UNIVERSIDADE FEDERAL DO PARÁ
INSTITUTO DE GEOCIÊNCIAS
PROGRAMA DE PÓS-GRADUAÇÃO EM GEOLOGIA E GEOQUÍMICA

TESE Nº 162

APLICAÇÃO DE RESÍDUOS DA MINERAÇÃO DE BAUXITA NA SÍNTESE DE GEOPOLÍMEROS

Tese apresentada por:

IGOR ALEXANDRE ROCHA BARRETO
Orientador: Prof. Dr. Marcondes Lima da Costa (UFPA)

BELÉM- PARÁ
2022

Universidade Federal do Pará
Instituto de Geociências
Programa de Pós-Graduação em Geologia e Geoquímica

APLICAÇÃO DE RESÍDUOS DA MINERAÇÃO DE BAUXITA NA SÍNTESE DE GEOPOLÍMEROS

TESE APRESENTADA POR:

IGOR ALEXANDRE ROCHA BARRETO
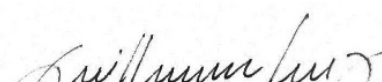
Como requisito parcial à obtenção do Grau de Doutor em Ciências na Área de GEOQUÍMICA E PETROLOGIA, Linha de Pesquisa MINERALOGIA E GEOQUÍMICA.

Data de Aprovação: 08 / 04 / 2022

Banca Examinadora:

Prof. Dr. Marcondes Lima da Costa
Orientadora – UFPA

Prof. Dr. Herbert Pöllmann
Membro – Martin-Luther Univ. Halle

Prof. Dr. Guilherme Frederico Bernardo L. e Silva
Membro – USP

Prof. Dr. José Roberto Zamian
Membro – UFPA

Prof. Dr. Rômulo Simões Angélica
Membro – UFPA

A Deus,
Aquele que é o maior responsável por todas as conquistas alcançadas no decorrer da minha vida;

A minha mãe, Nelma Franco Rocha da Silva, e aos meus avós, Neide Costa Franco Rocha e João Silva Rocha (*in memoriam*),

Por terem me proporcionado acesso à educação;
Por todo amor;
Por todo incentivo.

AGRADECIMENTOS

RESUMO

O processo de extração e beneficiamento dos depósitos de bauxitas da província bauxitífera de Paragominas/Rondon do Pará pode gerar grandes quantidades de resíduos, principalmente em duas etapas do processo: lavra e beneficiamento. Na etapa de lavra dos depósitos o "resíduo" é oriundo da retirada de uma espessa camada de material argiloso (conhecido como Argila de Belterra). Por outro lado, o "resíduo" do processo de beneficiamento é gerado após as etapas de britagem, moagem e lavagem, que originam uma ampla quantidade de material argiloso disperso em uma grande quantidade de água. Para o presente estudo selecionou Argila de Belterra dos depósitos de bauxita de Rondon do Pará, amostra de Argila de Lavagem de bauxita da empresa Hydro, uma amostra de caulim beneficiado da Imerys, da região do rio Capim, também no estado do Pará, uma amostra de microssílica comercial (Ecopower) e reagentes P.A da sigma (NaOH e KOH). As amostras e os geopolímeros foram caracterizados por Difração de Raios-X (DRX), Fluorescência de Raios-X (FRX), Análise Térmica Gravimétrica (TG), Calorímetro Exploratória Diferencial (DSC), Espectrometria de Emissão Ótica com Plasma Acoplado (ICP-OES) e Analisador de Partícula a Laser (APL). Geopolímeros foram sintetizados a partir da Argila de Belterra, microssílica e NaOH de acordo com o planejamento Box-Benkhen. Realizou-se também síntese de geopolímeros a partir de Argila de Belterra e caulim beneficiado (um estudo comparativo) usando KOH e microssílica. E por fim, geopolímeros foram sintetizados a partir da Argila de lavagem de Bauxita com NaOH e microssílica de acordo com o planejamento Doehlert. No estudo somente com a Argila de Belterra, o maior resultado de resistência resultado foi 47,78MPa e o menor resultado foi 7,05MPa. No estudo comparativo entre Argila de Belterra e caulim beneficiado, os melhores resultados de resistência a compressão foram obtidos com o caulim beneficiado. Os resultados de resistência a compressão dos geopolímeros sintetizados a partir da Argila de Lavagem variaram de 8.99 a 41.89MPa. Esses resultados demonstram o potencial positivo de ambos materiais para síntese de geopolímeros que podem ser usados como possíveis substitutos "Eco-friendly" para materiais tradicionais, principalmente, cerâmica e cimento.

Palavras-chave: Argila de Belterra; Argila de lavagem da bauxita; geopolímero; caulinita; metacaulinita.

ABSTRACT

The process of extraction and beneficiation of bauxite deposits in the bauxite province of Paragominas/Rondon do Pará can generate large amounts of waste, mainly in two stages of the process: mining and processing. In the mining stage of the deposits, the "residue" comes from the removal of a thick layer of clay material (known as Belterra Clay). On the other hand, the "residue" from the beneficiation process is generated after the crushing, grinding and washing stages, which give rise to a large amount of clay material dispersed in a large amount of water. For the present study, it selected Belterra clay from the bauxite deposits of Rondon do Pará, a sample of Bauxite Washing Clay from the Hydro company and a sample of kaolin benefited from Imerys Company. The samples and geopolymers were characterized by X-ray Diffraction (XRD), X-ray Fluorescence (FRX), Gravimetric Thermal Analysis (TG), Differential Exploratory Calorimeter (DSC), Optical Emission Spectrometry with Coupled Plasma (ICP-OES) and Laser Particle Analyzer (APL). Geopolymers were synthesized from Belterra clay, microsilica and NaOH according to the Box-Benkhen design. Synthesis of geopolymers from Belterra clay and beneficiated kaolin was also carried out (a comparative study) using KOH and microsilica. Finally, geopolymers were synthesized from Bauxite washing clay with NaOH and microsilica according to the Doehlert design. In the study with only Belterra clay, the highest resistance result was 47.78MPa and the lowest result was 7.05MPa. In the comparative study between Belterra Clay and beneficiated kaolin, the best results of compressive strength were obtained with the beneficiated kaolin. The compressive strength results of the geopolymers synthesized from the Washing Clay ranged from 8.99 to 41.89MPa. These results demonstrate the positive potential of both samples for the synthesis of geopolymers that can be used as possible "Eco-friendly" substitutes for traditional materials, mainly ceramics and cement.

Keywords: Belterra Clay; Bauxite washing clay; geopolymer; kaolinite; metakaolinite.

LISTA DE ILUSTRAÇÕES

LISTA DE TABELAS

SUMÁRIO

1 INTRODUÇÃO

O processo de extração e beneficiamento dos depósitos de bauxitas da província bauxitífera de Paragominas/Rondon do Pará pode gerar grandes quantidades de resíduos, principalmente em duas etapas do processo: lavra e beneficiamento. Na etapa de lavra dos depósitos o "resíduo" é oriundo da retirada de uma espessa camada de material argiloso (conhecido como Argila de Belterra) que é temporariamente arquivado dentro do processo conhecido como strip mining. Dependo da área de lavra, o capeamento do minério pode chegar até 20 metros de espessura. Por outro lado, o "resíduo" do processo de beneficiamento é gerado após as etapas de britagem, moagem e lavagem, que originam uma ampla quantidade de material argiloso disperso em uma grande quantidade de água. Esse material é depositado em bacias de rejeitos e correspondente 0,35-1,0 ton do minério. Apesar da grande quantidade de resíduos que é disponibilizada pelos 2 processos, esses materiais não possuem nenhuma aplicação pré-definida e são caracterizados como materiais estéreis e/ou nocivos ao meio ambiente. A composição mineralógica desses materiais é bastante semelhante, predominada pela presença do argilomineral caulinita, podendo apresentar gibbsita, goethita, hematita, anatásio e quartzo como minerais secundários.

A caulinita ($Al_2Si_2O_5(OH)_4$) é o argilomineral mais comumente encontrado na natureza. É um argilomineral do tipo 1:1. A sua estrutura é formada por uma folha tetraédrica de SiO_2 e uma folha octaédrica de $Al(OH)_6$ (Albach *et al.* 2019). Essas caraterísticas colaboram para que a caulinita seja utilizada em diversas aplicações. Porém, uma aplicação tem ganhado destaque nos dias atuais, que é o uso da caulinita, principalmente, quando calcinada a 600-750°C (formação da metacaulinita), como principal fonte de aluminossilicatos para produção de geopolímeros (Sun *et al.* 2018, Dupuy *et al.* 2019, Filipponi *et al.* 2021, Li *et al.* 2022).

Geopolímero é o termo utilizado para definir compostos inorgânicos amorfos e/ou cristalinos formados a partir de uma reação química entre compostos sólidos de aluminossilicato e solução de hidróxido alcalino altamente concentrada (Davidovits 1991c, González-García *et al.* 2022, Singh *et al.* 2015b, Siyal *et al.* 2016). Esse tipo de material é conhecido por apresentar diversas propriedades e características, que incluem: elevada resistência à compressão, baixa retração, cura rápida ou lenta, resistência a ácidos, resistência ao fogo e baixa condutividade térmica (Duxson *et al.* 2007, Junaid *et*

al. 2014). Essas propriedades não são um diferencial apenas do geopolímero, outros materiais podem exibir propriedades similares, como: materiais cerâmicos, cimento, concreto, entre outros. A vantagem do geopolímero em relação aos outros materiais, está relacionada ao seu processo de síntese que, normalmente, é realizado em baixas temperaturas e em curto intervalo de tempo, cooperando para a redução de emissão de CO_2 na atmosfera e do gasto energético, caracterizando-o como um produto amigável ao meio ambiente (Belmokhtar *et al.* 2017, Gomes Silveira *et al.* 2022, Hajimohammadi *et al.* 2018a, Kamseu *et al*. 2017, Koshy *et al.* 2019, Lemougna *et al.* 2017, McLellan *et al.* 2011, Petrus *et al*. 2021, Phoo-Ngernkham *et al.* 2015, Samarakoon e*t al.* 2019,Siyal *et al.* 2016).

1.1 OBJETIVOS

1.1.1 Objetivo geral

Identificar as propriedades dos geopolímeros sintetizados em diferentes condições de sínteses a partir de resíduos da mineração de bauxita (cobertura tipo Argila de Belterra e Argila de Lavagem de Bauxita) visando sua aplicação como material cerâmico e/ou cimento de baixa temperatura.

1.1.2 Objetivos específicos

- ✓ Sintetizar geopolímero com NaOH a partir de metacaulim vermelho proveniente da Argila de Belterra calcinada a 650°C;
- ✓ Avaliar o efeito do uso de KOH como ativador alcalino em dois tipos distintos de argilas cauliníticas;
- ✓ Investigar o desempenho da síntese de geopolímero a partir da Argila de Lavagem da Bauxita sem pré-tratamento térmico.

1.2 PROVENIÊNCIA NATURAL DA ARGILA DE BELTERRA E DA ARGILA DE LAVAGEM EMPREGADA NESTE ESTUDO

A argila de Belterra utilizada no presente trabalho (Argila de Belterra) provêm de uma lavra piloto de bauxita, denominada de Branco (Figura 1), situada no Platô Rondon Norte, Rondon do Pará. A argila de lavagem utilizada no trabalho é oriunda da extração de bauxita na região de Paragominas pela empresa Hydro (figura 2).

Os depósitos de bauxitas de Rondon do Pará e de Paragominas fazem parte da Província Bauxitífera de Paragominas, região leste do estado do Pará e oeste do estado do Maranhão, derivadas das sedimentares da Formações Itapecuru e Ipixuna (Greig 1977, Kotschoubey & Truckenbrodt 1981, Kotschoubey 2005). As bauxitas desta Província estão capeadas por espesso material argiloso, de coloração vermelha a amarela, equivalente à Argila de Belterra (Oliveira *et al*. 2016).
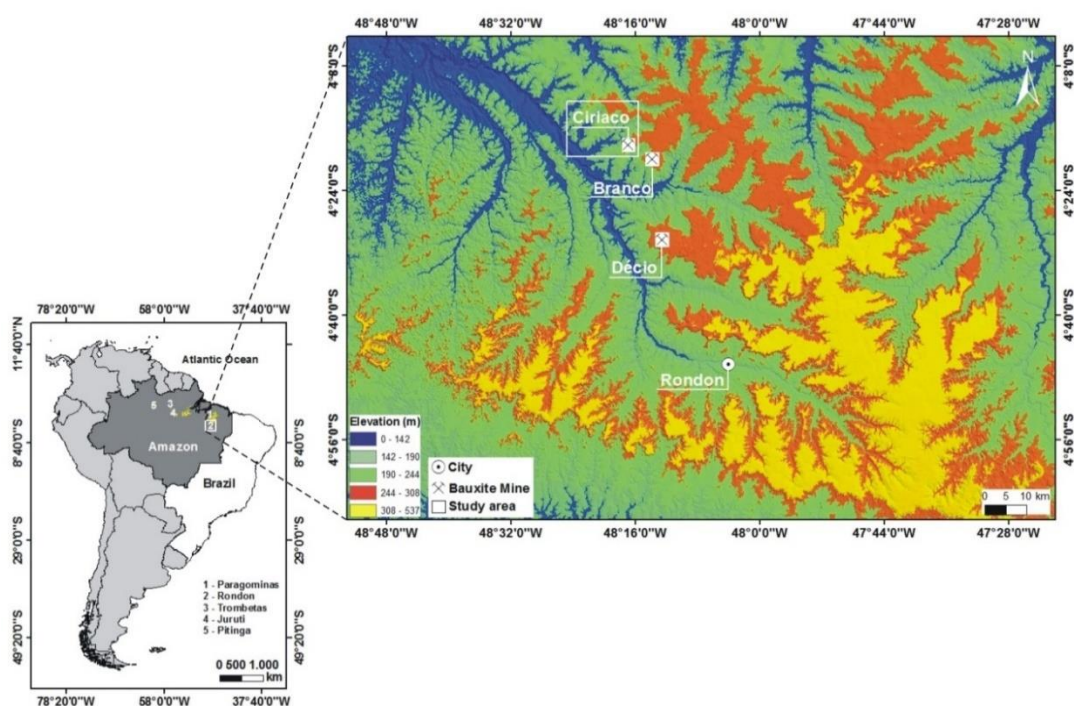
Figura 1 – Imagem SRTM da região de proveniência da Argila de Belterra, em domínio do município de Rondon do Pará. São indicadas as três lavras piloto, entre elas a Branco, de onde proveio a amostra empregada no presente estudo.
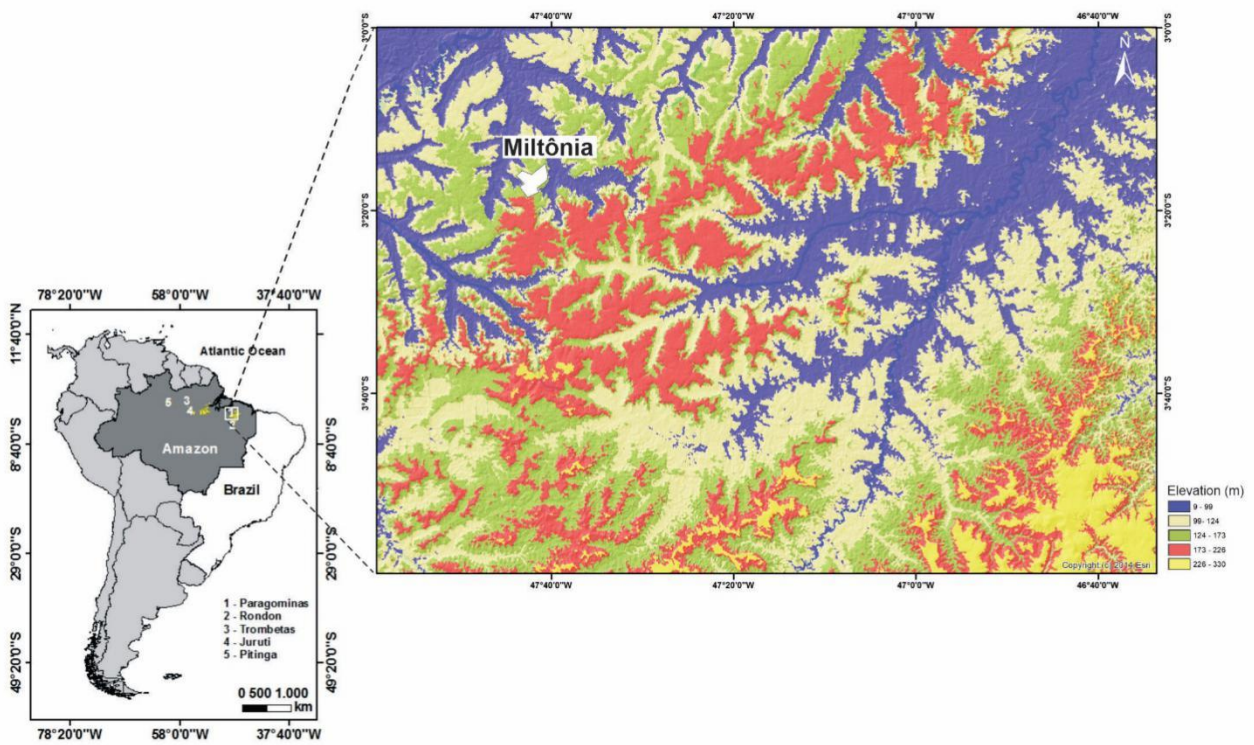
Figura 2 – Imagem SRTM da região de proveniência da Argila de Belterra, em domínio do município de Paragominas. É indicada a mina piloto Miltônia.

2 REVISÃO DA LITERATURA

2.1 GEOPOLÍMEROS

O termo geopolímeros é empregado para descrever uma classe de materiais inorgânicos amorfos "polímeros inorgânicos" que são formados a partir de uma reação de hidratação de aluminossilicatos com substâncias altamente alcalinas (J. Davidovits 1991ª, J. Davidovits 1991, Singh *et al*. 2015, Siyal et al. 2016, Ma et al. 2018, Rożek *et al*. 2019). O geopolímero tem composição química similar às zeólitas, diferenciando-se apenas em termos estruturais (Zhang *et al*. 2018). Além do termo geopolímero, esse tipo de material pode ser descrito na literatura por outras nomenclaturas, que podem depender da sua aplicação final. As nomenclaturas comumente utilizadas são: cimento ativado alcalinamente, cerâmica alcalina (devido sua alta estabilidade), geocimento, concreto de polímero inorgânico, entre outras alcalinas (Singh *et al*. 2015a).

O pesquisador francês Davidovits foi o principal precursor dos estudos desse novo tipo de material. A motivação dos seus estudos foram os incêndios catastróficos ocorridos sequencialmente na França em 1972, envolvendo plásticos orgânicos inflamáveis. Essas tragédias o motivaram junto com um grupo de pesquisadores a investigar materiais não inflamáveis que tivessem alta resistência ao calor. Os primeiros resultados revelaram um tipo de aluminossilicato que foi reestruturado devido à presença de uma solução altamente alcalina. Esse "novo aluminossilicato" foi nomeado pelo pesquisador de geopolímero (J Davidovits 1991, J Davidovits 1991a).

Davidovits avançou nas pesquisas desse novo material, registrando sua patente em 1979. Nesse mesmo ano ele fundou o Geopolymer Institute. O pesquisador prosseguiu no desenvolvimento desse tipo de material, obtendo diversas patentes.

Apesar de o produto ter sido patenteado por Davidovits, o pesquisador não foi o pioneiro na pesquisa desse tipo de material. Os estudos iniciais foram feitos na década de 70, ainda na antiga União Soviética. Os pesquisadores da União Soviética denominaram esse novo material de cimento de solo. Essa denominação foi atribuída pela origem do material utilizado, natural, e sua propriedade ligante, que era bem similar às características do cimento. O primeiro cimento de solo foi produzido através da mistura de materiais naturais à base de minerais aluminossilicatados que eram misturados com resíduos industriais ricos em componentes álcalis (Glukhovsky 1994). Glukhovsky, do Institueo de Engenharia de Kiev, na Ucrânia, foi o pesquisador responsável pela obtenção

desse material. Glukhovsky, assim como Davidovits, alertava para o fato de que cimentos da antiguidade eram produzidos dessa mesma forma e apresentavam uma alta durabilidade, além de resistência às intempéries (Davidovits & Morris 1988).

As pesquisas com esse tipo de material tornaram-se de extremo interesse para a o ramo de desenvolvimento de novos materiais e suas possíveis aplicações. Porém, a sua aplicabilidade depende exclusivamente das propriedades que ele possa apresentar como produtos finais. Essas propriedades serão consequências das matérias-primas utilizadas na síntese do geopolímero.

Os geopolímeros podem apresentar uma gama de propriedades e características, que incluem: elevada resistência à compressão, baixa retração, cura rápida ou lenta, resistência aos ácidos, resistência ao fogo e baixa condutividade térmica (Provis & van Deventer 2007, Junaid *et al*. 2014, Das *et al.* 2021.

2.1 FONTES DE ALUMINOSSILICATOS

A escolha da matéria-prima principal para síntese de geopolímeros (fonte aluminossilicatos) é um dos fatores que mais influenciam na obtenção de um bom produto. Elas que determinarão as características físicas e químicas que os geopolímeros irão apresentar. O resultado poderá ser refletido pelo meio da aquisição de produtos de baixa ou alta qualidade.

Diversos materiais já foram utilizados como precursores de geopolímeros. Esses materiais variam de um material natural: argilas e sedimentos (Dupuy *et al*. 2019); materiais oriundos de processos industriais, tais como: lama vermelha, cinzas volantes, resíduos da indústria de vidros, entre outros (Lemougna *et al*. 2017, Hajimohammadi *et al*. 2018a); e materiais sintetizados em laboratórios: zeólitas e compostos sintéticos de Al_2O_3 e SiO_2 (Król & Mozgawa 2019).

2.1.1 Argilas e rochas sedimentares

Esses materiais podem ser constituídos por diversas espécies de minerais, ou até mesmo por uma única (algo raro na natureza). O que caracteriza uma argila, é a presença predominante de argilominerais, cristais muito pequenos (<2μm), em plaquetas de contorno pseudo-hexagonais ou fibras (Barba 1997, Wenk *et al*. 2004, Velde & Meunier

2008, Teixeira 2009). Os argilominerais são filossilicatos, formados por duas, três ou quatro folhas, compostas por estruturas de tetraedros SiO_4 e octaédricas $[Mg(OH)_6]$ ou $[Al(OH)_6]$ (Luna 1999, Souza 2003, Moore & Reynolds 1997, Bergaya & Lagaly 2006). A combinação destas estruturas e composição química originam as diferentes espécies de argilominerais. E essas características irão determinar sua possível aplicação para síntese de geopolímeros.

Em geral os argilominerais são encontrados associados a outros minerais, como: calcita, dolomita, quartzo, pirita, feldspato, hematita, goethita, entre outros oxi/hidróxidos de ferro, além de matéria orgânica (Luna 1999).

Os principais argilominerais são: caulinita, illita, montimorilonita, clorita e paligorsquita (Vicenzi 1999).

A caulinita ($Al_2Si_2O_5(OH)_4$) é o argilomineral mais comumente encontrado nas rochas sedimentares e sedimentos, sendo o principal constituinte do caulim. Esse argilomineral, calcinado em temperaturas entre 600 e 800°C, conhecido como metacaulinita, é o material de partida mais utilizado na síntese de geopolímeros (Barbosa *et al*. 2018, Glid *et al*. 2017b, Yunsheng *et al*. 2010, Zhang *et al*. 2012b). A preferência pelo uso da metacaulinita em vez de caulinita oferece vantagens únicas em termos de alta reatividade e pureza, contribuindo para um geopolímero com melhor resistência à compressão e alta área superficial (Cheng *et al*. 2012, Yip et al. 2004).

A illita, com estrutura 2:1 ($K_{0,6}(H_3O)_{0,4}Al_{1,3}Mg_{0,3}Fe_{0,1}Si_{3,5}O_{10}(OH)_2(H_2O)$), é um argilomineral não expansivo, como a caulinita. O seu uso como material de partida para obtenção de geopolímeros foi utilizado após sua ativação térmica entre 550-950°C. Os estudos demonstraram que essa ativação aumentou sua reatividade na síntese de geopolímeros (Buchwald *et al*. 2009, Seiffarth *et al*. 2013, Sedmale *et al*. 2017). A presença de potássio em sua composição colabora nas etapas de dissolução e policondensação dos geopolímeros o que pode contribui para uma boa resistência mecânica (Xu & van Deventer 2000). Outro componente que pode influenciar nas propriedades dos geopolímeros é o Mg, porém não se sabe qual o efeito direto que sua presença pode acarretar, e se o mesmo seria positivo ou negativo (Xu & van Deventer 2000).

A montimorilonita, argilomineral do grupo das esmectitas, do tipo 2:1, $Na_{0,2}Ca_{0,1}Al_2Si_4O_{10}(OH)_2(H_2O)_{10}$, bastante expansivo com alta capacidade de absorver moléculas de água entre suas camadas t-o-t. Essa argila é a mais utilizada em processo de pilarização. Assim como a ilita, pressupõe-se que após a sua desidroxilação, esse

argilomineral possa apresentar reatividade a ativação alcalina (Sedmale *et al.* 2017). Devido sua alta absorção de água, argilas ricas neste mineral, apresentam uma forte disposição a causar trincas durante o processo de secagem (Luna 1999).

2.1.2 Resíduos industriais

O crescente desenvolvimento da indústria em seus diversos setores tem gerado uma quantidade razoável de resíduos, aparentemente, estéreis. Esse "problema" tem sido alvo de diversas discussões políticas em âmbito nacional e internacional, buscando soluções para o armazenamento adequado desses materiais. No entanto, a depender da composição, esses materiais podem ser empregados para produção de outros materiais, como cimentos, material cerâmico e síntese de novos materiais. Essas aplicações são alternativas para que esses resíduos tenham um destino sustentável (Belmokhtar *et al.* 2017, Gomes Silveira *et al.* 2022).

A utilização desse tipo de material para síntese de geopolímeros está sendo bastante abordado nos trabalhos atuais da área. Dentre os resíduos industriais, os mais aplicados para essa finalidade são: cinzas volantes, cinzas de casca de arroz, rejeitos de tratamento de água, rejeitos de vidros, lama vermelha, entre outros (Belmokhtar *et al.* 2017, Hajimohammadi *et al.* 2018, Kamseu *et al.* 2017, Koshy *et al.* 2019, Lemougna *et al.* 2017, Phoo-Ngernkham *et al.* 2015, Siyal *et al.* 2016).

Esses resíduos, em geral, são constituídos por altos percentuais de Al_2O_3 e SiO_2. A abundância desses compostos nesse tipo de material é um atrativo para sua aplicação em geopolímeros. Em contrapartida, esses materiais podem apresentar uma composição química bastante variada, com teores elevados de outros componentes, que podem influenciar nas propriedades finais dos geopolímeros (Phoo-Ngernkham *et al.* 2015, Siyal *et al.* 2016, Belmokhtar *et al.* 2017, Kamseu *et al.* 2017, Lemougna *et al.* 2017, Hajimohammadi *et al.* 2018, Koshy *et al.* 2019, Gomes Silveira *et al.* 2022).

As "impurezas" mais encontradas nesses tipos de materiais são: matéria orgânica, minerais de ferro, principalmente, hematita (Fe_2O_3) e goethita (FeO(OH), dolomita ($CaMg(CO_3)_2$), feldspatos, quartzo e minerais micáceos.

2.1.3   Materiais sintéticos

O uso de materiais sintéticos na síntese de geopolímeros é certeza de um produto com boas propriedades, pois o percentual de Al_2O_3 e SiO_2 é facilmente controlado. A natureza e o custo desse material não o tornam vantajoso, por conta disso, esse tipo de material é comumente utilizado como um aditivo para se atingir as razões molares desejadas no processo de síntese.

2.2 REAÇÃO DE GEOPOLIMERIZAÇÃO

A reação envolvida no processo de formação dos geopolímeros é exotérmica, considerada bastante rápida, em que aluminossilicatos, ativados alcalinamente, são parciais ou totalmente transformados em polímeros inorgânicos amorfos/semicristalinos (Cui *et al*. 2011). A fonte de aluminossilicatos é um dos principais medidores do mecanismo dessa reação. O que já é bastante conhecido na literatura é que o elevado grau de amorfismo desses aluminossilicatos favorece positivamente a formação do geopolímero (Yip *et al*. 2004, Cheng *et al*. 2012, Ma *et al*. 2018). Além dos aluminossilicatos, outros fatores que influenciam diretamente na obtenção de um "bom geopolímero" são o agente ativador (NaOH, KOH, Na_2SiO_3 e K_2SiO_3) e a quantidade de água (Singh *et al*. 2015a).

Compreender o mecanismo de reação que ocorre na formação dos geopolímeros é algo bastante importante. Essa reação é um processo químico bastante complexo que envolve diversas etapas que ainda não foram totalmente definidas na literatura, mas o princípio geral já está bem estabelecido (Alonso & Palomo 2001, van Jaarsveld *et al*. 2002, Duxson 2007, Dimas *et al*. 2009, Luukkonen *et al*. 2018). O processo de geopolimerização ocorre segundo as seguintes etapas:

(a) Dissolução dos aluminossilicatos em meio altamente alcalino;

(b) Reorganização e difusão dos íons com formação de uma estrutura coagulada;

(c) Reação de policondensação com formação de uma fase gel de aluminossilicato; e

(d) Transformação em estado sólido altamente endurecido.

A primeira etapa do processo de geopolimerização inicia-se com a dissolução de partículas sólidas de aluminossilicatos em meio altamente alcalino. O meio alcalino contribui para a quebra das ligações químicas covalentes Si—O—Si e Si—O—Al, favorecendo a liberação de espécies livres de tetraedros de $[SiO_4]^-$ e $[AlO_4]^-$ (Rahier e*t al*. 2007, Duxson *et al*. 2007, Komnitsas 2011, Yun-Ming et al. 2016). Considerando apenas um balanço de massa e de carga, a reação de dissolução e hidrólise que iniciam o processo de geopolimerização podem ser descritas da seguinte maneira:

(1) $Al_2O_3 + 3H_2O + 2OH^- \rightarrow 2\ [Al(OH)_4]^-$

(2) $SiO_2 + H_2O + OH^- \rightarrow [SiO(OH)_3]^-$

(3) $SiO_2 + 2OH^- \rightarrow [SiO_2(OH)_2]^{2-}$
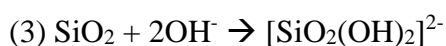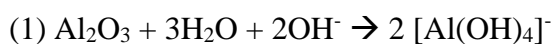
Essa primeira etapa libera moléculas de água e íons OH^- que normalmente são consumidos durante a dissolução. A água liberada durante essa etapa desempenha o papel de meio reacional, além de colaborar para o manuseio e conformação da "pasta" formada para uma possível aplicação(Duxson *et al*. 2007, Kaur *et al*. 2018). As reações (1) e (3) demonstram que a alcalinidade (concentração de $[OH]^-$) é um fator que influencia diretamente a taxa de dissolução da sílica (SiO_2) e da alumina (Al_2O_3), porém a temperatura e a reatividade da matéria prima em si também são fatores determinantes (Sagoe-Crentsil & Weng 2007, Jaarsveld & van Deventer 1999).

A segunda etapa é referente à condensação, onde as espécies químicas liberadas sofrem um rearranjo e formam um tipo de gel, definido como gel 1, resultado da interação entre as espécies de $[Al(OH)_4]^-$ e $[SiO(OH)_3]^-$ que são ligadas umas às outras pela atração entre um dos grupos OH^- a partir de $[SiO(OH)_3]^-$ e íons de Al^{+3} do $[Al(OH)_4]^-$, originando um complexo intermediário, com elevada concentração de Al (Zhuang *et al*. 2016). Mas a reação progride de forma contínua e mais espécies de Si-O são dissolvidas, formando a fase gel 2 que é caracterizada pelo enriquecimento de Si (Hassan *et al*. 2019). A ligação entre esses complexos é balanceada por íons de Na^+/ K^+ (Zhuang *et al*. 2016).

Conforme a "rede de gel" vai se estendendo inicia-se a formação de uma rede tridimensional de Al—O—Si (força da ligação 3,02KJ/mol), como resultado da condensação entre espécies de aluminatos e silicatos, caracterizando a formação do geopolímero (Rasaki *et al*. 2019). A força presente nas ligações dos geopolímeros é devido a diferença de eletronegatividade que existe entre os cátions (Al^{+3} e $Si^{+4)}$ e o ânion

(O^{2-}) (Hu *et al*. 2008). Essa etapa final da reação é evidenciada pelo endurecimento da pasta geopolimérica, que pode atingir uma resistência mecânica de 30 MPa mesmo sob cura a temperatura ambiente após um tempo de 24h (Rovnaník 2010).

A após as etapas acima se obtém o geopolímero (Fig. 2). Estudos demonstraram que suas propriedades são diretamente influenciadas por parâmetros como razão molar SiO_2/Al_2O_3, razão molar M_2O/Al_2O_3, razão molar SiO_2/M_2O e razão sólido/líquido (M é Na^+ ou K^+) (Dupuy *et al*. 2019, Singh *et al*. 2015b). A resistência mecânica do geopolímero é proporcional ao percentual de ativador alcalino presente em sua composição. O tempo de cura é influenciado pelo aumento de razão molar de SiO_2/Al_2O_3.
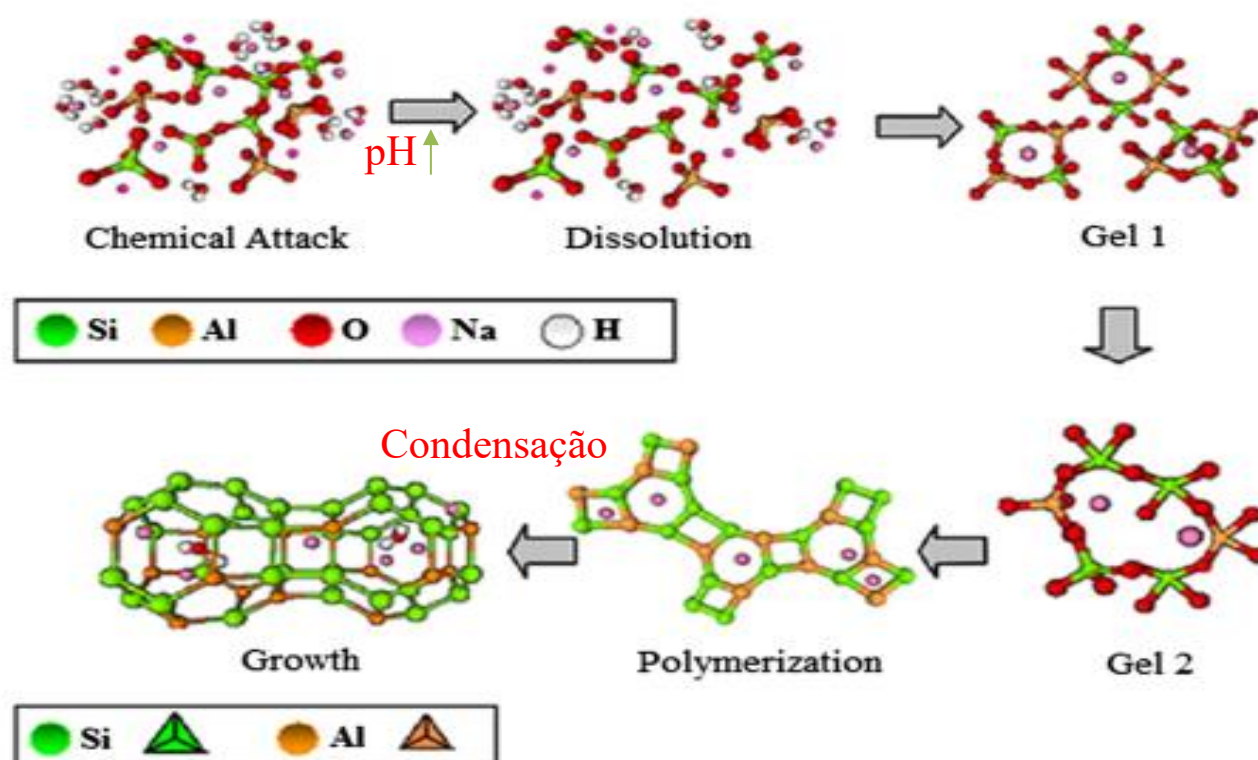
Figura 2- Reação de geopolimerização.
Adaptado de Yun-Ming *et al*. (2016).

2.3 APLICAÇÕES

As propriedades finais adquiridas pelos geopolímeros são bastante similares a produtos como cimentos, cerâmica e zeólita. Mas o que vai definir a sua melhor aplicação é a maneira que o geopolímero será sintetizado. As características comumente destacadas nesse produto são: alta resistência mecânica com pouco tempo de cura, resistência térmica, baixa retração após a queima, resistência a ataque ácido, agente adsorvente, entre outros (Duxson *et al*. 2007).

Yusheng *et al* 2010 investigaram o uso de geopolímero como um substituto para o cimento tradicional e obteve resultados expressivos em relação a resistência mecânica (34,9 Mpa).

Duxson *et al*. 2007 analisaram uso de geopolímero como um tipo de concreto, obtendo alta resistência após 24 horas de cura (60–70 Mpa). (Phoo-Ngernkham *et al*. 2015) também avaliou o uso do geopolímero como um substituto para concreto e obteve resistências elevadas após 28 dias de cura (171,7 e 173.0 Mpa).

Prud'homme *et al*. 2011 (a-b) estudaram o uso de diferentes tipos de argilas na formulação de geopolímero para a aplicá-los como materiais porosos para construção civil.

Bhattacharyya *et al*. *2012* produziram tijolos geopolimérico a partir de cinzas volantes. Os resultados mostraram-se satisfatórios, com percentuais aceitáveis de absorção de água (10-15%) e resistência mecânica entre 12-25MPa.

Lemougna *et al*. 2017 produziram cerâmica vermelha de baixa temperatura a partir de geopolímeros derivados de lama vermelha. Os resultados de absorção de água adequaram-se nas normas estabelecidas, com um percentual máximo de 18%. Os valores de resistência variaram de 4Mpa na temperatura mais baixa (60°C) e 55Mpa na temperatura mais alta (700°C). Sedmale *et al* 2017 também avaliaram a aplicação de material geopolimérico como um produto cerâmico, e assim como Lemougna *et al*. 2017, os melhores resultados foram obtidos na faixa de 600-700°C (25MPa).

Diversos autores têm estudado a capacidade de adsorção dos geopolímero:

- Cheng *et al*. 2012 analisou a capacidade de adsorção de 4 íons metálicos (Pb^{2+}, Cu^{2+}, Cr^{3+} e Cd^{2+}). O geopolímero mostrou-se com uma excelente capacidade de remoção desses íons do meio aquoso.
- Naghsh & Shams 2017 estudaram a capacidade de remoção de íons de Ca^{2+} e Mg^{2+} em diferentes formulações de geopolímero. As concentrações

máximas adsorvidas foram de 76,34 mg/g (Ca^{2+}) e 39,68 mg/g (Mg^{2+}) a 25 °C. Os autores concluíram que a capacidade de adsorção dos geopolímeros é diretamente proporcional à temperatura.

- Barbosa *et al*. 2018 também investigaram a capacidade de adsorção dos materiais geopoliméricos. Os autores estudaram o potencial de remoção de corantes orgânicos por material geopolimérico. O maior percentual removido foi de 70,8%. Segundo os autores esse percentual elevado demonstra que o geopolímero é um material interessante para remoção de resíduos orgânicos.

Moutinho *et al*. 2019 estudaram o uso de geopolímero como material de conservação para azulejos antigos. Os autores objetivaram preservar a degradação do material original e proteger o mesmo da ação da água da chuva, de substâncias químicas e ações mecânicas. Os resultados não se mostraram tão satisfatórios se comparado com outros materiais já utilizados para esse fim. Porém, as características apresentadas pelo geopolímero mostraram-se favoráveis para uma possível aplicação como material de restauro.

Panda et al. 2019 investigaram o uso de geopolímero como matéria prima para produção de concreto por meio de uma impressora 3D. Os Resultados mostraram que o produto final apresentou um desempenho mecânico anisotrópico e comportamento reológico bastante dependente da formulação estudada. Por conseguinte, os autores concluíram que o estudo pode ser aprimorado para se estabelecer uma formulação que possa apresentar a viscosidade adequada para se obter produtos com boa resistência mecânica.

3 MATERIAIS E MÉTODOS

3.1 MATERIAS-PRIMAS

Os materiais empregados para o desenvolvimento do presente trabalho (Figura 3) consistem em uma amostra representativa de Argila de Belterra (ABT-1/KLN-1) coletada a 50cm da superfície da mina piloto de Bauxita Branco que está situada no Platô Rondon Norte, Rondon do Pará-PA, Brasil; uma amostra de Argila de Lavagem de Bauxita (ALB-1) que foi coletada na empresa Mineração Paragominas S.A, Paragominas-PA, Brasil; uma amostra de caulim beneficiado da empresa Imerys (KLN-2); e regentes comerciais P.A da marca Sigma (NaOH   KOH). Adicionalmente foi utilizada uma amostra de microssílica comercial (Ecopowder) (MCR-1) que é fabricada a partir de finas partículas de SiO_2, geradas pelo processo de produção de silício metálico. Essa amostra foi utilizada para se obter as razões desejadas de SiO_2/Al_2O_3 nas sínteses dos geopolímeros.
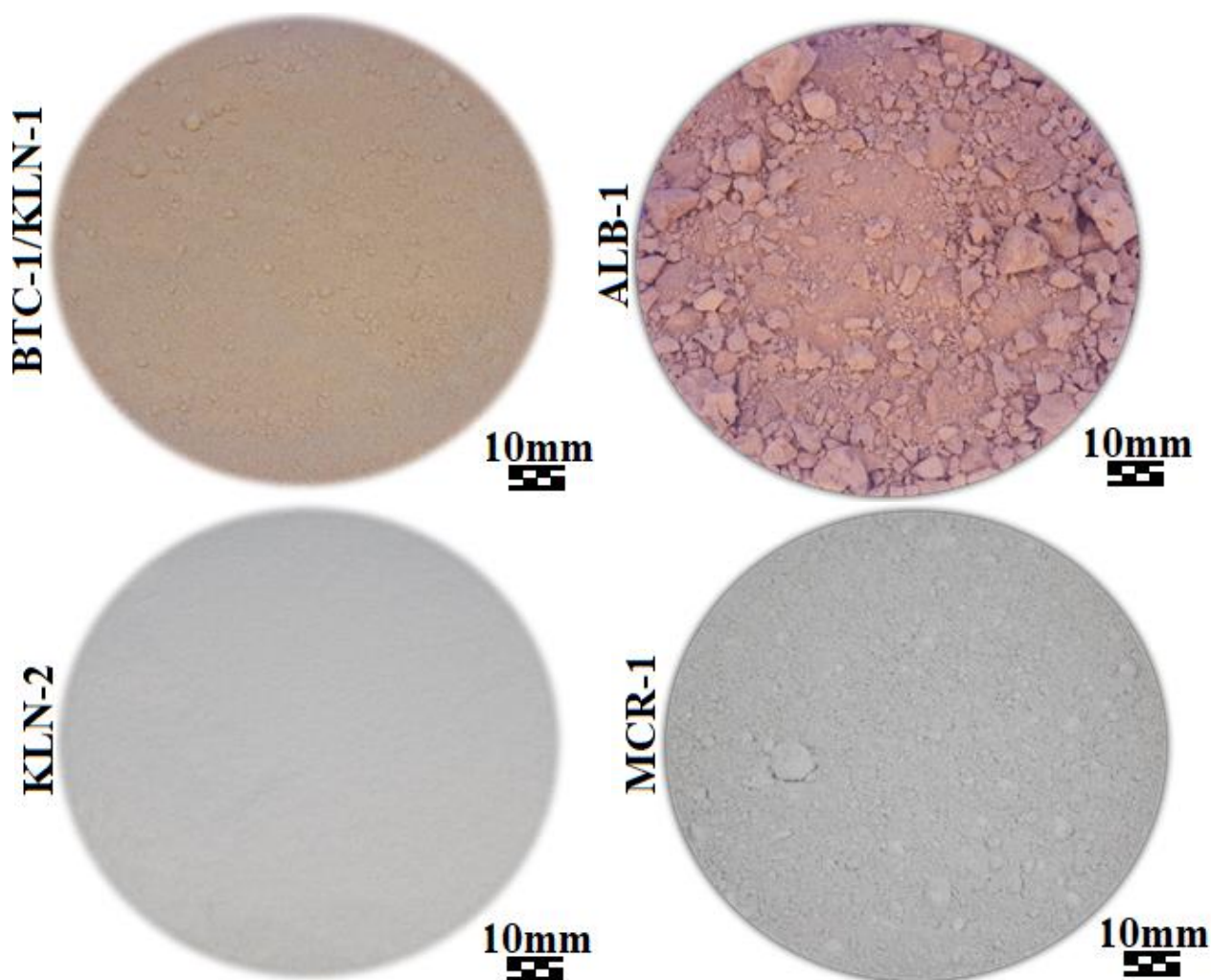
Figura 3- Imagens das amostras utilizadas no trabalho.

3.1.1   Composição mineralógica

A determinação das fases mineralógicas das amostras *in natura*, calcinadas e dos geopolímeros foi determinada por difração de raios-X segundo o método do pó. Empregou-se um difratômetro BRUKER, modelo D2 PHASER, com goniômetro θ / θ, raio: 141,1nm, ânodo de cobre com linha de emissão característica de 1,54 Å / 8,047 keV (Cu-Kα1) e potência máxima de 300W (30 kV x 10 mA). O detector utilizado nesse equipamento é o Linear Lynxeye com abertura de 5° 2θ e 192 canais. Esse mesmo método será utilizado para determinar os minerais presentes no geopolímero. As análises foram realizadas no Laboratório de Mineralogia, Geoquímica e Aplicações (LAMIGA-UFPA) do Instituto de Geociências da UFPA.

3.2.2 Composição química (FRX)

As análises químicas para determinação dos elementos maiores foram realizadas por Espectrometria de Fluorescência de Raios-X (FRX), através da confecção de pastilhas fundidas. As pastilhas foram preparadas com uma razão amostra/fundente (tetraborato de lítio) estabelecida segundo o método XRF79C_10. As análises foram realizadas no laboratório de análise químicas da empresa SGS GEOSOL, localizado em Vespasiano/MG.

A perda ao fogo (PF) de todas as amostras foi determinada através do método gravimétrico por calcinação a 1000ºC, a partir de amostras previamente secas.

3.2.3 Sílica reativa e alumina aproveitável

O percentual de sílica reativa e alumina aproveitável também foram realizados no laboratório de análise químicas da empresa SGS GEOSOL segundo o método estabelecido pela empresa (**ICP05V)**, que consiste na dissolução da amostra em solução concentrada de NaOH em um sistema com pressão e temperatura (150°C) controladas. A partir da solução obtida determinou-se a concentração de alumínio aproveitável por espectroscopia de emissão ótica com plasma indutivamente acoplado (ICP-OES). A fase sólida, resultante do estágio de dissolução foi dissolvida em solução de HCL, o que permitiu determinar o percentual de silica reativa por ICP-OES.

3.2.4 Quantificação da caulinita por estequiometria

A quantificação do percentual de caulinita por estequiometria foi determinada a partir dos resultados de sílica reativa.
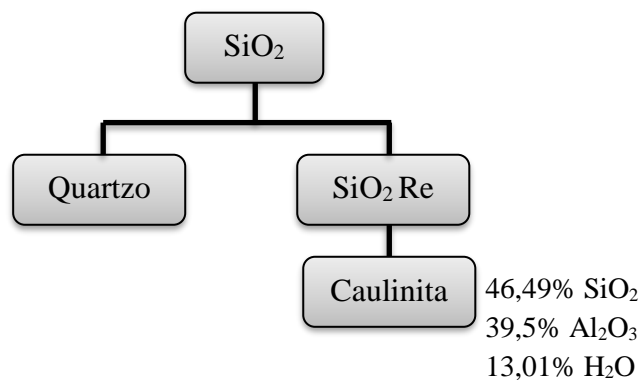
Figura 4- Fluxograma do cálculo estequiométrico utilizado para determinar o percentual de caulinita.

3.2.5 Distribuição do tamanho de partículas

As análises granulométricas foram realizadas para se avaliar qual a influência dos tamanhos dos grãos nas propriedades tecnológicas do produto final. Essa propriedade foi determinada pela técnica de difração de laser, com o equipamento Analysette Microtec Plus (Fritsch, Alemanha). O procedimento consiste em inserir uma alíquota da amostra de interesse moída e imersa em uma solução de água e três gotas de pirofosfato de sódio (10%). Este procedimento foi realizado no Laboratório de Mineralogia, Geoquímica e Aplicações (LAMIGA-UFPA) do Instituto de Geociências da UFPA.

3.2.6 Espectroscopia Infravermelha com transformada de Fourier (FTIR)

Esta técnica foi utilizada com a finalidade de complementar os resultados obtidos pela difração de raios-X. As análises foram feitas utilizando cerca de 0,0015g de amostra que foram misturadas e homogeneizada com 2g de brometo de potássio (KBr, Merck). Em seguida, pastilhas foram conformadas em moldes de aço na forma de discos de 14mm de diâmetro, e prensadas sob uma pressão de 8 Kbar, em prensa manual da marca Specac 8. As análises foram realizadas no equipamento Vertex 70, da Bruker, na faixa espectral

de 400-4000cm-1. Esse procedimento será realizado no Laboratório de Mineralogia, Geoquímica e Aplicações (LAMIGA-UFPA) do Instituto de Geociências da UFPA.

3.2.8 TG/DSC

Por meio destas análises, buscou-se entender qual o comportamento térmico e as possíveis reações que ocorrem durante o processo de aquecimento das amostras. As análises das amostras foram realizadas em um equipamento da NETZSCH, modelo STA 449 F5 Jupiter, com analisador térmico simultâneo, equipado com um forno cilíndrico vertical e fluxo de N2 de 50ml/s com uma taxa de aquecimento de 10°C/min, com uma faixa de temperatura de 30°C até 1100ºC. Este procedimento foi realizado no Laboratório de Mineralogia, Geoquímica e Aplicações (LAMIGA-UFPA) do Instituto de Geociências da UFPA.

3.3 FORMULAÇÃO E CARACTERIZAÇÃO DOS GEOPOLIMEROS

As metodologias de sínteses empregadas e constantes nos manuscritos foram estabelecidas de acordo com os objetivos específicos estabelecidos na tese. Esses objetivos foram construídos baseando-se em lacunas da literatura em relação as matérias-primas principais empregadas na tese (Argila de Belterra e Argila de Lavagem da Bauxita); nas diferentes propriedades exibidas pelos geopolímeros a depender do ativador alcalino (NaOH e KOH) e da matéria-prima precursora de geopolímero; e por fim, ao comportamento da síntese de geopolímero a partir de uma amostra sem qualquer método de preparação de amostra. Os métodos utilizados para alcançar esses objetivos estão listados abaixo:

- No primeiro manuscrito, aborda-se a aplicação de geopolímero sintetizado com NaOH a partir da Argila de Belterra calcinada a 650°C "metacaulim vermelho" em cerâmica vermelha de baixa temperatura. No presente trabalho buscava-se compreender como a amostra de Argila de Belterra se adequava aos principais parâmetros definidos pelo modelo de Taguchi (Nazari, 2013; Olivia & Nikraz, 2012): temperatura, Na_2O/Al_2O_3, SiO_2/Al_2O_3 e percentual de água. Os resultados do manuscrito revelaram que a síntese de geopolímero com NaOH a partir da Argila de Belterra se comportou se maneira semelhante a outros materiais já descritos na literatura, apresentando condições ótimas de síntese de: Na_2O/Al_2O_3

(1,1), SiO_2/Al_2O_3 (3,4-3,8), temperatura (100°C) e percentual de água (34,8%) (g/g).

- Compreendido o comportamento da síntese de geopolímero da amostra de Argila de Belterra com NaOH (ativador alcalino mais utilizado para síntese de geopolímero), o segundo manuscrito construiu-se com o objetivo de compreender a influência da composição mineralógica da Argila de Belterra (que além de caulinita, contém gibbsita, goethita, quartzo e anatásio) nas propriedades dos geopolímeros sintetizados com KOH. Para este estudo, além de uma amostra de Argila de Belterra, utilizou uma amostra de caulim beneficiado da empresa Imerys para servir como um "material de referência", sabendo-se que a mineralogia dessa amostra é apenas caulinita (>90%) e quartzo. Como o intuito do trabalho era avaliar as propriedades dos geopolímeros e não a sua possível aplicação, as amostras foram preparadas de modo a favorecer a reatividade: moagem em moinho de bolhas por aproximadamente 1 hora; peneiramento a 60 mesh; a fração passante foi calcinada a 750°C, temperatura em que favorece a metacaulinita é mais reativa. As condições de síntese ótimas encontradas no manuscrito um foram reaproveitadas e fixadas no manuscrito dois: razão de SiO_2/Al_2O_3 (3,4) e o percentual de água em (34,8%) (g/g).

  - O desenvolvimento do terceiro manuscrito que compõe a tese foi reflexo direto do conhecimento adquirido durante os dos dois primeiros manuscritos. O enfoque do terceiro manuscrito foi a aplicação da amostra de Argila de Lavagem da Bauxita como matéria-prima principal para síntese de geopolímero. Ao contrário dos manuscritos anteriores, a intenção deste manuscrito era usar a amostra da forma que ela é disponibilizada pela empresa mineração Paragominas S.A (Hydro), afim de tornar sua aplicação ainda mais viável e atrativa, evitando etapas, que apesar de usuais, encarecem ainda mais sua aplicação em geopolímero, como: moagem, peneiramento e calcinação a temperaturas acima de 500°C. A única etapa de preparação da amostra foi: secagem a 105°C/2h. Além da eliminação de etapas de preparação, o objetivo do terceiro manuscrito era testar razões mais baixas de Na/Al, considerando que o custo atual do NaOH é o que mais pesa negativamente para que o geopolímero seja considerável "economicamente inviável". Sendo assim resolveu-se testar razões mais baixas até do que a encontrada como ideal no manuscrito um (1,1). As razões testadas foram: 0,9, 0,8, 0,7, 0,6 e 0,5. A razão SiO_2/Al_2O_3 foi reaproveitada dos

manuscritos anteriores e fixada em 3,4, e o percentual de água em 15,5 % (g/g). O percentual de água utilizada neste artigo é inferior aos outros artigos por consequência da granulometria (< 400 mesh) e da não calcinação da amostra, o que colaborou para uma maior plasticidade da amostra quando misturada com água. O detalhamento das etapas de sínteses de cada artigo pode ser observado nos tópicos seguintes.

3.3.1 Preparação da amostra/síntese dos geopolímeros (Manuscrito 1)

A amostra de Argila de Belterra (ABT-1) foi seca em estufa durante um período de 24 horas sob temperatura de 110°C para retirada da umidade natural. Em seguida, a amostra foi moída em moinho de bolas (Marconi MA 500/CF) com uma rotação de 365,4 rpm, por um período de 1 hora. A amostra com a granulometria já reduzida foi calcinada a 650°C em forno mufla por duas horas para obtenção da metacaulinita.

A síntese dos geopolímeros foi realizada com base na Metodologia de Superfície de Resposta (MSR) baseada em um planejamento estatístico do tipo Box-Behnken (PBB) (tabela 2), com 12 experimentos e mais 5 réplicas no ponto central das variáveis, para determinar quais as melhores condições de síntese com base na resistência à compressão. A escolha das variáveis independentes foi feita de acordo com o modelo de Taguchi (Nazari, 2013; Olivia & Nikraz, 2012) que define apenas 4 parâmetros importantes: temperatura, Na_2O/Al_2O_3, SiO_2/Al_2O_3, e percentual de água. O planejamento foi realizado com 3 variáveis independentes (temperatura, Na_2O/Al_2O_3 e SiO_2/Al_2O_3), com três níveis (-1, 0 e +1) (tabela 2) e o percentual de água fixo em 34,8% (g/g). A variável dependente foi a resistência à compressão. Os dados do planejamento Box-Behnken foram tratados usando os programas Octave - 4.2.1 e Microsoft Excel 2016.

Os testes de absorção de água, porosidade aparente e densidade aparente foram realizados em todos os geopolímeros sintetizados no planejamento PBB, como complementação das propriedades tecnológicas.

Inicialmente, pesou-se quantidades estabelecidas da amostra ABT-1 e microssílica (MCR-1) (15,2g/5,4g; 17,5g/3,1g e 20,6g/0g) para se chegar ao peso de 20,6g em todas as formulações. A proporção em massa de ABT-1/MCR-1 foi pré-determinada de acordo com a razão SiO_2/Al_2O_3 desejada.

Após a mistura das amostras, a solução alcalina foi adicionada lentamente, homogeneizando-se em gral de porcelana, por aproximadamente 10 min. A pasta

geopolimérica foi, então, moldada em moldes de aço, na forma de prisma, com as seguintes dimensões: 50,0mmx20,0mmx10mm, e prensagem uniaxial de simples efeito sob uma pressão de 50 kgf/cm2 em Prensa Hidráulica (Karl Kolb, modelo PW-40). Após a conformação, os corpos de prova foram vedados em papel filme (controlar a umidade) e colocados na estufa a 40°C por 24h, em seguida a temperatura foi acrescida em 10°C/h até atingir a temperatura final estabelecida no planejamento (60°C, 80°C e 100°C).

Tabela 1- Variáveis independentes usadas no planejamento de experimento do tipo Box-Behnken.

Variáveis independentes	Unidade	Notação	Níveis		
			+1	0	-1
SiO_2/Al_2O_3	Razão molar	X1	3,8	2,9	2,0
Na_2O/Al_2O_3	Razão molar	X2	1,1	0,9	0,7
Temperatura	°C	X3	100	80	60

Tabela 2- Condições dos geopolímeros sintetizados de acordo com o planejamento do tipo Box-Behnken.

Experiments	Si/Al (X1)		Na/Al (X2)		Temperature (X3)	
	Coded	Real (molar ratio)	Coded	Real (molar ratio)	Coded	Real (°C)
1	-1	2	-1	0,7	0	80
2	1	3,8	-1	0,7	0	80
3	-1	2	1	1,1	0	80
4	1	3,8	1	1,1	0	80
5	-1	2	0	0,9	-1	60
6	1	3,8	0	0,9	-1	60
7	-1	2	0	0,9	1	100
8	1	3,8	0	0,9	1	100
9	0	2,9	-1	0,7	-1	60
10	0	2,9	1	1,1	-1	60
11	0	2,9	-1	0,7	1	100
12	0	2,9	1	1,1	1	100
13 (PC)	0	2,9	0	0,9	0	60

PC: ponto central.

3.3.2 Preparação da amostra/Síntese dos geopolímeros (Manuscrito 2)

A amostra de Argila de Belterra, nomeada nesse manuscrito de KLN-1, a amostra de caulim beneficiado da Imerys (KLN-2) e a amostras de microssílica (MCR-1) foram as matérias-primas utilizadas no artigo 2. As amostras foram secas em estufa durante um período de 24 horas sob temperatura de 110°C para retirada da umidade natural. Em seguida, as amostras foram moídas em moinho de bolas (Marconi MA 500/CF) com uma rotação de 365,4 rpm, por um período de 1 hora. No produto obtido na moagem, realizou-se o peneiramento em peneira com abertura de 60 mesh para retirada da fração de areia grossa. A fração obtida abaixo de 60mesh foi calcinada a 750 °C, por duas horas, para a completa desidroxilação da caulinita e sua transformação para metacaulinita.

A síntese seguiu as seguintes etapas (figura 5): as amostras KLN-1 e KLN-2 foram misturadas com a amostra MCR-1 em grau de porcelana até ser obtido uma mistura homogênea; a essa mistura adicionou-se lentamente uma solução de 7,2ml de KOH nas concentrações definidas na tabela 3; a pasta formada foi homogeneizada em grau de porcelana pelo período de 5min; a pasta geopolimérica foi então armazenada em estufa a 40°C pelo período de 1h; a pasta geopolimérica foi retirada da estufa e conformada em moldes de aço nas dimensões de 50mmx20mmx30mm com prensagem uniaxial de simples efeito sob uma pressão de 20 kgf/cm^2 em Prensa Hidráulica (Karl Kolb, modelo PW-40). Após a conformação, os corpos de prova foram vedados em papel filme (controlar a umidade) e colocados na estufa a 40°C por 24h, em seguida a temperatura foi acrescida em 10°C/h até atingir a temperatura final estabelecida nos experimentos.

As condições de sínteses estudadas foram: concentração molar, temperatura e tempo de cura. A razão molar Si/Al e o volume de água foram mantidos constantes em todas as sínteses, 3,4 Si/Al e 7,2ml de H_2O. Para avaliar a influência da concentração molar, soluções de KOH foram preparadas nas concentrações de 12, 13, 14, 15 e 16M, com temperatura final de cura de 70°C e tempo de cura de 24h. A temperatura foi avaliada nas condições fixas de concentração molar de KOH (16M), tempo de cura de 24h e temperaturas finais de 60, 70, 80, 90 e 100°C. A influência dos tempos de cura de 24, 48, 72, 96 e 120h foram analisados nas condições de 16M de KOH e temperatura de cura de 70°C.

Tabela 3- Condições de sínteses estudadas (Manuscrito 2).

Variáveis estudadas	Parâmetros estudados				
Concentração molar (M)	12	13	14	15	16
Temperatura (°C)	60	70	80	90	100
Tempo (h)	24	48	72	96	120

3.3.3 Síntese dos geopolímeros (Manuscrito 3)

A síntese dos geopolímeros foi realizada de acordo com a Metodologia de Superfície de Resposta (MSR) baseada em um planejamento de experimento do tipo Doehlert, com 6 experimentos e 3 réplicas no ponto central (tabela 2). Nesse tipo de planejamento são avaliadas a influência de 2 variáveis em relação a uma determinada resposta, uma variável é avaliada em 5 níveis distintos e a outra é analisada em 3 níveis.

As variáveis dependentes escolhidas no trabalho foram temperatura e razão Na/Al (tabela 1). A variável independente do planejamento é a resistência à compressão.

Para a síntese dos geopolímeros a amostra de argila de lavagem de bauxita (ALB-1) foi seca por 48h em temperatura ambiente e em seguida foi levada a estufa por mais 2h na temperatura de 105°C para acelerar a perda de umidade da amostra. Para conformação dos corpos de prova, pesou-se a mistura de 23g da amostra ALB-1 e 7g de microssílica comercial (MCR-1) para atingir a razão molar de Si/Al de 3,5. Essa mistura foi transferida para um grau de porcelana. A essa mistura adicionou-se lentamente uma solução de 4,6ml de NaOH que foi homogeneizada com pistilo por aproximadamente 5min. O volume de água foi mantido fixo em 4,6ml para que não ocorresse diferenças na hora da prensagem dos corpos de prova. A massa de NaOH em solução foi estabelecida pelas razões molares de Na/Al pré-definidas da tabela 1. A pasta geopolimérica formada foi reservada em potes de polietilenos que em seguida eram tampados, onde permaneciam em temperatura ambiente pelo período de 1h30min. Após esse período a pasta geopolimérica foi conformada em moldes de aço nas dimensões de 50mm x 20mm x 30mm com prensagem uniaxial de simples efeito sob uma pressão de 15 kgf/cm^2 em prensa hidráulica (Karl Kolb, modelo PW-40). Os corpos de prova conformados eram vedados em papel filme (controlar a umidade) e colocados na estufa a 40°C por 24h, em seguida a temperatura era acrescida em 10°C/h até atingir a temperatura final estabelecida nos experimentos.

Tabela 4 - Variáveis independentes com seus valores reais e codificados que serão utilizadas no planejamento estatístico de Doehlert.

Na/Al		Temperatura	
Codificada	Real	Codificada	Real
-1	0,5	-0,866	100
-0,5	0,6	0	275
0	0,7	0,866	450,0
0,5	0,8		
1	0,9		

Tabela 5- Matriz experimental e valores reais e codificados das variáveis independentes de acordo com o planejamento Doehlert.

Experimento	Temperatura		Na/Al	
	Codificada	Real	Codificada	Real
G1	0,866	450	0,5	0,8
G2	0,866	450	-0,5	0,6
G3	0	275	-1	0,5
G4	0,866	100	-0,5	0,6
G5	0,866	100	0,5	0,8
G6	0	275	1	0,9
G7	0	275	0	0,7
G8	0	275	0	0,7
G9	0	275	0	0,7

3.4 CARACTERIZAÇÃO DO PRODUTO FINAL

3.4.2 Absorção de água

Este parâmetro será avaliado através da relação entre os pesos secos e úmidos dos corpos prova. A obtenção do peso úmido requer a imersão dos corpos cerâmicos em água por, no mínimo, 24h. O peso úmido é determinado após a retirada da água superficial do corpo-de-prova.

$$Aa = (Mu - Ms)/Ms \times 100 (\%)$$

Onde:

Aa- indica a absorção de água, em porcentagem;

Mu- indica a massa do corpo saturado em água;

Ms- indica a massa do corpo seco

3.9.3 Porosidade aparente

A determinação da porosidade aparente dos corpos de prova será realizada de acordo com a norma C373-88 (ASTM), de acordo com a equação:

$$Pa = (Mu - Ms)/(Mu - Mi) \times 100 (\%)$$

Onde:

Pa - indica a porosidade aparente, em porcentagem;

Mu - é a massa dos corpos cerâmicos saturados com água;

Ms - é a massa dos corpos cerâmicos secos;

Mi -é a massa (g) do corpo cerâmico imerso em água.

3.9.4 Resistência mecânica à compressão (Manuscritos 1 e 3)

Os ensaios de resistência à compressão para o manuscrito 1 e 2 foram realizados em equipamento universal de ensaios, modelo 300/15 kN, Servo-plus evolution, da MSTEST, com velocidade de ensaio de 01MPa/seg, início do ensaio em 1N e fim de carga 30%. O teste foi realizado no laboratório de concretos da Faculdade de Arquitetura da UFPA.

3.9.4 Resistência mecânica à compressão (Manuscrito 2)

O teste de resistência à compressão dos CPs foi realizado em uma máquina universal de ensaios, da AROTEC, modelo WDW-100E, com célula de carga de 100 KN, velocidade de ensaio de 2KN/min, inicio de ensaio em 2N. Os testes foram realizados no laboratório de resistência do Instituto Federal do Pará (IFPA).

A resistência mecânica à compressão foi calculada segundo a equação:

$$\delta c = \frac{P}{A}$$

Onde:

Δc: tensão de ruptura à flexão (MPa);

P: carga de ruptura após secagem (N);

A:área total (mm^2)

4   RESULTADOS E DISCUSSÕES

Os resultados, discussões e conclusões específicas estão apresentados em forma de três manuscritos. O primeiro artigo, já publicado no periódico *Construction and Building Materials*, aborda o uso da Argila de Belterra (ABT) calcinada a 650°C na síntese de geopolímeros aplicados como material cerâmico de baixa temperatura. O segundo manuscrito investiga o comportamento da utilização de duas argilas cauliníticas distintas na síntese de geopolímeros com KOH. O manuscrito foi submetido à *Materials Chemistry and Physics*. O terceiro manuscrito é referente ao uso da Argila de Lavagem da Bauxita *in natura* (sem tratamento térmico) como matéria-prima principal para síntese de geopolímeros "Eco-Friendly". Esse manuscrito foi submetido à *Cement and Concrete Composites*.

4.1 USE OF THE CLAYEY COVER OF BAUXITE DEPOSITS OF THE AMZON REGION FOR GEOPOLYMER SYNTHESIS AND ITS APPLICATION IN RED CERAMICS
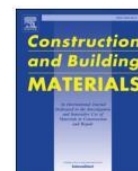
Use of the clayey cover of bauxite deposits of the Amazon region for geopolymer synthesis and its application in red ceramics

Igor Alexandre Rocha Barreto [a,*], Marcondes Lima da Costa [b]

[a] Program for Post-graduation in Geology and Geochemistry, Institute of Geosciences, UFPA, Belém, PA, Brazil
[b] Program for Post-graduation in Geology and Geochemistry, Institute of Geosciences, Federal University of Pará, UFPA, Brazil

ARTICLE INFO

ABSTRACT

The exploitation of bauxite deposits in the Amazon region is well known. Mining begins with the temporary or even permanent removal of an extensive surface layer of clayey material (Belterra clay) that can reach a thickness of up to 20 m. The mineralogical composition of this material has already been described in the literature and consists mainly of kaolinite. The extensive surface distribution of Belterra clay in the Amazon region and its composition is of interest in the evaluation of its viability for the synthesis of geopolymers. For the present study, a sample of Belterra clay (BTC-1) from the bauxite deposits of Rondon do Pará was selected, in addition to microsilica (MCR-1) (Ecopowder) and Sigma P.A. reagent (NaOH). The Belterra clay sample was characterized by X-ray diffraction (XRD), X-ray fluorescence (XRF), and thermogravimetric (TG) and differential scanning calorimetry (DSC) analyses. To determine the physical and mechanical properties of Belterra clay, geopolymers were synthesized using BTC-1, MCR-1, and NaOH with different Si/Al and Na/Al ratios according to the Box-Behnken design (BBD). Technological tests, including water absorption, apparent porosity, and compressive strength tests, were performed. Based on the BBD, the highest compressive strength was 47.78 MPa, and the lowest compressive strength was 7.05 MPa. BTC-1 showed potential for the synthesis of geopolymers with high mechanical strength and an acceptable percentage of water absorption.

1. Introduction

The exploitation of bauxite deposits in the Amazon region is well known. Mining begins with the temporary or even permanent removal of an extensive surface layer of clayey material (Belterra Clay) that can reach a thickness of up to 20 m. As the companies use the strip-mining process, the Belterra Clay, after removing bauxite for mining, it is returned to the area for the restoration of the landscape, because it has not yet been developed a consolidated application by companies.

The mineralogical composition of this material has already been described in the literature and consists mainly of kaolinite [1–4].

The unique composition of Belterra Clay and its ample availability have increased interest in the possibility of its technological application as a raw material for the production of red ceramics [2,3,5]. The results of previous studies have shown that the predominance of kaolinite directly affects the technical characteristics of ceramic products, exhibiting water absorption, apparent porosity, and mechanical strength characteristics that are not ideal, especially at lower firing temperatures. However, the technical properties can be considerably improved with the addition of at most 40% illitic clay, clayey silt, and yellow soil to the ceramic mass.

In contrast to the undesirable effects of large concentrations of kaolinite on the technical properties of ceramic products, desirable effects can be achieved with kaolinite as the main starting mineral in other applications, such as geopolymer synthesis [6–11].

Geopolymers are synthesized through a chemical reaction between solid aluminosilicate compounds and a highly concentrated alkaline hydroxide solution [12–15].

Geopolymers can exhibit diverse properties and characteristics, including a high compressive strength, low shrinkage, fast or slow curing, acid resistance, fire resistance, and low thermal conductivity [16–19]. Based on their properties, geopolymers have been attractive for applications in the civil construction sector (ceramic materials, concrete, and cement) because compared to the usual production methods, geopolymers have technical properties that can be obtained in short times and at lower temperatures, which reduces CO_2 emissions and energy expenditures and produces an environmentally friendly product [11,20,21].

Considering the extensive surface distribution of Belterra Clay in the Amazon region that can be obtained at a low or no cost by bauxite mining exploitation and its unique composition, which includes considerable concentrations of hematite and gibbsite compared to kaolinite (favorable to geopolymer synthesis), the objective of this study was to demonstrate that the Belterra clay from the bauxite deposits of Rondon do Pará in state of Pará, Brazil, which does not have any current application value, is a great material for the synthesis of geopolymers for use in the production of red ceramics at low temperatures, which can reduce CO_2 emissions in this industrial sector.

2. Materials and methods

2.1. Raw materials

The raw material used in this study consisted of a representative sample of Belterra Clay (BTC-1) from the Bauxite Branco pilot mine, located in the Rondon Norte Plateau in the municipality of Rondon do Pará. Approximately 20 kg of sample was collected at a depth of 50 cm. Additionally, a commercial microsilica sample (MCR-1) (Ecopowder) and pellet NaOH (Sigma-Aldrich) were used to obtain the desired SiO_2/Al_2O_3 and Na/Al_2O_3 ratios for geopolymer synthesis.

2.2. Sample characterization

2.2.1. Mineralogical composition

The mineralogical phases of the sample were determined by X-ray diffraction (XRD) according to the powder method. A BRUKER diffractometer, model D2 PHASER, with a θ/θ goniometer, a radius of 141.1 nm, a copper anode with a characteristic emission line of 1.54 Å/8.047 keV (Cu-Kα1), and a maximum power of 300 W (30 kV × 10 mA) was used. A linear Lynxeye detector with a 5° 2θ aperture and 192 channels was used. The analyses were performed at the Laboratory of Mineralogy, Geochemistry and Applications (LAMIGA-UFPA, for its acronym in Portuguese) of the Institute of Geosciences of the Federal University of Pará (UFPA).

2.2.2. Chemical composition with XRF

The major chemical elements of the sample BTC-1 were determined by X-ray fluorescence (XRF) spectrometry through the preparation of a fused pellet. The pellet was prepared with a sample/flux ratio (lithium tetraborate) established according to the XRF79C_10 method. The analysis of the BTC-1 sample was performed in the Chemical Analysis Laboratory of SGS GEOSOL, located in Vespasiano, State of Minas Gerais, Brazil.

The chemical composition of the MCR-1 sample was determined by XRF using a PANalytical Axios Minerals sequential wavelength-dispersive spectrometer with a ceramic X-ray tube, a rhodium (Rh) anode, and maximum power of 2.4 kW. The samples were prepared on a casting dish with a sample flux ratio of 0.8 g/8 g. The flux used was lithium tetraborate. This procedure was performed by the Laboratory of Mineral Characterization (Laboratório de Caracterização Mineral - LCM) of the Institute of Geosciences of the Federal University of Pará.

The loss on ignition (LOI) for both samples was determined via the gravimetric method by calcinating previously dried samples at 1000 °C.

2.2.3. Reactive silica/usable alumina and kaolinite percentages

To determine the percentage of kaolinite present in the sample, the percentages of reactive silica and usable alumina were determined. These analyses were performed in the Chemical Analysis Laboratory of SGS GEOSOL according to its established method (**ICP05 V**). The method consisted of sample digestion in an alkaline medium (NaOH) under a controlled pressure and temperature (150 °C). The concentration of usable alumina was determined by inductively coupled plasma optical emission spectroscopy (ICP-OES). The solid phase, resulting from the stage of the sample digestion, was dissolved in an HCl solution. The concentration of reactive silica was also determined by ICP-OES.

The kaolinite percentage was quantified from the results of chemical analysis and reactive silica.

2.2.4. Particle size determination

The particle size in the BTC-01 sample was determined by laser diffraction with Analysette MicroTec Plus equipment (Fritsch, Germany). The procedure consisted of inserting an aliquot of the sample of interest, which was disaggregated and immersed in a solution of water and three drops of sodium pyrophosphate (10%).

2.2.5. FTIr

Fourier transform infrared spectroscopy (FTIR) analysis of the *in natura* samples and the calcined Belterra clay sample (BTC-1, BTC-1 650 °C and MCR-1) were used to complement the XRD results. For this purpose, pellets were made with approximately 0.0015 g of sample and 2 g of potassium bromide (KBr, Merck). The pellets were placed in steel disc molds with a diameter of 14 mm and pressed with a pressure of 8 Kbar in a Specac 8 manual press. The analyses were performed in a Vertex 70 from Bruker in the spectral range of 400–4000 cm^{-1}.

2.2.6. TG/DSc

Thermogravimetric and differential scanning calorimetry (TG/DSC) analyses were performed with a NETZSCH model STA 449 F5 Jupiter with a simultaneous thermal analyzer equipped with a vertical cylindrical oven, an N_2 flow rate of 50 ml/s, a heating rate of 10 °C/min, and a temperature range of 30 °C to 1100 °C.

2.3. Geopolymer formulation and characterization

2.3.1. Geopolymer preparation/synthesis

The BTC-1 sample was dried in an oven for 24 h at 105 °C to ensure the removal of natural moisture and then ground in a ball mill (Marconi MA 500/CF) at 365.4 rpm for 1 h. Then the BTC-1 sample was calcined at 650 °C for 2 h for complete dehydroxylation of kaolinite and its transformation into metakaolinite. This temperature was determined after observing the TG/DSC curves.

The NaOH solutions were prepared considering the molar ratios of Na/Al that were predefined in the design of the experiments. The volume of water used to prepare the solutions was set at 7.8 ml (approximately 34.5% of the sample mass) for all formulations planned in the experimental design (Table 2).

Geopolymer synthesis was performed by using the response surface methodology (RSM) based on a Box-Behnken design (BBD) (Table 1 and Table 2), with 12 experiments and five replicates at the central point of the variables to determine the best synthesis conditions based on the compressive strength. The independent variables were chosen according to the Taguchi model [22,23], which defines only four important parameters: temperature, Na_2O/Al_2O_3, SiO_2/Al_2O_3, and water percentage. The design was performed with three independent variables (temperature, Na2O/Al2O3, and SiO2/Al2O3) and a central point in two-level factorial designs (−1, 0, and +1) (Table 2). The water percentage was fixed at 34.8% (g/g). The compressive strength was selected as the dependent variable because the increase in this property is one of the most important indicators of the geopolymerization reaction. The BBD data were processed using Octave – 4.2.1 software and Microsoft Excel 2016.

Table 1

Independent variables with the actual and coded values used in the BBD.

Independent variable	Units	Notation	Levels		
			+1	0	−1
SiO_2/Al_2O_3	Molar ratio	X1	3.8	2.9	2.0
Na_2O/Al_2O_3	Molar ratio	X2	1.1	0.9	0.7
Temperature	°C	X3	100	80	60

Table 2

Conditions of geopolymer synthesis according to the BBD.

Experiments	Si/Al (X1)		Na/Al (X2)		Temperature (X3)	
	Coded	Real (molar ratio)	Coded	Real (molar ratio)	Coded	Real (°C)
1	−1	2	−1	0.7	0	80
2	1	3.8	−1	0.7	0	80
3	−1	2	1	1.1	0	80
4	1	3.8	1	1.1	0	80
5	−1	2	0	0.9	−1	60
6	1	3.8	0	0.9	−1	60
7	−1	2	0	0.9	1	100
8	1	3.8	0	0.9	1	100
9	0	2.9	−1	0.7	−1	60
10	0	2.9	1	1.1	−1	60
11	0	2.9	−1	0.7	1	100
12	0	2.9	1	1.1	1	100
13 (CP)	0	2.9	0	0.9	0	60

CP: central point.

Water absorption, apparent porosity, and bulk density tests were performed on all geopolymers synthesized in the BBD design as a complement to the technical properties.

Initially, established quantities of the BTC-1 and MCR-1 samples were weighed (15.2 g/5.4 g, 17.5 g/3.1 g, and 20.6 g/0 g) so that all formulations would have a weight of 20.6 g. The BTC-1/MCR-1 mass ratio was predetermined according to the desired SiO_2/Al_2O_3 ratio.

After the samples were mixed, the alkaline solution was added slowly, and the mixture was homogenized in a porcelain mortar for approximately 10 min. A geopolymer paste was then molded into steel molds shaped as prisms with dimensions of 50.0 mm × 20.0 mm × 10 mm, which underwent simple effect uniaxial pressing at a pressure of 50 kgf/cm^2 in a hydraulic press (Karl Kolb, model PW- 40). After being shaped, the specimens were sealed in plastic wrap (moisture control) and placed in an oven at 40 °C for 24 h. Then, the temperature was increased at a rate of 10 °C/h until the final temperatures established in the design (60 °C (curing for 72 h), 80 °C (curing for 48 h), and 100 °C (24 h)) were reached.

2.4. Geopolymer characterization

2.4.1. Water absorption

This parameter was evaluated according to an adaptation of the ASTM C20-00 (Reapproved 2010) [24] standard through the relationship between the dry and wet specimen weights. To obtain the wet weight, the ceramic specimens were immersed in water for at least 24 h. The wet weight was determined after removing the surface water from the specimen.

$$Aw = (Ms - Md)/Md \times 100(\%)$$

where

Aw is the percent water absorption;
Ms is the mass of the specimen saturated with water; and
Md is the mass of the dry specimen.

2.4.2. Apparent porosity

The apparent porosity of the specimens was determined according to the ASTM C20–00 (Reapproved 2010) [24] standard through the following equation:

$$Pa = (Ms - Md)/(Ms - Mi) \times 100(\%)$$

where

Pa is the percent apparent porosity;
Ms is the mass of the specimen saturated with water;
Md is the mass of the dry specimen; and
Mi is the mass (g) of the ceramic specimen immersed in water.

2.4.3. Compressive strength after curing/drying

The compressive strength of the specimens was tested using a universal testing machine, model 300/15 kN, with servo-plus evolution control from MSTEST, with a test speed of 01 MPa/s, a beginning load of 1 N, and an ending load of 30%. The test was performed in the Concrete Laboratory of the School of Architecture of UFPA.

2.4.4. Effect of water on the compressive strength

After the Aw test, the specimens were dried according to the curing methodology established for each experiment. Then, compressive strength tests were performed only for the five replicates of the central point, and the results were compared with the compressive strengths of the dry specimens. Analysis of variance (ANOVA) was used to determine if there was a difference between the compressive strength results of the dry specimens and the compressive strength results after the Aw test.

3. Results

3.1. Chemical and mineralogical compositions

3.1.1. Mineralogical results (XRD) of the BTC-1 sample

The mineralogical composition of the BTC-1 sample can be observed in Fig. 1. The sample consists of kaolinite, which is the predominant
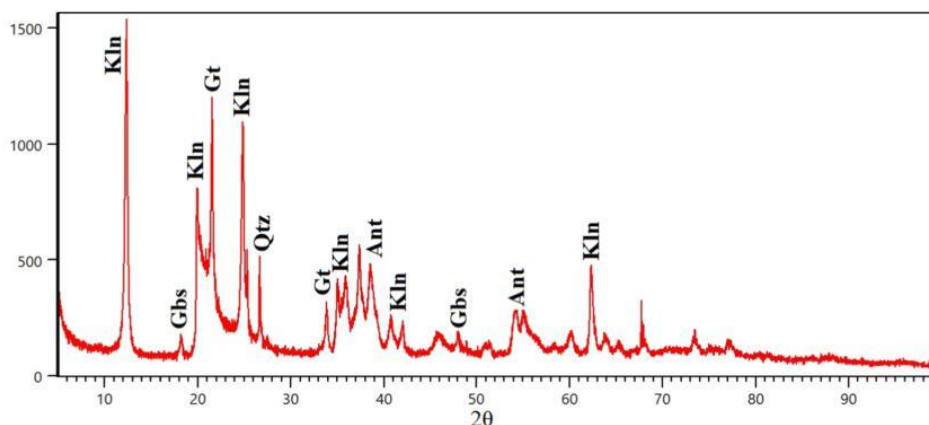
Fig. 1. XRD of the BTC-1 sample. Kaolinite (Kln), quartz (Qtz), goethite (Gt), and gibbsite (Gbs) are shown.
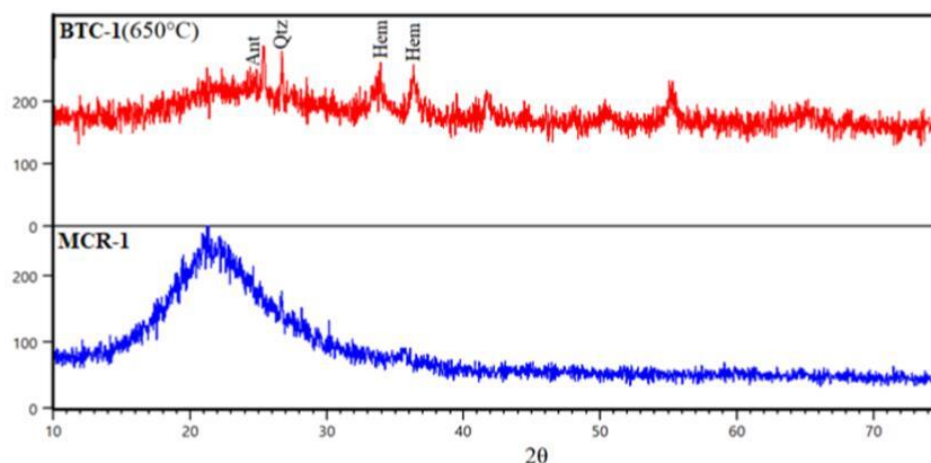
Fig. 2. Comparative mineralogy obtained by XRD: BTC-1 calcined at 650 °C and MCR-1.

mineral, in addition to gibbsite, quartz, goethite, and anatase in decreasing order of abundance (Fig. 2).

The predominance of kaolinite in the sample contributes to its application in geopolymer synthesis. Other minerals that are present in lower proportions can have some effect on geopolymer properties, such as the mechanism of the geopolymerization reaction (increasing or impairing its performance) [14,25–30].

Fig. 3. FTIR spectra of BTC-1 and MCR-1 *in natura* and BTC-1 calcined at 650 °C.

3.1.2. XRD of the BTC-1 sample calcined at 650 °C and the MCR-1 sample

The BTC-1 calcined at 650 °C is mainly composed of amorphous material, and the crystalline phases, which are present in small proportions, are represented by anatase, hematite, and quartz. Therefore, calcination of BTC-1 compared to its natural counterpart, leads to the complete destruction of kaolinite, the new formation of hematite at the expense of goethite, and the stabilization of anatase and quartz (beta quartz may be present). The accentuated background demonstrates the presence of amorphous compounds [31].

3.1.3. FTIR spectra of raw materials

The FTIR spectra of the in natura sample (Fig. 3) show bands in the regions of 3700, 3693, 3622, 3527, 3454, and 3394 cm^{-1} that are attributed to the axial deformation of the hydroxyl group [ν(OH)] of the mineral kaolinite [32–35]. The band at 1120 cm^{-1} is characteristic of the stretching of the bonds (Si, Al–O) [32]. In turn, the presence of the 914 cm^{-1} and 790 cm^{-1} bands is characteristic of the angular deformation and rotation of the Al–OH bond of the mineral gibbsite [34]. The band at 460 cm^{-1} can be attributed to the Si–O bonds of kaolinite. The axial deformation of the Si–O bond in the quartz can be observed by the presence of the 750 cm^{-1} band. These data reinforce the mineral analyses obtained by XRD.

The FTIR spectra of the 650 °C calcined BTC-1 and MCR-1 samples (Fig. 3) are typical of the metakaolinite/amorphous aluminum silicate phase and show a broad band at 3500 cm^{-1} that is attributed to the absorbed water, a band at 1100 cm^{-1} characteristic of the stretching of the Si–O bond of metakaolinite, and bands at 820 and 460 cm^{-1} that represent the Al–O and (Si, Al–O) bonds, respectively [19,36,37].

3.1.4. Chemical composition of the BTC-1 sample

The BTC-1 sample consists mainly of Al$_2$O$_3$ (34.9%), SiO$_2$ (36.3%), and Fe$_2$O$_3$ (12.2%) (Table 3). The percentage of reactive silica in the
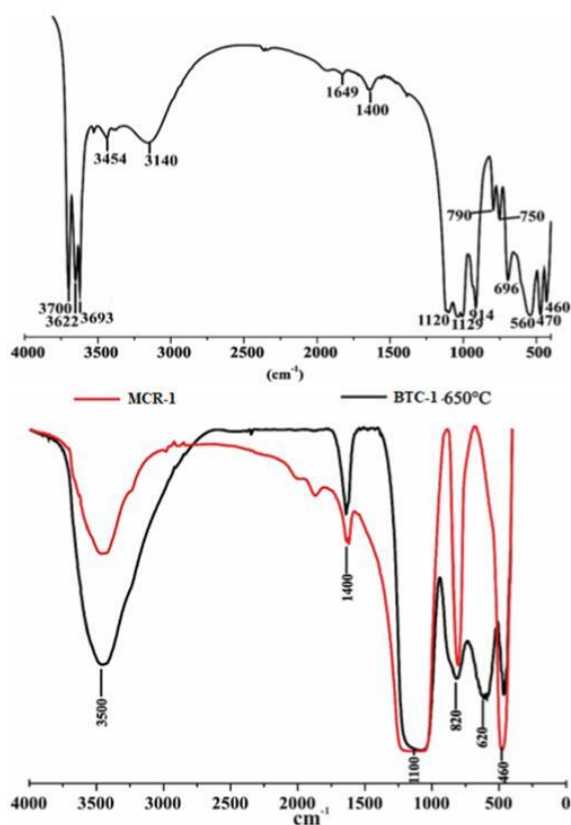
Table 3
Chemical composition (wt.%).

Composition	BTC-1 (%)	MCR-1 (%)
SiO$_2$	36.3	97.3
Al$_2$O$_3$	34.9	0.05
Fe$_2$O$_3$	12.2	0.05
LOI	14.74	0.69
Other	2.22	1.42
Total	100.36	99.51
SiO$_2$-Re	34.27	

SiO$_2$-Re: reactive silica.

Table 4
Conditions of geopolymer synthesis according to the BBD.

Exp. #	Coded variables				Response variable:
	X1 Si/Al	X2 Na/Al	X3 T	Molar Concentration	compressive strength (MPa)
1	−1	−1	0	12.46	31.09
2	1	−1	0	8.94	26.22
3	−1	1	0	19.48	24.71
4	1	1	0	14.37	36.56
5	−1	0	−1	15.65	7.05
6	1	0	−1	11.50	14.57
7	−1	0	1	15.65	36.08
8	1	0	1	11.50	45.82
9	0	−1	−1	10.86	23.66
10	0	1	−1	16.61	13.35
11	0	−1	1	10.86	32.52
12	0	1	1	16.61	46.78
13	0	0	0	13.73	36.97
14	0	0	0	13.73	35.84
15	0	0	0	13.73	41.98
16	0	0	0	13.73	40.11
17	0	0	0	13.73	40.10

Fig. 6. Water absorption and apparent porosity for all experiments.
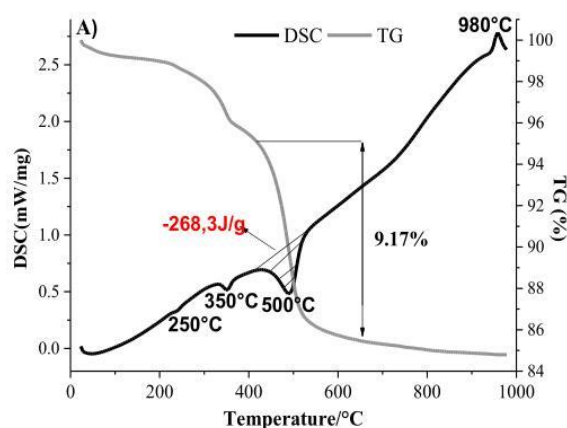
Fig. 4. DSC (Mw/mg)/TG (%) curves of the BTC-1 sample.
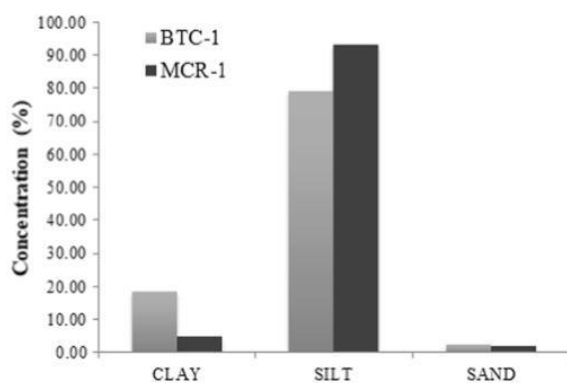
Fig. 5. Grain size composition of the samples.

sample is 34.27%. The MCR-1 sample displays a high SiO_2 content (97.3%), an amorphous silica compound, and 2.21% of other components.

The percentage of SiO_2-Re (reactive silica) allows us to indirectly calculate the percentage of kaolinite present in the sample and, therefore, the percentage of quartz: 73.62% of kaolinite and 2.37% of quartz.

Knowing the percentages of Al_2O_3 and SiO_2 belonging to kaolinite is the starting point for defining the Si/Al and Na/Al ratios used in the experimental design.

3.1.5. Thermal behavior of BTC-1

The Belterra Clay sample, BTC-1, exhibits three endothermic events and one exothermic event (Fig. 4). The first endothermic event (240–250 °C) is characteristic of the dehydroxylation of goethite; the second event at 350–360 °C refers to gibbsite dehydroxylation; the third and largest event at 500 °C confirms the dehydroxylation of kaolinite to form metakaolinite [38–40]; and finally, the only exothermic event at 980–985 °C reveals the formation of a new crystalline phase (mullite).

Based on the thermal behavior of the sample, a temperature of 650 °C is established for metakaolinite synthesis, considering that the dehydroxylation of the mineral kaolinite was complete at this temperature.

3.2. Physical characteristics

3.2.1. Particle size

The Belterra clay sample is mainly composed of a silt fraction (79%), followed by a clay fraction (18.66%) and a sand fraction of only 2.34% (Fig. 5). The MCR-1 sample has an even richer silt fraction (93.34%).

The particle size of the samples has a direct relationship with the surface area available for the aluminosilicate dissolution reaction

Table 5
ANOVA for the full model.

Source	SS	Degrees of freedom	Md	Model F	Tabulated F	R^2	Adjusted R^2
Model	2062.67	9	229.19	20.29	3.68	0.98	0.96
Error	79.08	7	11.30				
Total	2141.74	16	133.86				
Pure error	25.43	4	6.36	2.81	6.59		
Lack of fit	53.65	3	17.88				

[11,29,41], in which finer particles tend to be more rapidly dissolved than larger particles.

Despite the positive effect that finer particles have on the degree of dissolution of aluminosilicates, finer particles necessitate a meticulous curing/drying process (mentioned in the materials and methods section) to prevent the formation of cracks, which contribute to a loss of mechanical strength.

3.3. Geopolymer technical properties

3.3.1. Water absorption and apparent porosity

The water absorption (Aw) range for the experiments is between 12.9 and 19.86% (Fig. 6). All Aw values are below the maximum values (20 and 22%) established by the ABNT standards (2005a, 2005b) [42–44].

The large difference between the lowest Aw value (exp. 12; 12.9%) and the highest Aw value (exp. 6; 19.86%) may be due to the higher NaOH concentration (higher enthalpy of dissolution) and the higher final temperature in experiment 12, which may have affected the geopolymerization process and led to the formation of a more "hardened" geopolymer paste compared to the other pastes. Despite the difference between experiments 6 and 12, there is no considerable variation in Aw when the experiments are analyzed together. This similar behavior is due to the final curing/drying temperature, which does not reach values above 100 °C; thus, the temperature does not have a significant effect on Aw, as observed in studies that focus on higher curing temperatures [26].

The apparent porosity results are in the range of 0.73 to 1.23%. The low apparent porosity percentage presented by all experiments is mainly correlated with the water percentage used in the NaOH solution (34.5%), which contributes to the formation of a homogeneous and easily moldable geopolymer paste. The difference in particle size in the studied compositions and the force applied during the molding of the specimens affected the compaction of the grains in the specimens and inhibited the formation of voids (pores) [45].

Similar to the Aw results, temperature does not have a strong effect on the apparent porosity of the specimens. Temperature would have had a greater effect if curing had been performed at temperatures higher than 800 °C [26].

3.3.2. Mechanical compressive strength

3.3.2.1. Statistical parameters.
The mechanical compressive strength was >6.5 MPa for all of the compositions. These results are above the values established by the technical standards (ABNT, 2005a, 2005b) [42–44] for ceramic blocks (6.5 MPa) and roofing tiles (1.5 MPa).

Based on the BBD, the highest compressive strength value is 47.78 MPa, and the lowest compressive strength value is 7.05 MPa.

A value of 7.05 MPa was observed at the lowest temperature, the lowest Si/Al ratio, and an intermediate Na/Al ratio used in the experimental design, while a value of 47.78 MPa was displayed at the highest temperature, the highest Na/Al ratio, and an intermediate Si/Al ratio.

This behavior could indicate that an increase in temperature is favorable to the kinetics of the geopolymerization process, resulting in geopolymers with improved strength. Similar behaviors have been reported in the literature [46–50].

The enhancement in the compressive strength using 1.1Na/Al shows that the degree of reaction increases as Na/Al ratio increases. This conclusion is in line with findings in the literature [19]

Regression analysis is used to estimate the effect of the dependent variables on the mechanical strength results.

The table with the ANOVA data (Table 5) of the regression model (RM) shows that the model exhibits no lack of fit because the calculated F value (2.81)/tabulated F value (6.59) (Fig. 7) is less than 1. Other results that contribute to the assertion that the proposed model is statistically adequate are the high values of the correlation coefficients R^2 (explained variation) (0.98) and the adjusted R^2 (maximum explained variation) (0.96) (Fig. 8), which show that the proposed model fits the experimental values of mechanical strength.
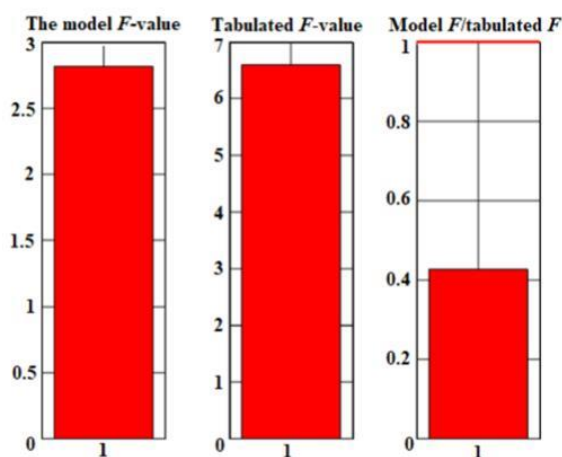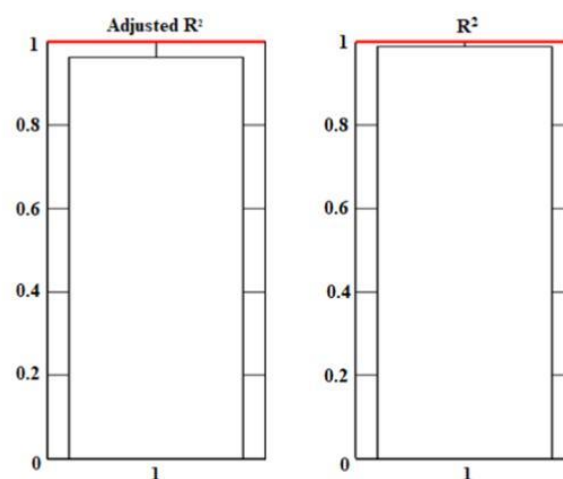

Fig. 7. Lack of fit.

Fig. 8. R^2 and adjusted R^2.
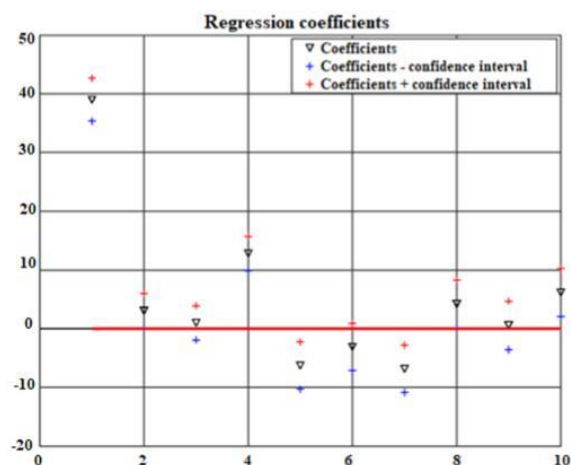
Fig. 9. Regression coefficients.

Fig. 10. Lack of fit.

Thus, the coefficients of the model are calculated based on the quadratic sum of the residuals 11.30 and a t value of 2.4469 with 95% confidence.

3.3.2.2. Coefficients of the RM (Regression Model). The coefficients of the model can be observed in Fig. 9. Ten coefficients are calculated: X0, X1, X2, X3, X1^2, X2^2, X3^2, (X1 × X2), (X1 × X3), and (X2 × X3). Considering the confidence interval for each coefficient, note that the coefficients X2 (Na/Al), X2^2, and (X1 × X3) ((Na/Al) × T) are not significant for the proposed model.

The Na/Al ratio (X2) alone does not directly affect the mechanical strength; however, this parameter affects the mechanical strength when combined with the other variables. Although the concentration of OH$^-$ (alkalinity of the medium) is an important factor for increasing the mechanical strength, the formation of high-strength geopolymers is favored by the presence of free SiO$_2$ from MCR-1 and by the curing temperature. This behavior is due to the silica in this sample reacting before the metakaolin silica [51–53] because the latter is not free.

3.3.2.3. New RM with only significant coefficients. The ANOVA table of the new RM can be seen in Table 6. Both the new model and the previous model exhibit no lack of fit, and the F calculated from the lack of fit is greater than the tabulated F (Fig. 10). The R^2 value (0.98) suggests that the regression equation is useful for determining the mechanical strength within the experimental range studied. This value suggests that 98% of the variations in mechanical strength are described through the independent variables.

The model coefficients are calculated based on the quadratic sum of the residuals 18.8023, and the t value = 2.2622 with 95% confidence.

3.3.2.4. Coefficients of the new RM. All the coefficients of the new model can be observed in Fig. 12. Six coefficients are calculated: X0, X1, X3, X1^2, X3^2, (X1 × X2), and (X2 × X3). In the new model, all the coefficients are significant. The relationship between the actual and predicted values of the model can be observed. The final equation of the
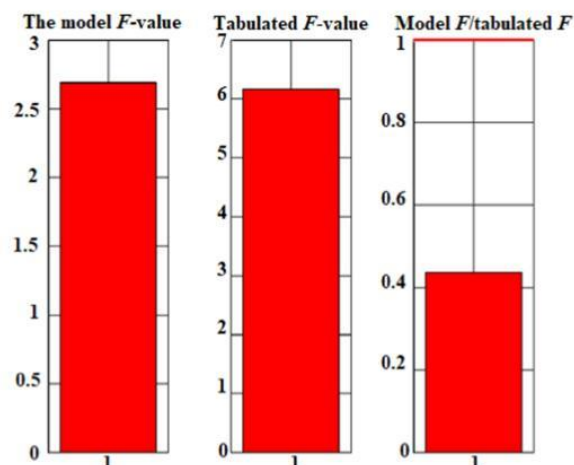
model is (Fig. 13).

Mechanical strength RM = 37.70 + 3.03X1 + 12.82X3 − 6.44X1^2 − 7.01X3^2 + 4.18X1 × X2 + 6.14X2xX3

3.3.2.5. Response surface and mechanical strength optimization. A three-dimensional surface plot of the response variable (mechanical strength) for the two experimental factors (Si/Al and Na/Al) and temperature fixed at the + 1 level (100 °C) is shown in Fig. 14. The surface shows the region of the experimental optimum (45 to 50 MPa) with Si/Al ratios between 3.4 and 4 and Na/Al ratios between 1.0 and 1.1.

Si/Al molar ratios between 3.4 and 3.8 and Na/Al molar ratios between 1.0 and 1.1 have already been demonstrated to be the ratios at
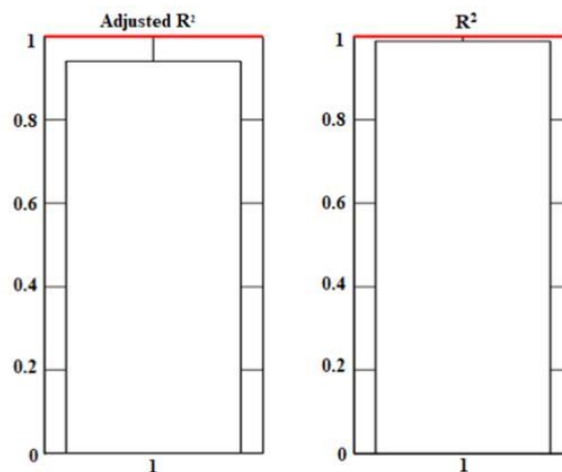
Fig. 11. R^2 and adjusted R^2.

Table 6
ANOVA for the recalculated model.

Source	SS	Degrees of freedom	Md	Model F	Tabulated F	R^2	Adjusted R^2
Model	2013.72	6.00	335.62	26.23	3.22	0.98	0.94
Error	128.02	10	12.80				
Total	2141.74	16	133.86	2.69	6.16		
Pure error	25.43	4	6.36				
Lack of fit	102.59	6	17.10				

which the geopolymers have the best mechanical properties [54–56].

3.3.2.6. Validation of the model. The optimal condition predicted by the response surface is tested. The experiment is performed with variable 1 at an Si/Al ratio of 3.4, variable 2 at an Na/Al ratio of 1.1, and variable 3 at 100 °C (Table 7). The experimental value found (47.489 ± 1.21) is very close to the value predicted by the response surface of ≅ 50 MPa (Fig. 11). This result contributes to the validation of the proposed model and indicates that the model has a good experimental fit.

The validation of the model leads to the conclusion that the studied material has desirable mechanical and structural properties for application in the construction industry and that these properties make it an ideal choice for this purpose [21].

3.3.2.7. Effect of water on compressive strength. The ANOVA and the results of the compressive strength (dry and after the Aw test) are shown in Table 7 and Table 8. The calculated F value is much lower than the tabulated F value, which implies acceptance of the null hypothesis: the mechanical strength of the "dry" specimens and that of the specimens
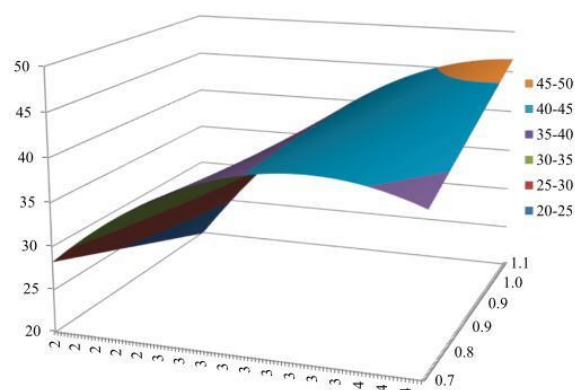
Fig. 14. Response surface plot of the compressive strength.

Table 7
Compressive strength of five replicates from central point experiments ("dry" and after immersion in water (Aw)).

Strength after Aw	Strength of "dry" specimens
42.23	36.97
36.29	35.84
40.64	41.98
40.92	40.11
35.06	40.10
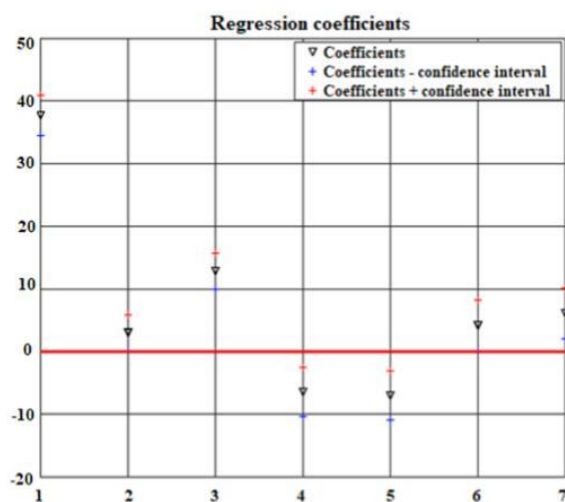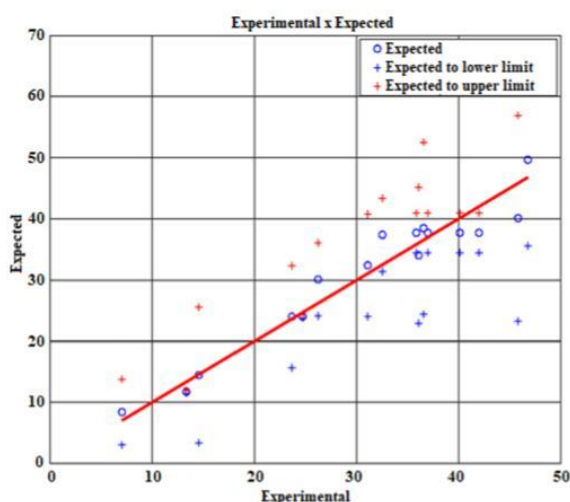
after Aw is statistically equal.

Immersion in water for 24 h does not affect the mechanical strength of the material, which shows that for this composition, there is no hydration of the Si–O–Si and Si–OH bonds that could weaken the geopolymer structure [26,57].

4. FTIR spectra of some geopolymers

Fig. 15 shows the IR spectra of compositions E-5, E12, E-CP, and BTC-1 (650 °C). A broad band observed in the range of 3300–3700 cm^{-1} is attributed to O–H stretching. The band at ~1600 cm^{-1} is attributed to the H–O–H bending vibration [58]. The band of BTC-1 (650 °C) at 1100 cm^{-1} shifted to a lower wavenumber (~980 cm^{-1}) in the geopolymers (E-5, E12, E-CP), indicating the formation of a geopolymer matrix (incorporation of Al in the geopolymer network) [59]. The higher intensity of this band, which indicated the lowest transmittance in the E-12 and E-CP compositions, was believed to contribute to a higher compressive strength (Table 4) [40]. The 820 cm^{-1} band in BTC-1 (650 °C) also shifted to a lower wavenumber (~717 cm^{-1}) in the geopolymers, which can be related to the tetrahedral groups AlO_4 and SiO_4 of the geopolymer matrix [19].

5. Conclusions

The predominance of kaolinite in Belterra Clay contributes to geopolymer synthesis and applications in low-temperature ceramic materials.

The best synthesis parameters were determined through BBD: 3.4–3.8Si/Al, 1–1.1Na/Al, and temperature of 100 °C.

The use of low temperatures for geopolymer synthesis contributes to an economic production process and can contribute to a reduction in CO_2 emissions.

The high strength exhibited by geopolymers means that they can be applied in cement/concrete to considerably reduce the CO_2 emissions of this sector, which is considered one of the world's largest CO_2 emitting agents.

Finally, the availability of Belterra Clay during bauxite mining and

Fig. 12. Regression coefficients.

Fig. 13. Expected values × experimental values.

Table 8
ANOVA for the replicates of compressive strength.

Source	SS	Degrees of freedom	Md	F	P value	Tabulated F
Between groups	0.0019331	1	0.0019331	0.000237365	0.988085	5.317655
Within the groups	65.15188425	8	8.14398553			
Total	65.15381735	9				
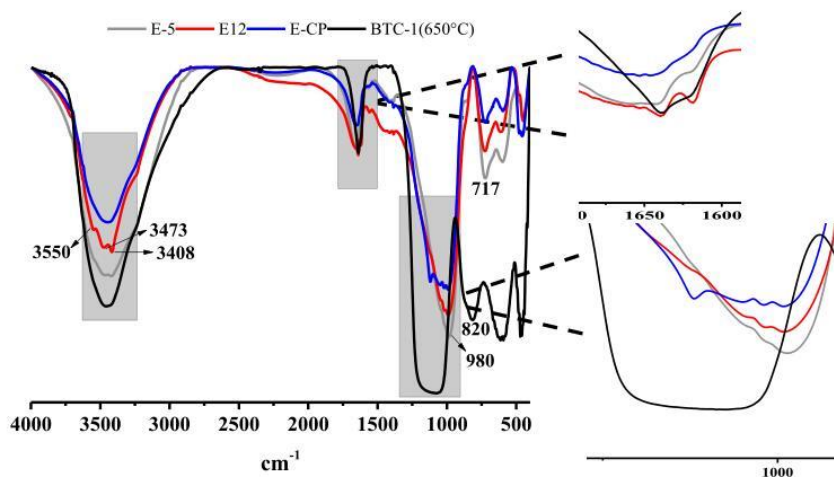
Fig. 15. IR spectra of compositions E-5, E12, E-CP, and BTC-1 (650 °C).

its technical characteristics, as presented in the study, indicate that this material is a positive alternative for the production of ceramic products and low-cost environmentally friendly cements/concretes.

CRediT authorship contribution statement

Igor Alexandre Rocha Barreto: Conceptualization, Methodology, Validation, Investigation, Formal analysis, Data curation, Writing - original draft, Writing - review & editing, Visualization. **Marcondes Lima da Costa:** Conceptualization, Methodology, Investigation, Writing - review & editing, Visualization, Funding acquisition, Project administration.

Declaration of Competing Interest

The authors declare that they have no known competing financial interests or personal relationships that could have appeared to influence the work reported in this paper.

References

[1] A.M.C. Horbe, M.L. da Costa, Lateritic crusts and related soils in eastern Brazilian Amazonia, Geoderma 126 (3-4) (2005) 225–239, https://doi.org/10.1016/j.geoderma.2004.09.011.

[2] I.A.R. Barreto, M.L. da Costa, Sintering of red ceramics from yellow Amazonian latosols incorporated with illitic and gibbsitic clay, Appl. Clay Sci. 152 (2018) 124–130, https://doi.org/10.1016/j.clay.2017.11.003.

[3] I.A.R. Barreto Marcondes Lima da Costa, Viability of Belterra clay, a widespread bauxite cover in the Amazon, as a low-cost raw material for the production of red ceramics Appl. Clay Sci. 162 2018 252 260 https:// doi.org/10.1016/j.clay.2018.06.010.

[4] L.B.A. Negrão, M.L. da Costa, H. Pöllmann, The belterra clay on the bauxite deposits of Rondon do Pará, Eastern Amazon, Brazilian Journal of Geology. 48 (2018) 473–484, https://doi.org/10.1590/2317–4889201820180128.

[5] L.B.A. Negrão, H. Pöllmann, M.L.d. Costa, Production of low-CO2 cements using abundant bauxite overburden "Belterra Clay", Sustainable Mater.Technol. 29 (2021) e00299, https://doi.org/10.1016/j.susmat.2021.e00299.

[6] Z. Zhang, H. Wang, J.L. Provis, F. Bullen, A. Reid, Y. Zhu, Quantitative kinetic and structural analysis of geopolymers. Part 1. the activation of metakaolin with sodium hydroxide, Thermochim Acta 539 (2012) 23–33, https://doi.org/10.1016/j.tca.2012.03.021.

[7] Y.M. Liew, C.Y. Heah, A.B. Mohd Mustafa, H. Kamarudin, Structure and properties of clay-based geopolymer cements: a review, Prog. Mater Sci. 83 (2016) 595–629, https://doi.org/10.1016/j.pmatsci.2016.08.002.

[8] M. Glid, I. Sobrados, H.B. Rhaiem, J. Sanz, A.B.H. Amara, Alkaline activation of metakaolinite-silica mixtures: role of dissolved silica concentration on the formation of geopolymers, Ceramics International. 43 (15) (2017) 12641–12650, https://doi.org/10.1016/j.ceramint.2017.06.144.

[9] T.R. Barbosa, E.L. Foletto, G.L. Dotto, S.L. Jahn, Preparation of mesoporous geopolymer using metakaolin and rice husk ash as synthesis precursors and its use as potential adsorbent to remove organic dye from aqueous solutions, Ceram. Int. 44 (1) (2018) 416–423, https://doi.org/10.1016/j.ceramint.2017.09.193.

[10] C. Ma, B. Zhao, S. Guo, G. Long, Y. Xie, Properties and characterization of green one-part geopolymer activated by composite activators, J. Cleaner Prod. 220 (2019) 188–199, https://doi.org/10.1016/j.jclepro.2019.02.159.

[11] M.H. Samarakoon, P.G. Ranjith, T.D. Rathnaweera, M.S.A. Perera, Recent advances in alkaline cement binders: a review, J. Cleaner Prod. 227 (2019) 70–87, https://doi.org/10.1016/j.jclepro.2019.04.103.

[12] P. Rożek, M. Król, W. Mozgawa, Geopolymer-zeolite composites: a review, J. Cleaner Prod. 230 (2019) 557–579, https://doi.org/10.1016/j.jclepro.2019.05.152.

[13] B. Singh, G. Ishwarya, M. Gupta, S.K. Bhattacharyya, Geopolymer concrete: a review of some recent developments, Constr. Build. Mater. 85 (2015) 78–90, https://doi.org/10.1016/j.conbuildmat.2015.03.036.

[14] A.A. Siyal, K.A. Azizli, Z. Man, L. Ismail, M.I. Khan, Geopolymerization kinetics of fly ash based geopolymers using JMAK model, Ceram. Int. 42 (14) (2016) 15575–15584, https://doi.org/10.1016/j.ceramint.2016.07.006.

[15] J. Davidovits, Geopolymers, J. Therm. Anal. 37 (8) (1991) 1633–1656, https://doi.org/10.1007/BF01912193.

[16] S. Selmani, A. Sdiri, S. Bouaziz, S. Rossignol, Geopolymers based on calcined tunisian clays: effects of alkaline solution on vibrational spectra and mechanical properties, Int. J. Miner. Process. 165 (2017) 50–57, https://doi.org/10.1016/j.minpro.2017.05.012.

[17] S. Selmani, A. Sdiri, S. Bouaziz, E. Joussein, S. Rossignol, Effects of metakaolin addition on geopolymer prepared from natural kaolinitic clay, Appl. Clay Sci. 146 (2017) 457–467, https://doi.org/10.1016/j.clay.2017.06.019.

[18] H.Y. Zhang, J.C. Liu, B.o. Wu, Mechanical properties and reaction mechanism of one-part geopolymer mortars, Constr. Build. Mater. 273 (2021) 121973, https://doi.org/10.1016/j.conbuildmat.2020.121973.

[19] N.g. Hui-Teng, H. Cheng-Yong, L. Yun-Ming, M.M.A.B. Abdullah, K. Ern Hun, H. M. Razi, N.g. Yong-Sing, Formulation, mechanical properties and phase analysis of fly ash geopolymer with ladle furnace slag replacement, J. Mater. Res. Technol. 12 (2021) 1212–1226, https://doi.org/10.1016/j.jmrt.2021.03.065.

[20] B.C. McLellan, R.P. Williams, J. Lay, A. van Riessen, G.D. Corder, Costs and carbon emissions for geopolymer pastes in comparison to ordinary portland cement, J. Cleaner Prod. 19 (9–10) (2011) 1080–1090, https://doi.org/10.1016/j.jclepro.2011.02.010.

[21] A. Hassan, M. Arif, M. Shariq, Use of geopolymer concrete for a cleaner and sustainable environment – a review of mechanical properties and microstructure, J. Cleaner Prod. 223 (2019) 704–728, https://doi.org/10.1016/j.jclepro.2019.03.051.

[22] M. Olivia, H. Nikraz, Properties of fly ash geopolymer concrete designed by Taguchi method, Mater. Des. 36 (2012) 191–198, https://doi.org/10.1016/j.matdes.2011.10.036.

[23] A. Nazari, Compressive strength of geopolymers produced by ordinary portland cement: application of genetic programming for design, Mater. Des. 43 (2013) 356–366, https://doi.org/10.1016/j.matdes.2012.07.012.

[24] ASTM, C20–00, Standard test methods for apparent porosity, water absorption, apparent specific gravity, and bulk density of burned refractory brick and shapes by boiling water, American Society for Testing and Materials. 00 (2015) 1–3, https://doi.org/10.1520/C0020–00R10.2.

[25] T. Phoo-Ngernkham, A. Maegawa, N. Mishima, S. Hatanaka, P. Chindaprasirt, Effects of sodium hydroxide and sodium silicate solutions on compressive and shear bond strengths of FA-GBFS geopolymer, Constr. Build. Mater. 91 (2015) 1–8, https://doi.org/10.1016/j.conbuildmat.2015.05.001.

[26] P.N. Lemougna, K. tuo Wang, Q. Tang, X. min Cui, Synthesis and characterization of low temperature (<800 °C) ceramics from red mud geopolymer precursor, Constr. Build. Mater. 131 (2017) 564–573. https://doi.org/10.1016/j.conbuildmat.2016.11.108.

[27] N. Belmokhtar, M. Ammari, J. Brigui, L. Ben allal, Comparison of the microstructure and the compressive strength of two geopolymers derived from Metakaolin and an industrial sludge, Constr. Build. Mater. 146 (2017) 621–629, https://doi.org/10.1016/j.conbuildmat.2017.04.127.

[28] E. Kamseu, L.M. Beleuk à Moungam, M. Cannio, N. Billong, D. Chaysuwan, U. C. Melo, C. Leonelli, Substitution of sodium silicate with rice husk ash-NaOH solution in metakaolin based geopolymer cement concerning reduction in global warming, J. Cleaner Prod. 142 (2017) 3050–3060, https://doi.org/10.1016/j.jclepro.2016.10.164.

[29] A. Hajimohammadi, T. Ngo, A. Kashani, Glass waste versus sand as aggregates: the characteristics of the evolving geopolymer binders, J. Cleaner Prod. 193 (2018) 593–603, https://doi.org/10.1016/j.jclepro.2018.05.086.

[30] N. Koshy, K. Dondrob, L. Hu, Q. Wen, J.N. Meegoda, Synthesis and characterization of geopolymers derived from coal gangue, fly ash and red mud, Constr. Build. Mater. 206 (2019) 287–296, https://doi.org/10.1016/j.conbuildmat.2019.02.076.

[31] S.F.S. Rodrigues, M.L. da Costa, H. Pöllmann, D.C. Kern, M.I. da Silveira, R. Kipnis, Pre-historic production of ceramics in the amazon: provenience, raw materials, and firing temperatures, Appl. Clay Sci. 107 (2015) 145–155, https://doi.org/10.1016/j.clay.2015.01.016.

[32] J.A. Mbey, F. Thomas, C.J. Ngally Sabouang, Liboum, D. Njopwouo, An insight on the weakening of the interlayer bonds in a Cameroonian kaolinite through DMSO intercalation, Appl. Clay Sci. 83–84 (2013) 327–335, https://doi.org/10.1016/j.clay.2013.08.010.

[33] V.C. Farmer, Transverse and longitudinal crystal modes associated with OH stretching vibrations in single crystals of kaolinite and dickite, 56 (2000) 927–930.

[34] H.T. Roudouane, J.A. Mbey, E.C. Bayiga, P.D. Ndjigui, Characterization and application tests of kaolinite clays from Aboudeia (southeastern Chad) in fired bricks making, Scientific African. 7 (2020) e00294, https://doi.org/10.1016/j.sciaf.2020.e00294.

[35] M.A. Qtaitat, I.N. Al-Trawneh, Characterization of kaolinite of the Baten El-Ghoul region/south Jordan by infrared spectroscopy, Spectrochimica Acta - Part A: Molecular and Biomolecular Spectroscopy. 61 (2005) 1519–1523, https://doi.org/10.1016/j.saa.2004.11.008.

[36] P. Baran, M. Nazarko, E. Włosińska, A. Kanciruk, K. Zarębska, Synthesis of geopolymers derived from fly ash with an addition of perlite, J. Cleaner Prod. 293 (2021) 126112, https://doi.org/10.1016/j.jclepro.2021.126112.

[37] Z. Li, S. Zhang, Y. Zuo, W. Chen, G. Ye, Chemical deformation of metakaolin based geopolymer, Cem. Concr. Res. 120 (2019) 108–118, https://doi.org/10.1016/j.cemconres.2019.03.017.

[38] B. Caglar, B. Afsin, A. Tabak, Benzamide species retained by DMSO composites at a kaolinite surface, J. Therm. Anal. Calorim. 87 (2) (2007) 429–432, https://doi.org/10.1007/s10973–005–7472–3.

[39] S.A. Drweesh, N.A. Fathy, M.A. Wahba, A.A. Hanna, A.I.M. Akarish, E.A. M. Elzahany, I.Y. El-Sherif, K.S. Abou-El-Sherbini, Equilibrium, kinetic and thermodynamic studies of Pb(II) adsorption from aqueous solutions on HCl-treated Egyptian kaolin, J. Environ. Chem. Eng. 4 (2) (2016) 1674–1684, https://doi.org/10.1016/j.jece:2016.02.005.

[40] M. Issaoui, L. Limousy, B. Lebeau, J. Bouazizi, M. Fourati, Design and characterization of flat membrane supports elaborated from kaolin and aluminum powders, C. R. Chim. 19 (4) (2016) 496–504, https://doi.org/10.1016/j.crci.2015.10.011.

[41] W. Hu, Q. Nie, B. Huang, X. Shu, Q. He, Mechanical and microstructural characterization of geopolymers derived from red mud and fly ashes, J. Cleaner Prod. 186 (2018) 799–806, https://doi.org/10.1016/j.jclepro.2018.03.086.

[42] ANBT, NBR 15270–1: Componentes cerâmicos. Parte 1: Blocos cerâmicos para alvenaria de vedação - Terminologia e requisitos, Associação Brasileira de Normas Técnicas. (2005) 15.

[43] ABNT Associação Brasileira de Normas Técnicas, Alvenaria estrutural - Blocos cerâmicos Parte 3 Métodos de ensaio 09/08 2017 34 https://www.abntcolecao.com.br/unisinos/pdfview/viewer.aspx?Q=AC344710F7027AC9CEC0C45 89CEB1C7F8FE99DE63B82A59E15FE5D2B69B57C5F.

[44] ABNT, NBR 15270-2: Componentes cerâmicos Parte 2: Blocos cerâmicos para alvenaria estrutural – Terminologia e requisitos, Associação Brasileira de Normas Técnicas. (2017) 15.

[45] B. Panda, G.B. Singh, C. Unluer, M.J. Tan, Synthesis and characterization of one-part geopolymers for extrusion based 3D concrete printing, J. Cleaner Prod. 220 (2019) 610–619, https://doi.org/10.1016/j.jclepro.2019.02.185.

[46] F. Colangelo, G. Roviello, L. Ricciotti, V. Ferrández-Mas, F. Messina, C. Ferone, O. Tarallo, R. Cioffi, C.R. Cheeseman, Mechanical and thermal properties of lightweight geopolymer composites, Cem. Concr. Compos. 86 (2018) 266–272, https://doi.org/10.1016/j.cemconcomp.2017.11.016.

[47] S.K. John, Y. Nadir, K. Girija, Effect of source materials, additives on the mechanical properties and durability of fly ash and fly ash-slag geopolymer mortar: a review, Constr. Build. Mater. 280 (2021) 122443, https://doi.org/10.1016/j.conbuildmat.2021.122443.

[48] M.H. Al-Majidi, A. Lampropoulos, A. Cundy, S. Meikle, Development of geopolymer mortar under ambient temperature for in situ applications, Constr. Build. Mater. 120 (2016) 198–211, https://doi.org/10.1016/j.conbuildmat.2016.05.085.

[49] H.T.B.M. Petrus, F.I. Fairuz, N. Sa'dan, M. Olvianas, W. Astuti, S.N.A. Jenie, F. A. Setiawan, F. Anggara, J.J. Ekaputri, I.M. Bendiyasa, Green geopolymer cement with dry activator from geothermal sludge and sodium hydroxide, J. Cleaner Prod. 293 (2021) 126143, https://doi.org/10.1016/j.jclepro.2021.126143.

[50] O. Ayeni, A.P. Onwualu, E. Boakye, Characterization and mechanical performance of metakaolin-based geopolymer for sustainable building applications, Constr. Build. Mater. 272 (2021) 121938, https://doi.org/10.1016/j.conbuildmat.2020.121938.

[51] K. Sagoe-Crentsil, L. Weng, Dissolution processes, hydrolysis and condensation reactions during geopolymer synthesis: Part IIHigh Si/Al ratio systems, J. Mater. Sci. 42 (9) (2007) 3007–3014, https://doi.org/10.1007/s10853–006–0818–9.

[52] J.G.S. Van Jaarsveld, J.S.J. Van Deventer, Effect of metal contaminants on the formation and properties of waste-based geopolymers, Cem. Concr. Res. 29 (1999) 1189–1200, https://doi.org/10.1016/S0008–8846(99)00032–0.

[53] M.L. Granizo, M.T. Blanco-Varela, S. Martínez-Ramírez, Alkali activation of metakaolins: parameters affecting mechanical, structural and microstructural properties, J. Mater. Sci. 42 (9) (2007) 2934–2943, https://doi.org/10.1007/s10853–006–0461–x.

[54] J.L. Provis, J.S.J. van Deventer, Geopolymerisation kinetics. 1. In situ energy-dispersive X-ray diffractometry, Chem. Eng. Sci. 62 (9) (2007) 2309–2317, https://doi.org/10.1016/j.ces.2007.01.027.

[55] P.D. Silva, K. Sagoe-Crentsil, V. Sirivivatnanon, Kinetics of geopolymerization: role of Al2O3 and SiO2, Cem. Concr. Res. 37 (4) (2007) 512–518, https://doi.org/10.1016/j.cemconres.2007.01.003.

[56] D. Khale, R. Chaudhary, Mechanism of geopolymerization and factors influencing its development: a review, J. Mater. Sci. 42 (3) (2007) 729–746, https://doi.org/10.1007/s10853–006–0401–x.

[57] P.N. Lemougna, U.F. Chinje Melo, M.P. Delplancke, H. Rahier, Influence of the chemical and mineralogical composition on the reactivity of volcanic ashes during alkali activation, Ceram. Int. 40 (1) (2014) 811–820, https://doi.org/10.1016/j.ceramint.2013.06.072.

[58] G. Ishwarya, B. Singh, S. Deshwal, S.K. Bhattacharyya, Effect of sodium carbonate/sodium silicate activator on the rheology, geopolymerization and strength of fly ash/slag geopolymer pastes, Cem. Concr. Compos. 97 (2019) 226–238, https://doi.org/10.1016/j.cemconcomp.2018.12.007.

[59] A. Nikolov, H. Nugteren, I. Rostovsky, Optimization of geopolymers based on natural zeolite clinoptilolite by calcination and use of aluminate activators, Constr. Build. Mater. 243 (2020) 118257, https://doi.org/10.1016/j.conbuildmat.2020.118257.

4.2 SYNTHESIS OF GEOPOLYMER WITH KOH BY TWO KAOLINITIC CLAYS FROM THE AMAZON: INFLUENCE OF DIFFERENT SYNTHESIS PARAMETERS ON THE COMPRESSIVE STRENGTH

Igor Alexandre Rocha Barreto[1]; Marcondes Lima da Costa[2]

[1]Program for Post-graduation in Geology and Geochemistry, Institute of Geosciences, UFPA, Belém (PA), Brazil. E-mail: igorrochaq@gmail.com, igor.barreto@icen.ufpa.br;
[2]Program for Post-graduation in Geology and Geochemistry, Institute of Geosciences, Federal University of Pará – UFPA, Brazil. E-mails: mlc@ufpa.br, marcondeslc@gmail.com.

HIGHLIGHTS

- The studied samples show different degree of disorder in the kaolinite mineral

- The curing temperature was the most important parameter that contributed to the development of strength in the geopolymers

- Mechanical strength of up to 64.38MPa was obtained by geopolymers.

- The clay with the simplest accessory mineralogy exhibited the best mechanical strength results.

ABSTRACT

The term geopolymer refers to "inorganic polymers" formed by a chemical reaction between solid aluminosilicate compounds and a highly concentrated alkaline hydroxide solution. The properties of geopolymers mostly result from the chemical and mineralogical composition of the material used as a source of aluminosilicates. Considering the influence of the starting material for the synthesis of geopolymers, the present study evaluates the use of two different types of kaolin in the synthesis of geopolymers using KOH as an alkaline activator. For the present study, a sample of Belterra clay (KLN-1) from the bauxite deposits of Rondon do Pará, a sample of processed kaolin (KLN-2), and microsilica (MCR-1) (Ecopower) and PA reagent from Sigma (KOH) were selected. The samples were characterized by X-ray diffraction (XRD), X-ray fluorescence (XRF), thermogravimetric analysis (TGA), differential scanning calorimetry (DSC) and Fourier transform infrared (FTIR) spectroscopy. For the synthesis of the geopolymers, the KLN-1 and KLN-2 samples were calcined at 750 °C for 2 h. The syntheses of the geopolymers were performed at different KOH molar concentrations (12, 13, 14, 15 and 16), at different curing temperatures (60, 70, 80, 90 and 100 °C) and for different curing times (24, 48, 72, 96, and 120 h). The geopolymers were characterized by mechanical strength testing and FTIR. The samples had different mineralogical compositions, which contributed to different compressive strength results. The samples showed greater resistance at concentrations of 12 and 16 M. The curing temperature of 80 °C exhibited better mechanical compressive strength. At 120 h, the best compressive strength value was obtained, indicating that a longer time favored the geopolymerization reaction. The best compressive strength results were obtained in the sample with the lowest amount of "impurities" (KLN-2). This result allows us to conclude that the accessory minerals present in the KLN-1 sample may have interfered with the mechanism of the geopolymerization reaction.

Keywords: kaolinite**,** metakaolin, structural disorder, compressive strength.

1 INTRODUCTION

Geopolymers are a class of amorphous inorganic materials: "inorganic polymers" that are formed from a hydration reaction of aluminosilicates with high alkalinity (Adjei et al., 2022; Al-Majidi et al., 2016; Davidovits, 1991b; Singh et al., 2015c; Siyal et al., 2016). The geopolymer formation reaction is quite complex, but the basic principle has already been well established. The reaction consists of the dissolution of aluminum and silica (present in the material used as a source of aluminosilicates) in contact with a highly alkaline solution, forming oligomers that undergo polycondensation to form three-dimensional structures, specifically, polysialate ($-Si-O-Al-O)_n$ and polysialate-siloxo ($-Si-O-Al-O-Si-O)_n$ (Davidovits, 1991b; John et al., 2021). In addition to the term geopolymer, this type of material is described in the literature by other names: alkaline activated cement, alkaline ceramic (due to its high stability), geocement, and inorganic polymer concrete, among other alkaline materials (Singh et al., 2015).

Research on this type of material continues to grow in the scientific community. Studies have shown that its applicability can be quite diverse: traditional cement (Yunsheng et al., 2010b) concrete (Alnahhal et al., 2022; Phoo-Ngernkham et al., 2015), red ceramic (Lemougna et al., 2017; Barreto et al., 2021), porous block for civil construction (Prud'homme et al., 2011), and material for preservation of old ceramic tiles (Moutinho et al., 2019).

The application of a geopolymer depends on its final properties. These properties are directly influenced by the choice of the main raw material (aluminosilicate source) used in their synthesis. The chemical and mineralogical composition of the raw material determines the technological properties of the final product (John et al., 2021).

Several materials have already been used as geopolymer precursors. These materials vary from natural materials, such as clays, sediments and rocks (Dupuy et al., 2019; Kaze et al., 2021); to materials from industrial processes, such as red mud, fly ash, and waste from the glass industry (Hajimohammadi et al., 2018a; Lemougna et al., 2017); to materials synthesized in laboratories, such as zeolites and synthetic Al_2O_3 and SiO_2 (Król & Mozgawa, 2019).

Of the various sources of aluminosilicates, clays have been the main natural source for the synthesis of geopolymers. Kaolinite, calcined at temperatures between 600-800 °C (metakaolinite), is the most widely used starting material in the synthesis of geopolymers (Autef et al., 2013; Barbosa et al., 2018; Glid et al., 2017b; Kaze et al., 2021;

Perná et al., 2019; Yunsheng et al., 2010a; Z. Zhang et al., 2012a). The benefits of using clays as a source of aluminosilicates in the synthesis of geopolymers are undeniable; however, these materials are rarely made only of clay minerals, and "impurities" are almost always found in clays; despite the consensus that these impurities can influence the final product, it is not known which properties each compound or element may influence. The "impurities" most found in these types of materials include organic matter, iron minerals, mainly hematite (Fe_2O_3) and goethite ($FeO(OH)$, gibbsite ($Al(OH)_3$), dolomite ($CaMg(CO_3)_2$), feldspars, quartz, and micaceous minerals.

Based on the above, the aim of the present study is to evaluate the performance of 2 different samples in the synthesis of geopolymers using KOH as an alkaline activator. One sample is composed of almost 100% kaolinite (processed kaolin), and another sample is composed of 76% kaolinite and approximately 24% other accessory minerals (yellow latosol).

2 MATERIALS AND METHODS

2.1 RAW MATERIAL

For the development of the study, two distinct samples of kaolinitic clays were used. The first sample consists of a representative sample of Belterra clay (KLN-1), collected 50 cm from the top of a bauxite pilot mine called Branco. The mine is located on the Rondon Norte Plateau in the municipality of Rondon do Pará-Pará. The second sample used in the study was a sample of processed kaolin from the company Imerys (KLN-2). Additionally, a commercial microsilica sample (MCR-1) (Ecopower) was used to achieve a Si/Al ratio of 3.4, as defined in the present study.

2.2 SAMPLE CHARACTERIZATION

2.2.1 Mineralogical identification

The identification of the mineralogical phases of the *in natura* and calcined samples was performed through powder X-ray diffraction (XRD) with a BRUKER diffractometer, model D2 PHASER, with a θ/θ goniometer, radius: 141.1 nm, angle range of 0-70°, step de 0.01°, timer step per step 1s copper anode with characteristic emission line of 1.54 Å/8.047 keV (Cu-Kα1), and maximum power of 300 W (30 kV x 10 mA). The detector used in this equipment was a Linear Lynxeye with a 5° 2θ aperture and 192

channels. The analyses were performed at the Laboratory of Mineralogy, Geochemistry and Applications (LAMIGA) of the Institute of Geosciences of the Federal University of Pará (UFPA).

2.2.2 Chemical analysis (XRF)

The chemical analyses of the Belterra clay samples were performed by X-ray fluorescence spectrometry (XRF) on fused pellets. The tablets were prepared with a sample/flux ratio (lithium tetraborate) established according to the XRF79C_10 method. The analyses were performed in the chemical analysis laboratory of the company SGS GEOSOL, located in Vespasiano/MG.

The loss on ignition (LOI) of all samples was determined by the gravimetric method by calcination at 1000 °C from previously dried samples.

2.2.3 Determination of the reactive silica and available alumina

The determination of the reactive silica and available alumina was performed in the chemical analysis laboratory of the company SGS GEOSOL according to a method established by the company (ICP05V) that consists of the dissolution of the sample in concentrated NaOH solution in a system with pressure and temperature (150 °C) control. From the obtained solution, the usable aluminum concentration was determined with inductively coupled plasma optical emission spectroscopy (ICP–OES). The solid phase, resulting from the dissolution stage, was dissolved in HCl solution, which allowed the determination of the percentage of reactive silica by ICP–OES.

2.2.5 Granulometric analysis

The particle size analysis was performed after grinding and sieving with size 60 mesh to reproduce the particle size of the samples during the synthesis of the geopolymers. For this purpose, the laser diffraction technique was applied through an Analysette Microtec Plus (Fritsch, Germany). The procedure consisted of inserting an aliquot of the ground sample of interest in a solution of water and three drops of sodium pyrophosphate (10%). This procedure was performed at the LAMIGA of the Institute of Geosciences of UFPA.

2.2.6 Characterization by FTIR

Fourier transform infrared (FTIR) spectroscopy was used to complement the results obtained by XRD. The analyses were performed using approximately 0.0015 g of sample mixed and homogenized with 2 g potassium bromide (KBr, Merck). Then, pellets were formed in steel molds in the form of discs 14 mm in diameter and pressed under a pressure of 8 kbar in a Specac 8 manual press. The analyses were performed in a Vertex 70 instrument from Bruker in the spectral range of 400-4000 cm^{-1}. This procedure was performed at the LAMIGA of the Institute of Geosciences of UFPA.

2.2.8 Evaluation of the materials with TGA/DSC

Thermogravimetric analysis (TGA)/differential scanning calorimetry (DSC) can be used to understand the thermal behavior and the possible reactions that occur during the process of heating samples. The analyses of the samples were performed with a NETZSCH model STA 449 F5 Jupiter, with a simultaneous thermal analyzer equipped with a vertical cylindrical oven and N2 flow of 50 ml/s at a heating rate of 10 °C/min and a temperature range of 30 °C to 1100 °C. This procedure was performed at the LAMIGA of the Institute of Geosciences of UFPA.

2.3 FORMULATION AND CHARACTERIZATION OF GEOPOLYMERS

2.3.1 Sample preparation

The raw materials were dried in an oven for 24 h at 110 °C to remove the natural moisture. Then, the samples were ground in a ball mill (Marconi MA 500/CF) with a rotation of 365.4 rpm for a period of 1 h. Sieving was performed on the product obtained from the grinding with a 60-mesh aperture to remove the coarse sand fraction.

The fraction obtained smaller than the size 60 mesh was calcined at 750 °C for two hours for the complete dehydroxylation of kaolinite and its transformation into metakaolinite, a source of amorphous aluminosilicate for the synthesis of geopolymers.

2.3.2 Conditions for the synthesis of geopolymers

The synthesis conditions of the geopolymers were established to evaluate the influence of the molar concentration, temperature and curing time on the mechanical strength of the geopolymers. The Si/Al molar ratio and the water volume were kept constant in all syntheses, with 3.4 Si/Al and 7.2 ml of H_2O. To evaluate the influence of the molar concentration, KOH solutions were prepared at concentrations of 12, 13, 14, 15 and 16 M, with a final curing temperature of 70 °C and curing time of 24 h. The temperature was evaluated under fixed conditions of KOH molar concentration (16 M), with a curing time of 24 h and final temperatures of 60, 70, 80, 90 and 100 °C. The influence of curing times of 24, 48, 72, 96 and 120 h was analyzed under conditions of 18 M KOH and curing temperature of 70 °C.

Table 1- Synthesis conditions studied.

Variable studied	Values studied				
Molar concentration (M)	12	13	14	15	16
Temperature (°C)	60	70	80	90	100
Time (h)	24	48	72	96	120

2.3.3 Synthesis of geopolymers

To determine the mechanical strength of the geopolymers, the KLN-1, KLN-2 and MCR-1 samples were weighed according to the ratios predefined in Section 3.2.2 and Table 1. The synthesis was performed through the following steps (Figure 1): the KLN-1 and KLN-2 samples were mixed with the MCR-1 sample in a mortar until a homogeneous mixture was obtained; a solution of 7.2 ml of KOH was slowly added to this mixture at the concentrations defined in Table 1. The paste formed was homogenized in a mortar for a period of 5 min. The geopolymeric paste was then stored in an oven at 40 °C for 1 h. The geopolymer paste was removed from the oven and formed into steel molds in dimensions of 50 mm x 20 mm x 30 mm with simple uniaxial pressing under a pressure of 20 kgf/cm^2 in a hydraulic press (Karl Kolb, model PW-40). After the conformation, the specimens were sealed in film paper (moisture control) and placed in an oven at 40 °C for 24 h. Then, the temperature was increased by 10 °C/h until the final temperature established in the experiments was reached.

KLN-1   KLN-2   **: Δ40°C (24h)

Δ750°C (2h)   (60, 70, 80, 90, 100°C)

Alkaline activator (KOH)   "Red metakaolin"   Metakaolin   **   Geopolymer
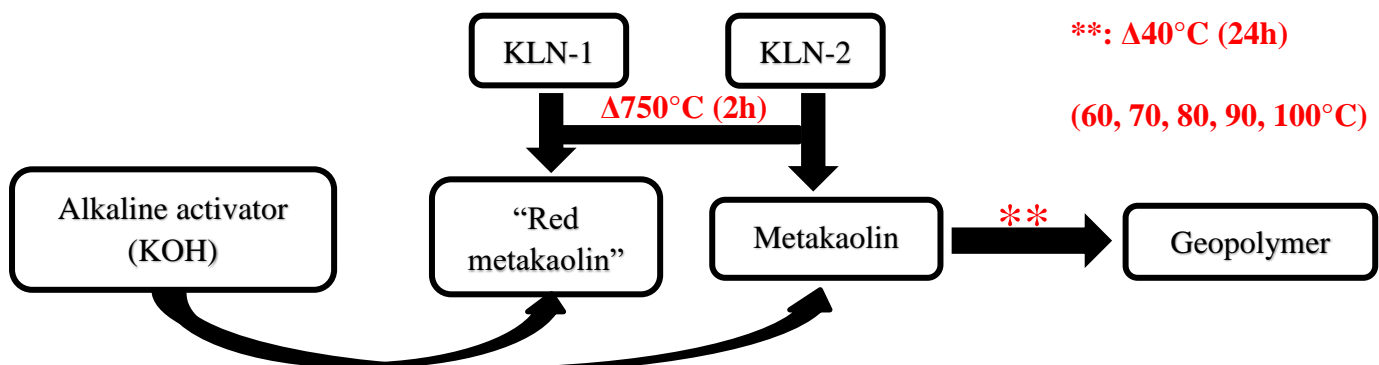
Figure 1- Flowchart of the process for obtaining geopolymers.

3.3.4 Mechanical compressive strength

The mechanical strength of the respective specimens was determined by the flexural tensile strength (FTS) at three points. The test was performed in an AROTEC universal testing machine, model WDW-100E, with a 100 kN load cell, test speed of 2 kN/min, and initial load of 2 N. The tests were performed in the resistance laboratory of the Federal Institute of Pará (IFPA).

3 RESULTS

3.1 CHEMICAL AND MINERALOGICAL CHARACTERIZATION

3.1.1 Mineralogical composition of the in natura samples by XRD

The mineralogy of the samples used in the present study can be seen in Figure 2. The clay mineral kaolinite is the predominant mineral in the two samples studied. The predominance of kaolinite in the samples is beneficial for the synthesis of geopolymers considering that this calcined mineral (metakaolinite) is the most commonly used precursor in the synthesis of geopolymers (Glid et al., 2017b; Barbosa et al., 2018; Ayeni et al., 2021a; Hui-Teng et al., 2021).

In structural terms, there are significant differences in the half-height widths of the kaolinite peaks of the samples. The value of the half-height width of peak 001 of sample KLN-1 (0.3115) is 2 times higher than that of peak 001 in sample KLN-2 (0.1425), which may indicate structural disorder in the kaolinite crystals present in KLN-1. The TGA/DSC results corroborate this statement. This degree of disorder in the kaolinite of Belterra clay has been found in previous studies (Negrão, Costa, Pöllmann, et al., 2018; Negrão, da Costa, et al., 2018; Negrão, Pöllmann, et al., 2021).

In the Belterra clay (KLN-1) sample, the minerals gibbsite, quartz, goethite, and anatase are present as accessory minerals. In the "reference" sample, in addition to the characteristic kaolinite peaks, small quartz peaks are present.

The presence of a small mineral assemblage in the KLN-1 sample may have a positive or even negative influence on the properties of the geopolymer (Phoo-ngernkham *et al.* 2015, Lemougna *et al.* 2017, Siyal *et al.* 2016, Belmokhtar *et al.* 2017, Kamseu *et al.* 2017, Hajimohammadi *et al.* 2018, Koshy *et al.* 2019). However, the KLN-2 sample, which practically has only kaolinite in its composition, can be an important meter for evaluating the influence of other minerals on the final properties of the geopolymer.

A-anatase;G-gibbsite;Gt-goethite;Kaol-kaolinite;Q-quartz.
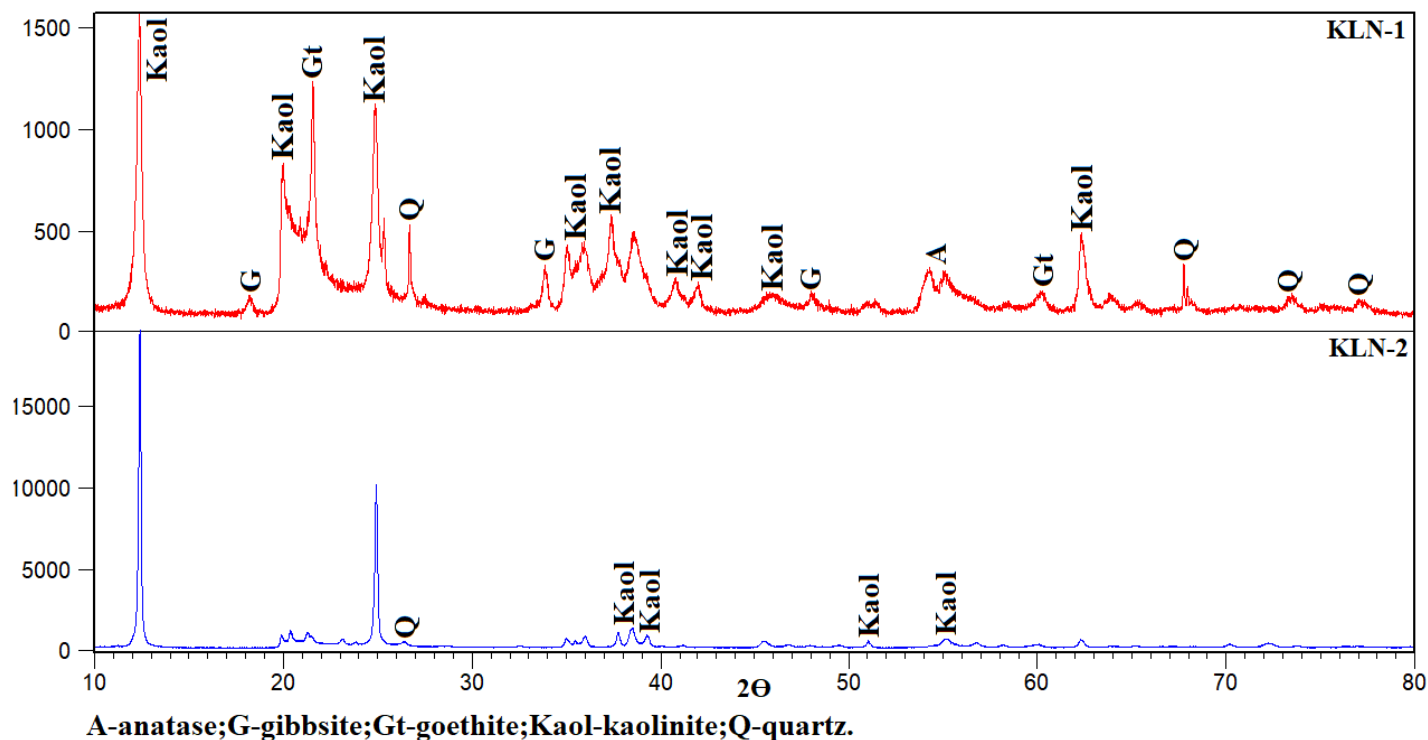
Figure 2 - Mineralogical compositions according to the XRD of the in natura samples.

3.1.2 Mineralogical transformations of the samples calcined at 750 °C and commercial microsilica by XRD

After calcination (Figure 3), minerals such as anatase and quartz remain stable or metastable in the KLN-1 samples (750 °C). The neoformation of hematite in these samples, resulting from the dehydroxylation of goethite, is also observed.

The most important aspect of these results is the presence of a high background, characteristic of the presence of amorphous compounds (Rodrigues et al., 2015). In the KLN-2 and SiO_2 samples, the presence of these compounds is well evidenced by a high rounded peak that characterizes a domain of amorphous materials in their compositions.
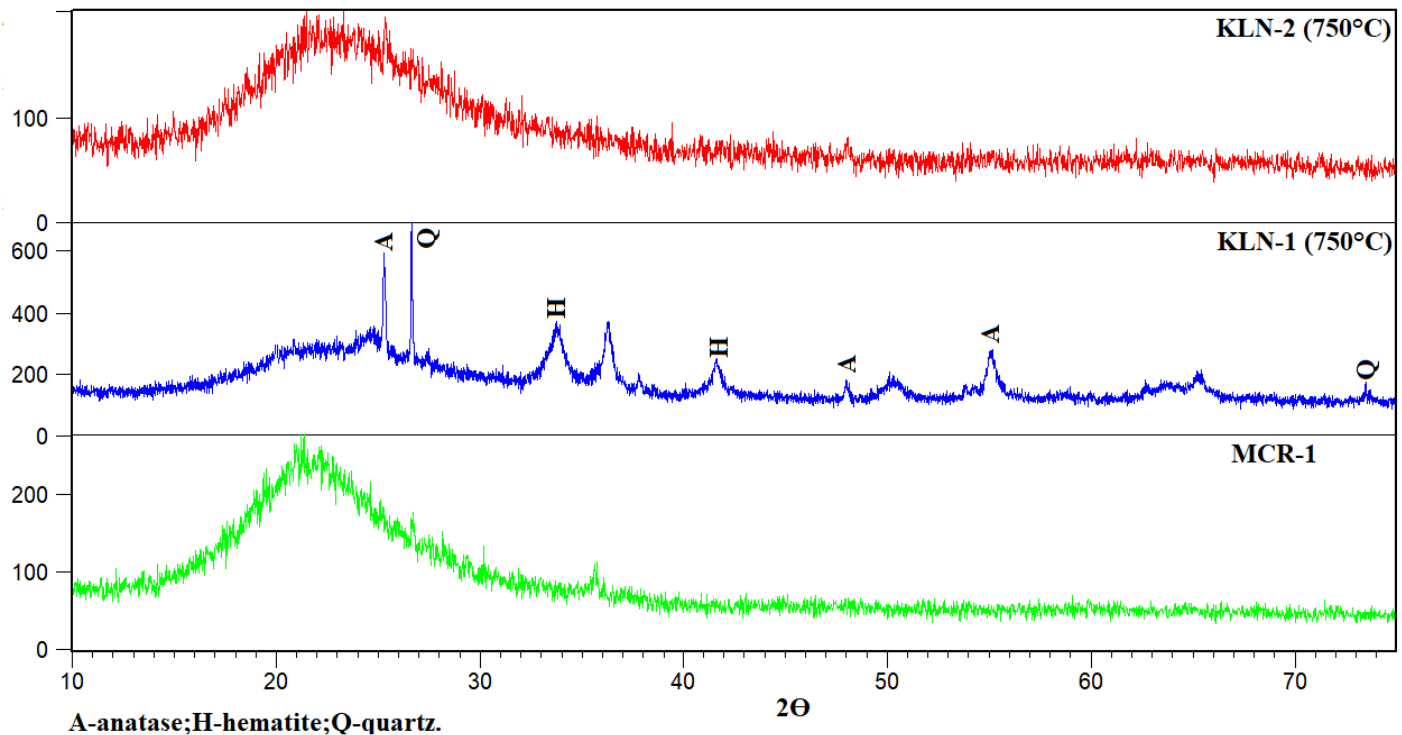
Figure 3 - Mineralogical composition according to the XRD of the calcined samples and amorphous SiO_2.

3.1.2 Behavior of the samples according to FTIR

The FTIR spectra of the in natura samples (Figure 4) show bands characteristic of the narrowing of the bonds of OH (3700-3620 cm^{-1}) and (Si, Al-O) 1120 cm^{-1} present in the kaolinite mineral (Ayeni et al., 2021a). A band at 460 cm^{-1} can also be attributed to the Si-O bonds of the kaolinite.

The spectra of the calcined samples are typical of the metakaolinite phase, showing a broad band at 3500 cm^{-1} that is attributed to the absorbed water; one band at 1100 cm^{-1} characteristic of the stretching of the Si-O bond of metakaolinite; and bands at 820 and 460 cm^{-1}, which represent to the Al-O and (Si, Al-O) bonds, respectively (Fialips et al., 2000; Frost & Vassallo, 1996; Ríos et al., 2009).
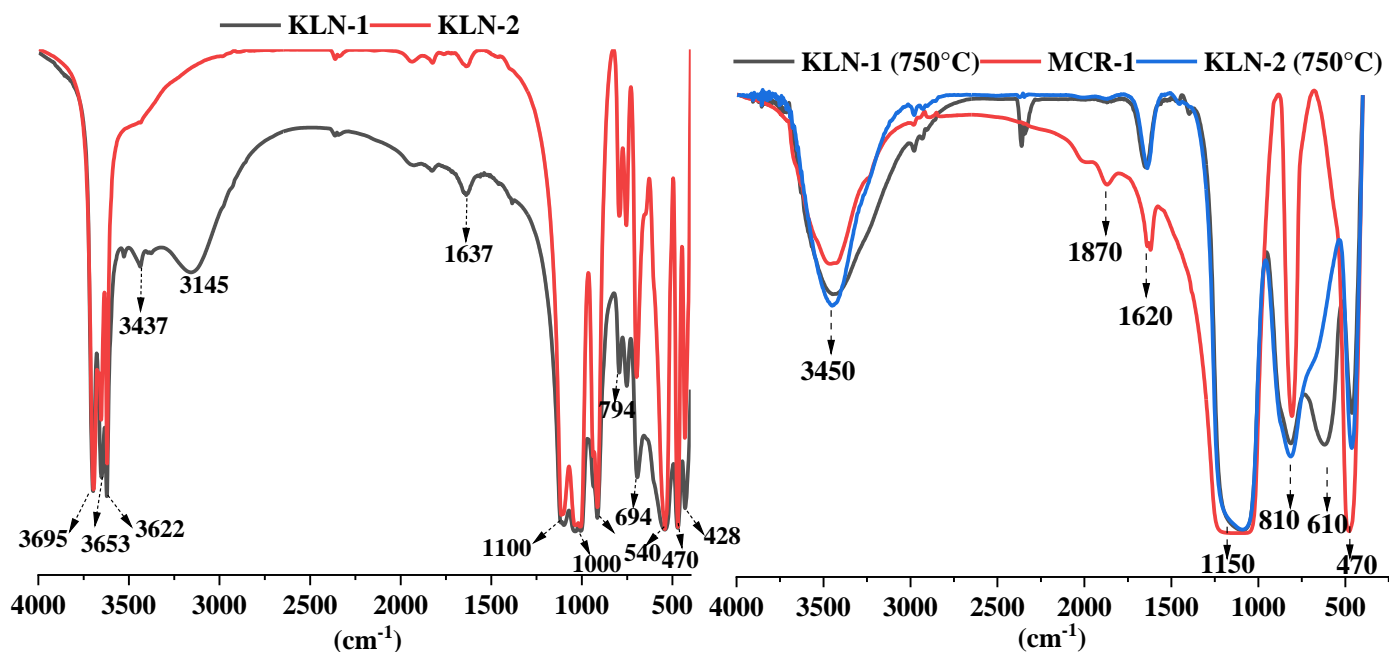
Figure 4 - Spectral behaviors according to the FTIR spectra of the in natura samples and those calcined at 750 °C.

3.1.3 Chemical compositions of the samples

The chemical compositions of the samples are shown in Table 2. The KLN-1 sample consists of 36.3% SiO_2, 34.9% Al_2O_3, 12.2% Fe_2O_3 and 2.22% other elements in lower concentrations. The KLN-2 sample consists mainly of SiO_2 (47.19%) and Al_2O_3 (39.19%). The MCR-1 sample consists of 97.4% SiO_2 and 1.42% other elements.

Determining the percentages of Al_2O_3 and SiO_2 from kaolinite is crucial for the study of the samples as a source of aluminosilicates for geopolymer synthesis.

The SiO_2 levels are correlated with the presence of kaolinite and quartz, as can be observed in Figure 2. The percentage of SiO_2-Re allowed us to differentiate by means of stoichiometric calculation what percentage of SiO_2 is present in the kaolinite and, consequently, the quartz percentage. The percentage of kaolinite in the KLN-1 sample is 73.62% and 99.21% in the KLN-2 sample. These results are used to establish the molar ratios studied in the design of the experiments.

Table 2- Chemical compositions of the samples.

Sample	SiO_2	Al_2O_3	Fe_2O_3	FP	Other	Total	SiO_2-Re
KLN-1	36.3	34.9	12.2	14.74	2.22	100.36	34.27
KLN-2	47.08	39.19	0.43	13.85	0.65	101.2	46.18
MCR-1	97.4	0.05	0.05	0.69	1.42	99.51	- -

SiO_2-Re: reactive SiO_2.

3.1.4 Thermal behavior

The results of the thermal analysis (Figure 5) show the thermal behavior of the studied samples. The KLN-1 sample has three endothermic events (with associated mass loss) and one exothermic event. The first endothermic event (240-250 °C) is characteristic of the dehydroxylation of goethite; the second event occurs between 350-360 °C and refers to the dehydroxylation of the mineral gibbsite; the third and largest event occurs at 500 °C, confirming the dehydroxylation of kaolinite for the formation of metakaolinite (Caglar *et al*. 2009, Drweesh *et al*. 2016, Issaoui *et al*. 2016); and finally, the only exothermic event at 980-985 °C reveals the formation of a new crystalline phase (mullite).

The KLN-2 sample shows only one endothermic event, at 530 °C, with a high variation in enthalpy (-307.4 J/g), characterizing a high concentration of kaolinite in its composition.

The difference in kaolinite dehydroxylation temperature in the samples may be due to the difference in crystallinity reported in the XRD results (Figure 2). Thus, the kaolinite mineral present in the KLN-1 sample undergoes dehydroxylation at lower temperatures due to the disorder present in the crystal structure.
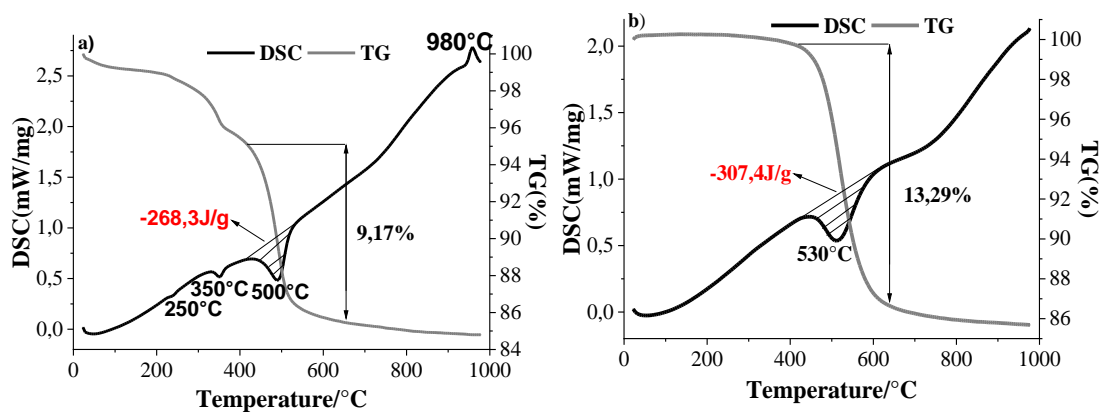
Figure 5 - Thermal behaviors according to the TGA/DSC curves of the studied samples. a): KLN-1, B): KLN-2.

3.2 PHYSICAL CHARACTERISTICS OF THE SAMPLES

3.1.1 Particle size

Figure 6 shows the particle size distribution of the studied samples. The Belterra clay samples have the highest silt fraction percentage (65.78), with 27.70% the sand fraction and 6.50% clay fraction. The KLN-1 sample having highest percentage of silt fraction can be attributed to the predominance of kaolinite in the sample, as observed by the results of the chemical analysis, XRD and TGA/DSC.

The MCR-1 sample has the highest silt fraction content (93.34%), with lower percentages of clay (4.85%) and sand (1.81%) fractions.

In addition to the chemical and mineralogical composition, the particle size of the samples can directly influence the synthesis mechanism of the geopolymer. The dissolution of aluminosilicates is expected to occur more rapidly in the sample with the smallest particle size (KLN-2) (larger surface area) than in the sample with the largest particle size (KLN-1) (Hajimohammadi et al., 2018b).
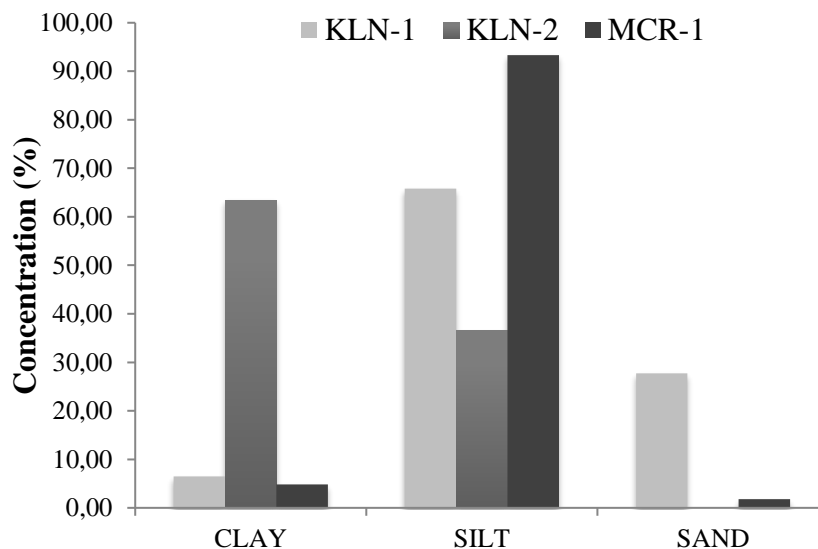
Figure 6 - Particle size distributions of the studied samples.

3.3 GEOPOLYMER CHARACTERIZATION

3.3.1 Mechanical compressive strength

3.3.1 Regarding the molar concentration

The compressive strength of the geopolymers based on the molar concentration (Figure 7) shows a different behavior of the samples at the different concentrations studied.

The KLN-2 sample showed the highest mechanical strength values at concentrations of 12M (25.85 MPa) and 16 M (25.24 MPa). The lowest resistance value in the KLN-2 sample was obtained at 14 M (12.33 MPa). The KLN-1 sample had the lowest strength at 16 M (6.31 MPa) and the highest strength at 13 M (12.06 MPa).

The variation in the mechanical strength values of the samples at the different concentrations showed that under the studied conditions (70 °C and 3.4 Si/Al ratio), the molar concentration does not contribute significantly to the increase in the mechanical strength of the geopolymers. A trend is observed in the KLN-2 sample, where resistance values are higher at extreme, minimum and maximum concentrations, and lower values at intermediate concentrations. In the KLN-1 sample, the mechanical strength tends to increase with increasing molar concentration up to 14 M and then tends to decrease. This

increase in resistance to 14 M was also observed in studies that used NaOH as an alkaline activator (Ayeni et al., 2021).

The difference in the strength values between the samples under the same conditions can be attributed to the mineralogical and physical characteristics of the studied samples.

In the KLN-2 sample, kaolinite is the only mineral that may have favored the geopolymerization reaction, whereas in the KLN-1 sample, the other existing minerals may have impaired the reaction mechanism.
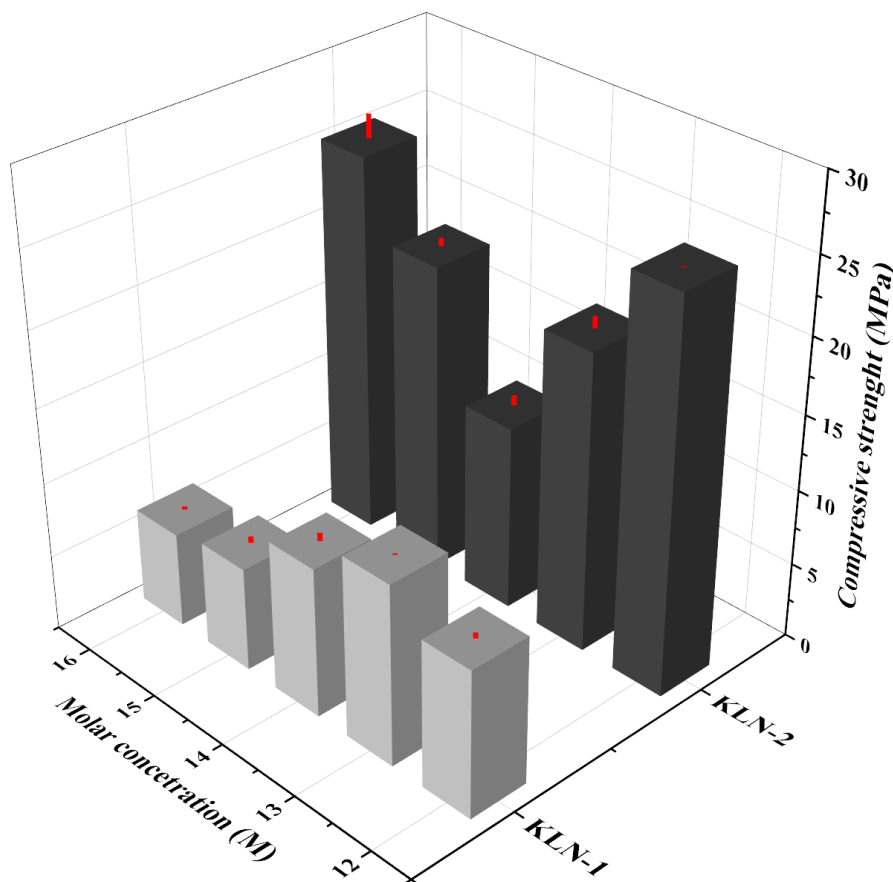
Figure 7- Compressive strength of the geopolymers obtained at different molar concentrations.

3.3.2 Temperature variation

The mechanical strength results based on temperature are shown in Figure 8. The mechanical strength values of the 2 samples showed a similar trend. The resistance increases until the temperature of 80 °C and then tends to decrease until the temperature of 100 °C.

The lowest mechanical strength value for the KLN-2 sample was at 90 °C (22.32 MPa), while the highest was at 80 °C (64.38 MPa). In the KLN-1 sample, the lowest value was also obtained at 90 °C (8.25 MPa) and the highest at 80 °C (17.08 MPa).

Analyzing the results obtained, we can infer that the curing temperature exerts a strong influence on the strength gain under the studied conditions (1.1 Na/Al and 3.4 Si/Al). This increase in strength gain suggests that the geopolymerization reaction was favored with the increase in temperature (Ayeni et al., 2021a; Mohajerani et al., 2019).

At 80 °C, the geopolymer hardening step probably occurred, which does not imply that all the water present in the geopolymer was evaporated. In fact, the higher strength value at 80 °C may be an indication that there was still moisture in the geopolymer at 80 °C, and the elimination of this moisture at temperatures of 90 and 100 °C resulted in a loss of strength at these temperatures. High values of mechanical strength at 80 °C were also observed in the syntheses of geopolymers with NaOH (Chindaprasirt et al., 2007; Sagawa et al., 2015); however, when compared with the results presented in this study, we can infer that under the same synthesis conditions, NaOH contributed more favorably to resistance gain.
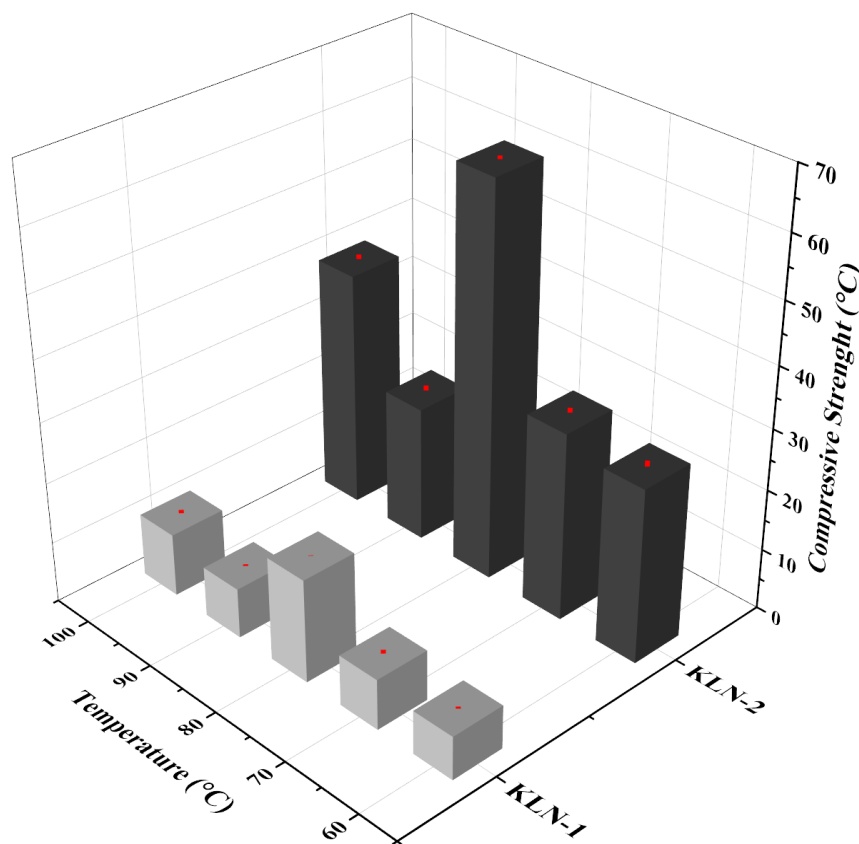
Figure 8- Compressive strength of the geopolymers obtained at different curing temperatures.

3.3.3 Curing time variation

The compressive strength results at different curing times are shown in Figure 9. The geopolymers of the two samples show an increase in strength with increasing curing time.

In the KLN-2 sample, the resistance after the first 24 h of curing is 14.29 MPa. After 48 h of curing, the resistance value increases to 25.74 MPa. For the 72-h and 96-h curing times, the resistance values do not undergo considerable changes, with 20.69 MPa at 72 h and 26.41 MPa at 96 h. However, after 120 h of curing, the resistance value increases sharply, reaching a value of 55.51 MPa.

The KLN-1 sample shows a value of 6.58 MPa in the first 24 h of curing, and at 48 h, the resistance value increases to 13.16 MPa. Similar the KLN-2 sample, the resistance values at 72 h (14.58 MPa) and 96 h (15.56) are not very different from the values obtained at 48. At 120 h, there is a significant increase in the mechanical strength value to 21.52 MPa.

These compressive strength results allow us to assume that in the first hours of curing, the geopolymerization reaction occurs more rapidly, which explains the strength gain in the 48-hour curing time. After 48 h of curing, the geopolymerization reaction occurs more slowly, showing resistance gain only after 120 h of curing. This behavior demonstrates that the curing time of geopolymers synthesized with KOH is the same behavior observed in geopolymers that use NaOH as an alkaline activator (Ayeni et al., 2021a; H. Y. Zhang et al., 2021).

When the same curing time is analyzed for the two samples, we observe a large difference in the compressive strength values, and based on the results already presented, this difference may be related to the differences in the mineralogical and particle size composition of the studied samples.
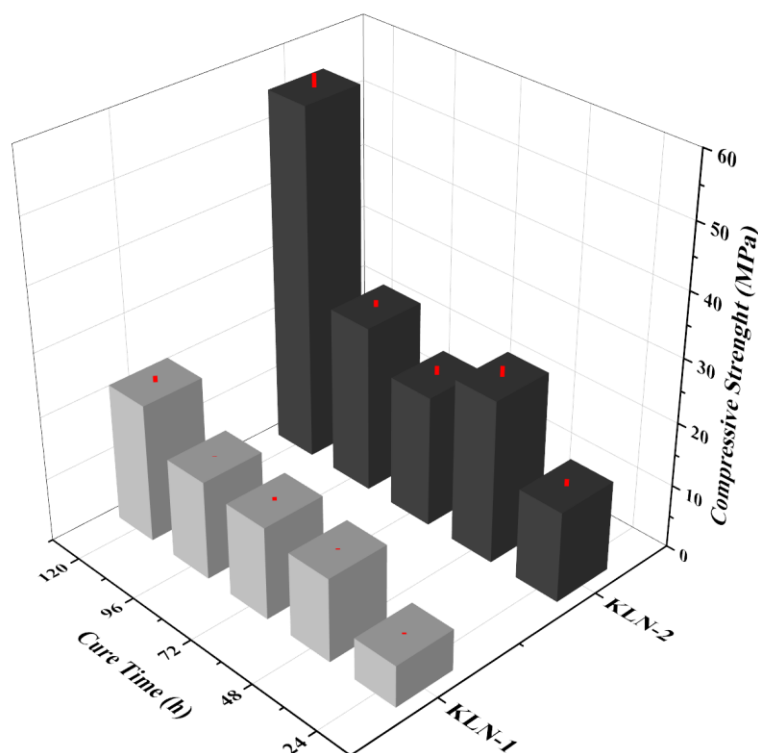
Figure 9- Compressive strengths of the geopolymers at different curing times.

3.3.4 Variation in the FTIR results with the molar concentration

The FTIR spectra of the geopolymers of the two samples synthesized at different molar concentrations are shown in Figure 10. The stretching of the H-O-H bond is represented at 3444-3450 cm^{-1} (Tang et al., 2021). The absorption band at 1645 cm^{-1} can be attributed to the vibration of the hydroxyl group (OH^{-}). Note that this band is displaced since in the calcined samples, there is a band at 1620 cm^{-1} (Figure 4). This band is related to the water present in the geopolymer structure (Yan et al., 2016; Li et al., 2022).

The band at 1110-1130 cm^{-1} is related to the asymmetric vibration of the Si-O-Al bond in the geopolymer (Costa et al., 2021). This is the main band indicating the formation of a geopolymer (Hui-Teng et al., 2021). The absorption band at 700-717 cm^{-1} corresponds to the stretching of the Al-O bond. The bands at 590 cm^{-1} and 475-460 cm^{-1} may be related to the symmetric stretching of the Si-O-Al bond and the flexion vibration of the Si-O-Si bond present in the geopolymer, respectively (Costa et al., 2021; Liu et al., 2020; Qureshi & Panesar, 2019).

The intensity of the band at 1110-1130 cm^{-1} has a direct relationship with the results of compressive strength; the higher its intensity, the greater compressive strength is expected (Hui-Teng et al., 2021). In the KLN-1 sample, it is observed that the highest intensity of this band occurs at concentrations of 12, 13 and 14 M, the concentrations that exhibit the highest compressive strength. In the KLN-2 sample, the highest intensity for the 1130 cm^{-1} band occurs at 16 M and 12 M, for which the best compressive strength results are also obtained.
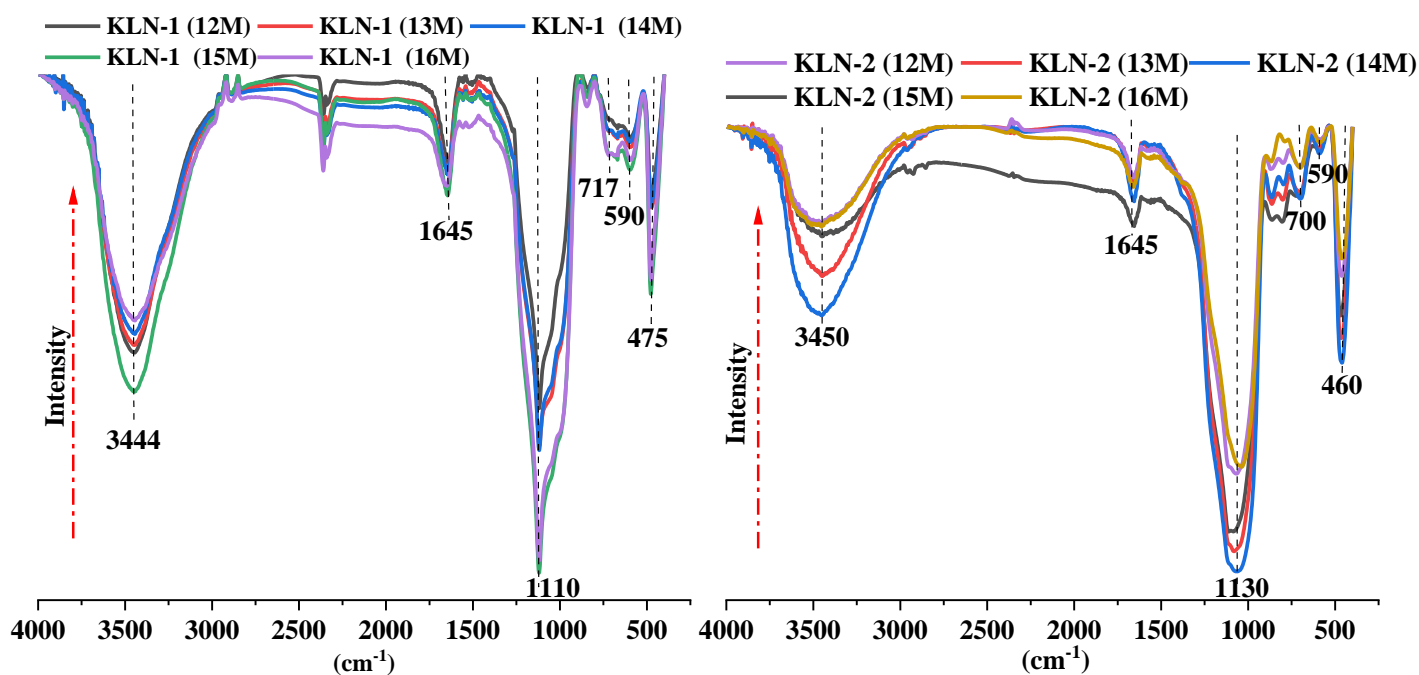
Figure 10- FTIR spectral behaviors of the geopolymers obtained at different molar concentrations.

3.3.5 Geopolymers at different temperatures according to FTIR

Figure 11 shows the spectra of the geopolymers at different temperatures. The absorption bands are practically the same as those reported in the previous figure, showing bands characteristic of the HOH bond (3444 cm^{-1}), stretching of the OH bond at 1645-1655 cm^{-1} and asymmetric vibration of the Si-O-Al bond at 1115-1120 cm^{-1}. Bands are also observed at 695-717 cm^{-1} (stretching of the Al-O bond), 560-590 cm^{-1} (symmetric stretching of the Si-O-Al bond) and 460-475 cm^{-1} (flexion vibration of the Si-O-Si bond).

The band intensity at 1115-1120 cm^{-1} is in agreement with the results of compressive strength, with higher intensities at temperatures of 80, 70 and 100 °C, in both samples. The intensity of the band at 717-695 cm^{-1} may also have a direct relationship with the compressive strength of the geopolymers (Perná et al., 2019; Ayeni et al., 2021b).
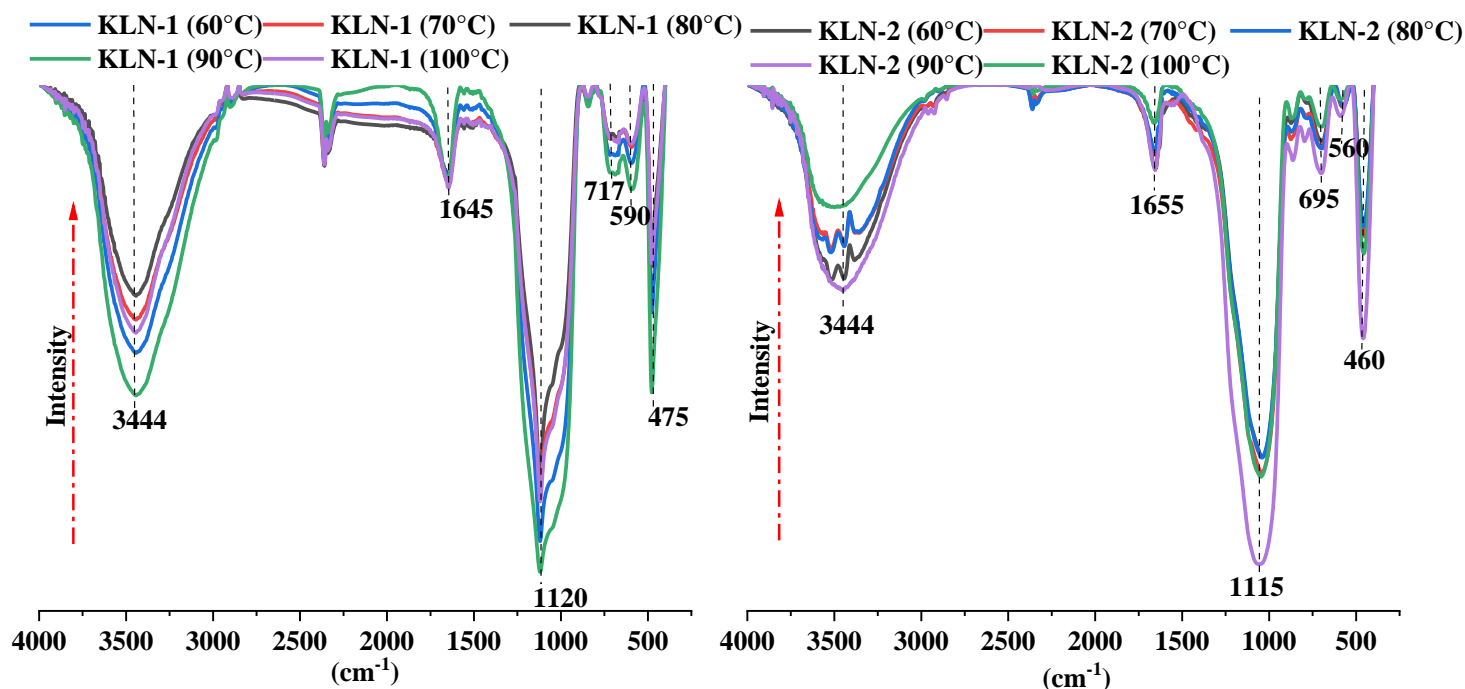
Figure 11- FTIR spectral behavior of the geopolymers obtained at different curing temperatures.

3.3.6 Variation in the FTIR results of the geopolymers with the curing time

The effectiveness of the geopolymer synthesis based on the curing time can be observed from the FTIR results (Figure 12). Similar to the results based on molar concentration and temperature, the intensity of the bands 1120-1130 cm^{-1} (Si-O-Al) and 795-717 cm^{-1} (stretching of the Al-O bond) follows the same trend, with the intensity of the bands being directly proportional to the compressive strength values shown in Figure 8. The highest intensity in these regions is observed at 120 h of curing in both samples, while the lowest intensity is observed at 24 h of curing.

In the spectra of the figures, bands occur in the regions of 3444 cm^{-1} (HOH), 1645-1656 cm^{-1} (OH-), 699-717 cm^{-1} (Al-O), 586-590 cm^{-1} (Si-O-Al) and 453-475 cm^{-1} (Si – O-Si).
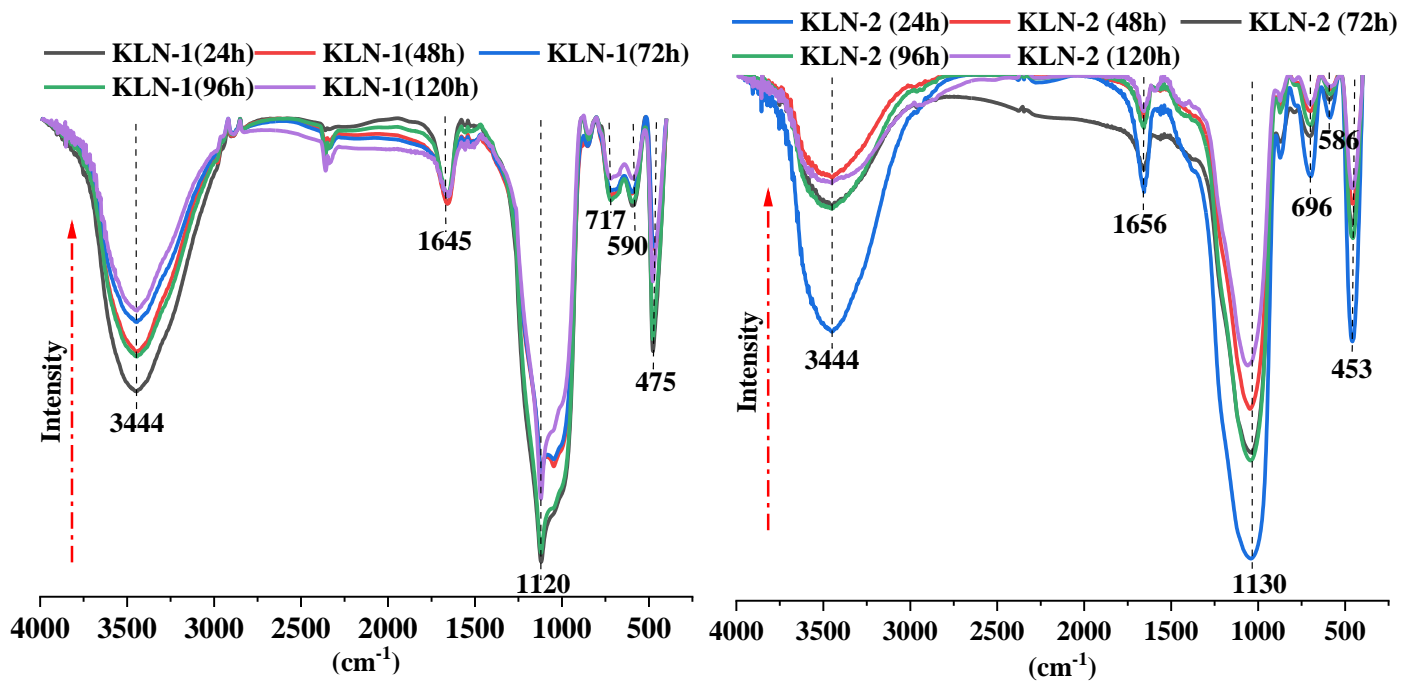
Figure 12- FTIR spectral behaviors of the geopolymers obtained at different curing times.

4 CONCLUSIONS

The results showed that the mineralogical and particle size differences directly impacted the resistance gain of the geopolymers synthesized with KOH. The clay with the simplest accessory mineralogy and with smaller particle sizes (KLN-2) exhibited the best mechanical strength results.

The variations with the molar concentration of KOH showed similar behavior between the samples, showing greater resistance at the lowest concentration, 12 M, and as the concentration increased to 13, 14 and 15 M, no major differences were observed in the resistance gain; the increase in resistance became more significant at the 16 M concentration.

The curing temperature was an important parameter that contributed to the development of strength in the geopolymers of the 2 samples studied. An increase in the curing temperature from 60 to 80 °C resulted in better compressive strength, but with an increase in temperature to 90 and 100 °C, there was a significant loss of strength. This behavior indicated that at higher temperatures, there was possibly a reduction in the gel phase available for the reaction, which resulted in low resistance gain.

The resistance gain occurred gradually with increasing curing time. The results of resistance allowed us to infer that the reaction mechanism was more accelerated in the first 48 h, when there was a significant resistance gain. At 72 h and 96 h, the resistance gain was quite irrelevant, becoming more perceptible only after 120 h.

Considering the points highlighted above, we can conclude that molar concentration, temperature and curing time are key factors for resistance gain. Regarding the influence of the precursor on geopolymer synthesis, we can say that the greater the mineral diversity is, the lower the resistance acquired by the geopolymers.

5 ACKNOWLEDGMENTS

REFERENCES

Adjei, S., Elkatatny, S., Aggrey, W.N., Abdelraouf, Y., 2022. Geopolymer as the future oil-well cement: A review. Journal of Petroleum Science and Engineering. https://doi.org/10.1016/j.petrol.2021.109485

Al-Majidi, M.H., Lampropoulos, A., Cundy, A., Meikle, S., 2016. Development of geopolymer mortar under ambient temperature for in situ applications. Construction and Building Materials 120, 198–211. https://doi.org/10.1016/j.conbuildmat.2016.05.085

Alnahhal, A.M., Alengaram, U.J., Yusoff, S., Darvish, P., Srinivas, K., Sumesh, M., 2022. Engineering performance of sustainable geopolymer foamed and non-foamed concretes. Construction and Building Materials 316, 125601. https://doi.org/10.1016/j.conbuildmat.2021.125601

Autef, A., Joussein, E., Poulesquen, A., Gasgnier, G., Pronier, S., Sobrados, I., Sanz, J., Rossignol, S., 2013. Influence of metakaolin purities on potassium geopolymer formulation: The existence of several networks. Journal of Colloid and Interface Science 408, 43–53. https://doi.org/10.1016/j.jcis.2013.07.024

Ayeni, O., Onwualu, A.P., Boakye, E., 2021a. Characterization and mechanical performance of metakaolin-based geopolymer for sustainable building applications. Construction and Building Materials 272, 121938. https://doi.org/10.1016/j.conbuildmat.2020.121938

Ayeni, O., Onwualu, A.P., Boakye, E., 2021b. Characterization and mechanical performance of metakaolin-based geopolymer for sustainable building applications.

Construction and Building Materials 272, 121938. https://doi.org/10.1016/j.conbuildmat.2020.121938

Barbosa, T.R., Foletto, E.L., Dotto, G.L., Jahn, S.L., 2018. Preparation of mesoporous geopolymer using metakaolin and rice husk ash as synthesis precursors and its use as potential adsorbent to remove organic dye from aqueous solutions. Ceramics International 44, 416–423. https://doi.org/10.1016/j.ceramint.2017.09.193

Barreto, I. A. R., Costa, M. L., 2021. Use of the clayey cover of bauxite deposits of the Amazon region for geopolymer synthesis and its application in red ceramics. Construction and Building Materials 300, 124318. https://doi.org/10.1016/j.conbuildmat.2021.124318

Chindaprasirt, P., Chareerat, T., Sirivivatnanon, V., 2007. Workability and strength of coarse high calcium fly ash geopolymer. Cement and Concrete Composites 29, 224–229. https://doi.org/10.1016/j.cemconcomp.2006.11.002

Costa, L.M., Almeida, N.G.S., Houmard, M., Cetlin, P.R., Silva, G.J.B., Aguilar, M.T.P., 2021. Influence of the addition of amorphous and crystalline silica on the structural properties of metakaolin-based geopolymers. Applied Clay Science 215, 106312. https://doi.org/10.1016/j.clay.2021.106312

Davidovits, J., 1991. GEOPOLYMERS Inorganic polymerie new materials, Journal ofThamalAnalysis.

Dupuy, C., Havette, J., Gharzouni, A., Texier-Mandoki, N., Bourbon, X., Rossignol, S., 2019. Metakaolin-based geopolymer: Formation of new phases influencing the setting time with the use of additives. Construction and Building Materials 200, 272–281. https://doi.org/10.1016/j.conbuildmat.2018.12.114

Fialips, C., Petit, S., Decarreau, A., Beaufort, D., Umr-cnrs, L.H.A.S.A., Poitiers, U. de, Pineau, R., Cedex, F.-P., 2000. I N F L U E N C E OF S Y N T H E S I S pH ON KAOLINITE " C R Y S T A L L I N I T Y " A N D S U R F A C E PROPERTIES 48, 173–184.

Frost, R.A.Y.L., Vassallo, A.M., 1996. THE D E H Y D R O X Y L A T I O N OF THE KAOLINITE CLAY M I N E R A L S U S I N G I N F R A R E D EMISSION S P E C T R O S C O P Y 44, 635–651.

Glid, M., Sobrados, I., Rhaiem, H. ben, Sanz, J., Amara, A.B.H., 2017a. Alkaline activation of metakaolinite-silica mixtures: Role of dissolved silica concentration on the formation of geopolymers. Ceramics International 43, 12641–12650. https://doi.org/10.1016/j.ceramint.2017.06.144

Glid, M., Sobrados, I., Rhaiem, H. ben, Sanz, J., Amara, A.B.H., 2017b. Alkaline activation of metakaolinite-silica mixtures: Role of dissolved silica concentration on the formation of geopolymers. Ceramics International 43, 12641–12650. https://doi.org/10.1016/j.ceramint.2017.06.144

Hajimohammadi, A., Ngo, T., Kashani, A., 2018a. Glass waste versus sand as aggregates: The characteristics of the evolving geopolymer binders. Journal of Cleaner Production 193, 593–603. https://doi.org/10.1016/j.jclepro.2018.05.086

Hajimohammadi, A., Ngo, T., Kashani, A., 2018b. Glass waste versus sand as aggregates: The characteristics of the evolving geopolymer binders. Journal of Cleaner Production 193, 593–603. https://doi.org/10.1016/j.jclepro.2018.05.086

Hui-Teng, N., Cheng-Yong, H., Yun-Ming, L., al Bakri Abdullah, M.M., Hun, K.E., Razi, H.M., Yong-Sing, N., 2021. Formulation, Mechanical Properties and Phase Analysis of Fly Ash Geopolymer with Ladle Furnace Slag Replacement. Journal of Materials Research and Technology 12, 1212–1226. https://doi.org/10.1016/j.jmrt.2021.03.065

John, S.K., Nadir, Y., Girija, K., 2021. Effect of source materials, additives on the mechanical properties and durability of fly ash and fly ash-slag geopolymer mortar: A review. Construction and Building Materials 280, 122443. https://doi.org/10.1016/j.conbuildmat.2021.122443

Kaze, C.R., Lecomte-Nana, G.L., Adesina, A., Nemaleu, J.G.D., Kamseu, E., Chinje Melo, U., 2021. Influence of mineralogy and activator type on the rheology behaviour and setting time of laterite based geopolymer paste. Cement and Concrete Composites 104345. https://doi.org/10.1016/j.cemconcomp.2021.104345

Król, M., Mozgawa, W., 2019. Zeolite layer on metakaolin-based support. Microporous and Mesoporous Materials 282, 109–113. https://doi.org/10.1016/j.micromeso.2019.03.028

Lemougna, P.N., Wang, K. tuo, Tang, Q., Cui, X. min, 2017. Synthesis and characterization of low temperature (<800 °C) ceramics from red mud geopolymer precursor. Construction and Building Materials 131, 564–573. https://doi.org/10.1016/j.conbuildmat.2016.11.108

Li, M., Luo, R., Qin, L., Liu, H., Duan, P., Jing, W., Zhang, Z., Liu, X., 2022. High temperature properties of graphene oxide modified metakaolin based geopolymer paste. Cement and Concrete Composites 125, 104318. https://doi.org/10.1016/j.cemconcomp.2021.104318

Liu, X., Jiang, J., Zhang, H., Li, M., Wu, Y., Guo, L., Wang, W., Duan, P., Zhang, W., Zhang, Z., 2020. Thermal stability and microstructure of metakaolin-based geopolymer blended with rice husk ash. Applied Clay Science 196, 105769. https://doi.org/10.1016/j.clay.2020.105769

Mohajerani, A., Suter, D., Jeffrey-Bailey, T., Song, T., Arulrajah, A., Horpibulsuk, S., Law, D., 2019. Recycling waste materials in geopolymer concrete. Clean Technologies and Environmental Policy 21, 493–515. https://doi.org/10.1007/s10098-018-01660-2

Moutinho, S., Costa, C., Cerqueira, Â., Rocha, F., Velosa, A., 2019. Geopolymers and polymers in the conservation of tile facades. Construction and Building Materials 197, 175–184. https://doi.org/10.1016/j.conbuildmat.2018.11.058

Negrão, L.B.A., Costa, M.L. da, Pöllmann, H., Horn, A., 2018a. An application of the Rietveld refinement method to the mineralogy of a bauxite-bearing regolith in the Lower Amazon. Mineralogical Magazine 82, 413–431. https://doi.org/10.1180/minmag.2017.081.056

Negrão, L.B.A., da Costa, M.L., Pöllmann, H., 2018b. The Belterra Clay on the bauxite deposits of Rondon do Pará, Eastern Amazon. Brazilian Journal of Geology 48, 473–484. https://doi.org/10.1590/2317-4889201820180128

Negrão, L.B.A., Pöllmann, H., Cortinhas Alves, T.K., 2021. Mineralogical appraisal of bauxite overburdens from Brazil. Minerals 11. https://doi.org/10.3390/min11070677

Perná, I., Šupová, M., Hanzlíček, T., Špaldoňová, A., 2019. The synthesis and characterization of geopolymers based on metakaolin and high LOI straw ash. Construction and Building Materials 228, 116765. https://doi.org/10.1016/j.conbuildmat.2019.116765

Phoo-Ngernkham, T., Maegawa, A., Mishima, N., Hatanaka, S., Chindaprasirt, P., 2015. Effects of sodium hydroxide and sodium silicate solutions on compressive and shear bond strengths of FA-GBFS geopolymer. Construction and Building Materials 91, 1–8. https://doi.org/10.1016/j.conbuildmat.2015.05.001

Prud'homme, E., Michaud, P., Joussein, E., Peyratout, C., Smith, A., Rossignol, S., 2011. In situ inorganic foams prepared from various clays at low temperature. Applied Clay Science 51, 15–22. https://doi.org/10.1016/j.clay.2010.10.016

Qureshi, T.S., Panesar, D.K., 2019. Impact of graphene oxide and highly reduced graphene oxide on cement based composites. Construction and Building Materials 206, 71–83. https://doi.org/10.1016/j.conbuildmat.2019.01.176

Ríos, C.A., Williams, C.D., Fullen, M.A., 2009. Applied Clay Science Nucleation and growth history of zeolite LTA synthesized from kaolinite by two different methods. Applied Clay Science 42, 446–454. https://doi.org/10.1016/j.clay.2008.05.006

Rodrigues, S.F.S., Costa, M.L. da, Pöllmann, H., Kern, D.C., Silveira, M.I. da, Kipnis, R., 2015. Pre-historic production of ceramics in the Amazon: Provenience, raw materials, and firing temperatures. Applied Clay Science 107, 145–155. https://doi.org/10.1016/j.clay.2015.01.016

Sagawa, Y., Ota, S., Harada, K., Nishizaki, T., Goda, H., 2015. Utilization of Fly Ash with Higher Loss on Ignition for Geopolymer Mortar. Advanced Materials Research 1129, 614–620. https://doi.org/10.4028/www.scientific.net/AMR.1129.614

Singh, B., Ishwarya, G., Gupta, M., Bhattacharyya, S.K., 2015. Geopolymer concrete: A review of some recent developments. Construction and Building Materials. https://doi.org/10.1016/j.conbuildmat.2015.03.036

Siyal, A.A., Azizli, K.A., Man, Z., Ismail, L., Khan, M.I., 2016. Geopolymerization kinetics of fly ash based geopolymers using JMAK model. Ceramics International 42, 15575–15584. https://doi.org/10.1016/j.ceramint.2016.07.006

Tang, J., Ji, X., Liu, X., Zhou, W., Chang, X., Zhang, S., 2021. Mechanical and microstructural properties of phosphate-based geopolymers with varying Si/Al molar ratios based on the sol-gel method. Materials Letters 131178. https://doi.org/10.1016/j.matlet.2021.131178

Yan, S., He, P., Jia, D., Yang, Z., Duan, X., Wang, S., Zhou, Y., 2016. Effects of treatment temperature on the reduction of GO under alkaline solution during the preparation of graphene/geopolymer composites. Ceramics International 42, 18181–18188. https://doi.org/10.1016/j.ceramint.2016.08.134

Yunsheng, Z., Wei, S., Zongjin, L., 2010a. Composition design and microstructural characterization of calcined kaolin-based geopolymer cement. Applied Clay Science 47, 271–275. https://doi.org/10.1016/j.clay.2009.11.002

Yunsheng, Z., Wei, S., Zongjin, L., 2010b. Composition design and microstructural characterization of calcined kaolin-based geopolymer cement. Applied Clay Science 47, 271–275. https://doi.org/10.1016/j.clay.2009.11.002

Zhang, H.Y., Liu, J.C., Wu, B., 2021. Mechanical properties and reaction mechanism of one-part geopolymer mortars. Construction and Building Materials 273. https://doi.org/10.1016/j.conbuildmat.2020.121973

Zhang, Z., Wang, H., Provis, J.L., Bullen, F., Reid, A., Zhu, Y., 2012. Quantitative kinetic and structural analysis of geopolymers. Part 1. the activation of metakaolin with sodium hydroxide. Thermochimica Acta 539, 23–33. https://doi.org/10.1016/j.tca.2012.03.021

4.3 SYNTHESIS OF "ECOFRIENDLY" GEOPOLYMERS FROM BAUXITE WASHING WASTE: AN ALTERNATIVE TO MINIMIZE CO$_2$ EMISSIONS

Igor Alexandre Rocha Barreto[1]; Marcondes Lima da Costa[2]; Leonardo Boiadeiro Ayres Negrão

[1]Program for Post-graduation in Geology and Geochemistry, Institute of Geosciences, UFPA, Belém (PA), Brazil. E-mail: igorrochaq@gmail.com, igor.barreto@icen.ufpa.br; [2]Program for Post-graduation in Geology and Geochemistry, Institute of Geosciences, Federal University of Pará – UFPA, Brazil. E-mails: mlc@ufpa.br, marcondeslc@gmail.com. [3]Institute of Geosciences and Geography, Department of Mineralogy and Geochemistry, Martin Luther University Halle-Wittenberg, Halle, Germany. E-mail: boiadeiro.negrao@gmail.com.

HIGHLIGHTS

- The kaolinite present in the sample has a low structural order.
- The geopolymers synthesized at the highest Na/Al ratios (0.8 and 0.9) showed lower compressive strength.
- The maximum resistance obtained was 41.89 MPa.
- The percentage of sodalite directly influences the resistance of the geopolymer.

ABSTRACT

Civil construction is one of the most important sectors of the world economy due to the rapid growth in global population. Concrete is one of the most essential products in this sector. Ordinary Portland cement is the major ingredient of traditional concrete. The manufacture of Portland cement is one of the main sources of atmospheric CO_2 emissions. Considering the problems involved with the use of Portland cement, the present study seeks to synthesize geopolymer from bauxite washing waste (clay) as an alternative to Portland cement. For the purposes of the study, a sample of bauxite washing clay from the company Mining Paragominas, a sample of commercial microsilica from Ecopower and NaOH P.A. from Sigma were used. Geopolymer synthesis was performed according to a Doehlert-type experimental design. The in natura samples were characterized by XRD, FT-IR, TG-DSC, XRF and ICP–OES. The geopolymers were characterized by XRD, FT-IR and mechanical compressive strength testing. The washing clay sample consists of kaolinite (45%), gibbsite (34%), goethite (11%), hematite (7%), anatase (2%) and amorphous phases (1%). The compressive strength values ranged from 8.99 to 41.89 MPa. The best compressive strength results were obtained at a low Na/Al ratio (0.5-0.6) and low curing temperature, which favors the application of the material for the synthesis of geopolymers, contributing to lower energy expenditure and also to lower CO_2 emissions.

Keywords: Kaolinite, Doehlert, hydrosodalite.

1 INTRODUCTION

Civil construction is one of the most important sectors of the world economy due to the rapid growth of global population. Concrete is one of the most essential products for this sector and is usually used in the construction of infrastructure (buildings, houses, etc.), roads, dams, tunnels and elevated tracks[1–3]. The attraction of this product is its unique properties, especially mechanical strength and hardness [3]. The annual production of concrete is approximately 10 billion tons.

Ordinary Portland cement is the major ingredient of traditional concrete. It acts as a binder in concrete, conferring thermal properties, as well as high strength and durability when combined with water. Despite its attractive properties, the use of Portland cement is questionable in an environmental context, not because of its use, but because of its manufacturing process. The manufacture of Portland cement requires the use of high temperatures and an amount of limestone, which makes its production one of the main sources of atmospheric CO_2 emissions [1,3–5].

Many alternatives have been considered to mitigate the effects of the use of Portland cement in civil construction. Among the solutions suggested by the scientific community, geopolymers have gained prominence as an "eco-friendly" substitute for Portland cement. Geopolymers are amorphous/crystalline inorganic polymers synthesized from the reaction of aluminosilicates with a highly alkaline solution[6–8].

The characteristics that make the use of geopolymers feasible are the type of raw material used and the low energy cost required for their production. Numerous materials can be used as precursors of geopolymers, such as clay waste[1], fly ash[9], natural pozzolan[10], red mud and glass waste[4], iron/nickel slag [11], and rice husk ash[12]. Depending on the mineral composition of the material used in the synthesis, thermal pretreatment is sometimes applied to the material to improve its reactivity during the synthesis process.

Currently, the material that stands out the most for this application is tailings/residues from industrial activities, especially mining activities, due to the high volume of residues that can be formed during mining and processing[4]. A branch of mining that generates a large amount of waste is the processing of bauxite ore in the Amazon region. This activity produces a high volume of waste, which is usually deposited in "tailings ponds" where the material remains static and, because it is considered sterile, has no specific destination. The mineralogical composition of this material varies and

includes minerals rich in Al_2O_3 (gibbsite and kaolinite), SiO_2 (kaolinite), Fe_2O_3 (hematite and goethite) and TiO_2 (anatase). Finding a sustainable and economically viable application for this material is one of the dilemmas faced by companies that generate this waste. Based on the mineralogical characteristics of this material and the large amount available, the present study aims to synthesize geopolymers without any thermal pretreatment from bauxite washing clay of the Mining Company Paragominas SA (Norsk Hydro), located in Paragominas-PA, Brazil.

2 MATERIALS AND METHODS

2.1 RAW MATERIAL

The material used in the study was bauxite washing clay (ALB-1) from the company Mineração Paragominas S.A (Hydro), located in the municipality of Paragominas, Pará, Brazil. The sample was collected directly from the "waste tailpipe" with the aid of a hose that transported the sample to the collection container. The collection was performed by company employees. In addition to ALB-1, a commercial microsilica sample (MCR-1) from Ecopower was used to obtain the desired Si/Al ratio in the study.

2.2 SAMPLE CHARACTERIZATION

2.2.1 Mineralogical identification by XRD

Identification of the mineralogical phases of the *in natura* and calcined samples was performed by powder X-ray diffraction (XRD). A BRUKER diffractometer (model: D2 PHASER) with a θ/θ goniometer, radius: 141.1 nm, angular range of 0-70°, step of 0.01°, time per step of 1 s, and a copper anode with a characteristic emission line of 1.54 Å/8.047 keV (Cu-Kα1) and a maximum power of 300 W (30 kV x 10 mA) was used. The detector was a Linear Lynxeye with a 5° 2θ aperture and 192 channels. The analyses were performed at the Laboratory of Mineralogy, Geochemistry and Applications (LAMIGA-UFPA) of the Institute of Geosciences of UFPA.

2.1.1 Quantification of the mineral phases

The quantification of the mineral phases was obtained from XRD Rietveld refinements. The crystallographic information files (.cif data) used in the refinements were obtained from the Inorganic Crystal Structure Database (ICSD) from FIZ Karlsruhe and are displayed in Table 1.

The amorphous contents were quantified using the external standard method[13]. For this quantification, a pure, single crystal of hyaline quartz was ground to powder, xrd-measured under the same conditions as the samples, refined with the Rietveld method and used as an external crystalline standard. Here, the amorphous content includes amorphous, possibly low-ordered phases (i.e., "low-crystallinity" phases) that result in misfits in the Rietveld refinements or no characterized phases present in minor contents.

Due to the high complexity of the XRD patterns, with peaks characteristic of amorphous and low-ordered phases, the phase and amorphous amounts obtained in the Rietveld refinements are considered semiquantitative results.

Table 1 - Phases and ICSD codes used in the Rietveld refinements.

Phase	Chemical formula	Space group	ICSD code	Reference
anatase	TiO_2	$I4_1/amd$	92363	[14]
gibbsite	$Al(OH)_3$	$P2_1$	6162	[15]
goethite	$(Fe_{0.83}Al_{0.17})O(OH)$	Pnma	109411	[16]
hematite	Fe_2O_3	R-3c	82137	[17]
hydrosodalite	$Na_8(Al_6Si_6O_{24})(OH)_2(H_2O)_2$	P222	20630	[18]
hydrosodalite	$Na_8(Al_6Si_6O_{24})(OH)_2$	P-43n	60840	[19]
hydrosodalite	$Na_{3.68}(Al_{3.6}Si_{8.4}O_{24})(H_2O)_{1.2}$	P-43m	201587	[20]
kaolinite	$Al_2Si_2O_5(OH)_4$	P1	63192	[21]
quartz	SiO_2	$P3_121$	16331	[22]
zeolite Na-K-4	$(Na_{7.36}H_{1.64})Al_9Si_{15}O_{48}(H_2O)_{4.68}$	Pm-3m	85517	[23]

2.2.2 Chemical analysis (XRF)

Chemical analysis of the samples was performed by X-ray fluorescence spectrometry (XRF) through the preparation of fused pellets. The tablets were prepared with a sample/flux ratio (lithium tetraborate) established according to the XRF79C_10 method. The analyses were performed in the chemical analysis laboratory of the company SGS GEOSOL, located in Vespasiano/MG.

The loss on ignition (LOI) of all samples was determined by the gravimetric method by calcination at 1000 °C of previously dried samples.

2.2.3 Determination of reactive silica and available alumina

The percentage of reactive silica and available alumina was determined in the chemical analysis laboratory of the company SGS GEOSOL according to the method established by the company (ICP05V), which consists of dissolving the sample in concentrated NaOH solution in a system with controlled pressure and temperature (150 °C). From the obtained solution, the usable aluminum concentration was determined by inductively coupled plasma optical emission spectroscopy (ICP–OES). The solid phase resulting from the dissolution step was dissolved in HCl solution, which allowed determination of the percentage of reactive silica by ICP–OES.

2.2.6 Material characterization by Fourier transform infrared spectroscopy (FT-IR)

Fourier transform infrared spectroscopy (FT-IR) was used to complement the XRD results for the samples and geopolymers. This technique was also used to characterize the "white powder" that was observed mainly on the surface of the geopolymers. The analyses were performed using approximately 0.0015 g of sample that was mixed and homogenized with 2 g of potassium bromide (KBr, Merck). Then, pellets were formed in steel molds in the form of discs 14 mm in diameter and pressed under a pressure of 8 kbar in a Specac 8 manual press. The analyses were performed in a Vertex 70 instrument (Bruker) in the spectral range of 400-4000 cm^{-1}. This procedure was performed at LAMIGA-UFPA of the Institute of Geosciences of UFPA.

2.2.8 TG/DSC analysis

Thermogravimetry/differential scanning calorimetry (TG/DSC) analysis was performed to understand the thermal behavior and possible reactions during the heating process of the investigated samples. Samples were analyzed in an STA 449 F5 Jupiter instrument (NETZSCH) with a simultaneous thermal analyzer equipped with a vertical cylindrical oven under N_2 flow of 50 ml/s, a heating rate of 10 °C/min, and temperature range of 30 °C to 1100 °C. This procedure was performed at LAMIGA-UFPA of the Institute of Geosciences of UFPA.

2.3 SYNTHESIS AND CHARACTERIZATION OF GEOPOLYMERS

2.3.3 Synthesis of geopolymers

The synthesis of the geopolymers were performed according to response surface methodology (RSM) based on a Doehlert design, with 6 experiments and 3 replicates at the central point (Table 2). In this type of planning, the influence of 2 variables in relation to a given response is evaluated: one variable is evaluated at 5 different levels, and the other is analyzed at 3 levels. The dependent variables chosen in the study were temperature and Na/Al ratio (Table 1). The independent variable was compressive strength.

For geopolymer synthesis, ALB-1 was dried at 48 h at room temperature and then transferred to an oven for another 2 h at 105 °C to accelerate the loss of moisture in the sample. To form the specimens, a mixture of 23 g of ALB-1 and 7 g of MCR-1 were weighed to reach a molar Si/Al ratio of 3.5. This mixture was transferred to a porcelain vessel. To this mixture was slowly added a solution of 4.6 ml NaOH, which was homogenized with a pestle for approximately 5 min. The water volume was fixed at 4.6 ml so that there were no differences in the pressing time of the specimens. The mass of NaOH in solution was established by the molar ratio of Na/Al predefined in Table 1. The formed geopolymer paste was reserved in polyethylene pots, which were then capped and held at room temperature for 1 h 30 min. After this period, the geopolymer paste was molded in steel molds (dimensions of 50 mm x 20 mm x 30 mm) with uniaxial pressing under a pressure of 15 kgf/cm^2 in a hydraulic press (Karl Kolb, model PW-40). The shaped specimens were sealed in film paper (for moisture control) and placed in an oven at 40 °C for 24 h. Then, the temperature was increased by 10 °C/h until reaching the final temperature established in the experiments.

Table 1 - Independent variables with their real and coded values used in the Doehlert statistical design.

Na/Al		Temperature	
Coded	Real	Coded	Real
-1	0,5	-0,866	100
-0,5	0,6	0	275
0	0,7	0,866	450,0
0,5	0,8		
1	0,9		

Table 2 - Experimental matrix and real and coded values of the independent variables.

	Temperature		Na/Al	
Exp.	Coded	Real	Coded	Real
G1	0.866	450	0.5	0.8
G2	0.866	450	-0.5	0.6
G3	0	275	-1	0.5
G4	0.866	100	-0.5	0.6
G5	0.866	100	0.5	0.8
G6	0	275	1	0.9
G7	0	275	0	0.7
G8	0	275	0	0.7
G9	0	275	0	0.7

3.3.4 Mechanical compressive strength

Compressive strength testing of the specimens was performed in a universal testing machine (300/15 kN, Servo-plus evolution, MSTEST) with a test speed of 0.1 MPa/sec, initial test value of 1 N and final load of 30%. The test was performed in the concrete laboratory of the Architecture School of UFPA.

3 RESULTS AND DISCUSSION

3.1 Sample characterization

3.1.1 Mineralogy obtained by XRD

. The mineralogy of ALB-1 sample consists of kaolinite (45%), gibbsite (34%), goethite (11%), hematite (7%), anatase (2%) and amorphous phase (1%) (Figure 1). This mineralogical composition is very similar to bauxite clay cover [24]. kaolinite present in the sample has a low structural order, showing an anomalous diffractogram that results in miss-fit in the Rietveld refinement; similar behavior was also observed in the refinement of kaolinite in bauxites of the Amazon and in their corresponding cover (Belterra clay)[25–27]. The low structural order of the kaolinite contributes to greater reactivity of this mineral, which favors the use of the sample in the synthesis of geopolymers without thermal pretreatment.

The high percentage of gibbsite can react with NaOH, similar to what occurs in the Bayer process.

Al-goethite, hematite and anatase minerals are inert under the studied synthesis conditions, but the presence of these minerals can influence both the synthesis mechanism and the final properties of geopolymers.
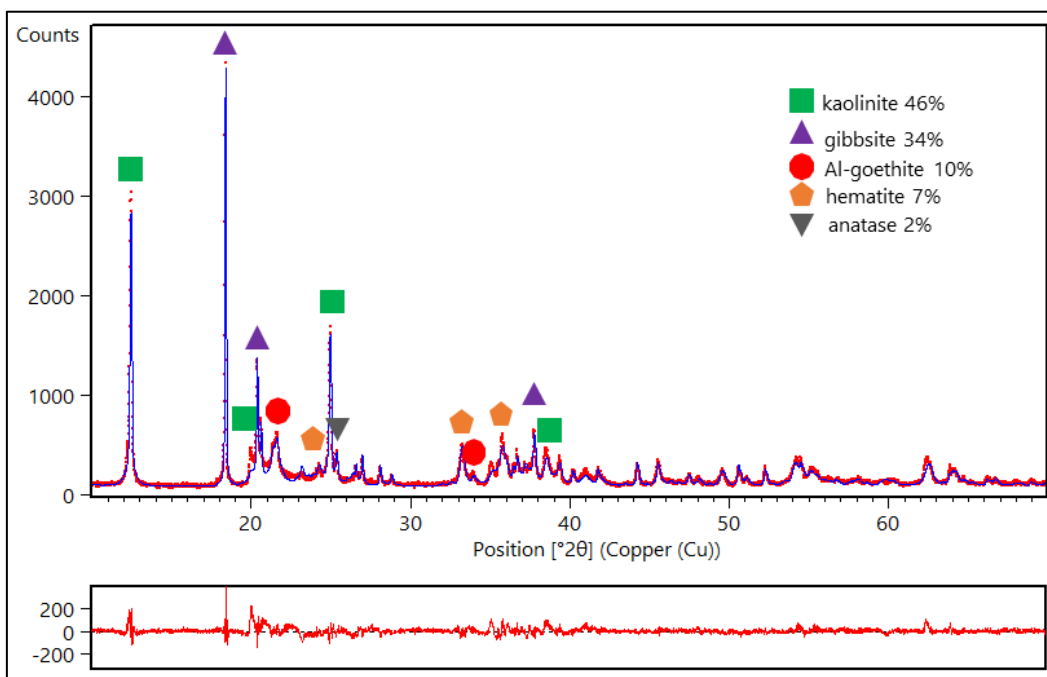

Figure 1- Rietveld-refined XRD results for ALB-1: GOF: 1.61, Rwp: 11.87.

3.1.2 Chemical composition

The chemical analyses of the samples show the main chemical constituents (as oxides) present in the samples (Table 2). As expected, ALB-1 shows high percentages of Al_2O_3 (41.12%), SiO_2 (23.00%) and Fe_2O_3 (15.35%). The percentages of SiO_2 and reactive silica are related to kaolinite, indirectly revealing percentages of 48.45% and 47.26% of this mineral, respectively, a result similar to that obtained by the semiquantitative analysis of the Rietveld-refined XRD data (Figure 1). The Al_2O_3 content is attributed to kaolinite and gibbsite (also Al-goethite) present in the sample. The Fe_2O_3 content is attributed to goethite and hematite.

The MCR-1 sample is mainly composed of SiO_2 (97.4%) and contains 1.42% other compounds.

The chemical analysis results allowed to calculate the Si/Al and Na/Al ratios used in the syntheses of the geopolymers.

Table 2- Chemical composition of the samples.

Sample	SiO$_2$	Al$_2$O$_3$	Fe$_2$O$_3$	LOI	Others	Total	SiO$_2$-Re
ALB-1	23.00	41.12	15.35	18.73	2.45	100.65	22.00
MCR-1	97.4	0.05	0.05	0.69	1.42	99.51	- -

SiO$_2$-Re: reative SiO$_2$

3.1.3 FT-IR spectra of in natura samples

Figure 2 shows the FT-IR results for the studied samples. The spectrum of ALB-1 shows characteristic peaks of the kaolinite phase, with absorption bands at 3437, 3525, 3620 and 3695 cm^{-1} that are related to O-H bonds. The absorption at 1635 cm^{-1} is attributed to the vibration of water molecules. The band at 1100 cm^{-1} is attributed to the stretching of Si-O bonds of kaolinite. The symmetric stretching of the Si–O–Si bonds of kaolinite is indicated by the absorption band at 1010 cm^{-1}. The bands at 912 cm^{-1} and 796 cm^{-1} are related to the angular deformation vibration of Al–OH bonds and the translational vibration of –OH (Al–OH) bonds of gibbsite. The bands at 468 and 750 cm^{-1} are characteristic of the symmetric stretching of Al–O bonds. The absorption band at 538 cm^{-1} is related to the angular deformation of Fe-O bonds. These results are in agreement with those obtained by[28–32].

The MCR-1 material shows a wide band at 3452 cm^{-1} and a band at 1620 cm^{-1}, which are characteristic of physically adsorbed water on the sample surface[10]. A band

between 1000 and 1250 cm^{-1} is observed, which is attributed to Si-O bonds in amorphous aluminosilicates. The bands at 806 and 478 cm^{-1} are related to Al–O bonds (Si,Al–O)[30].
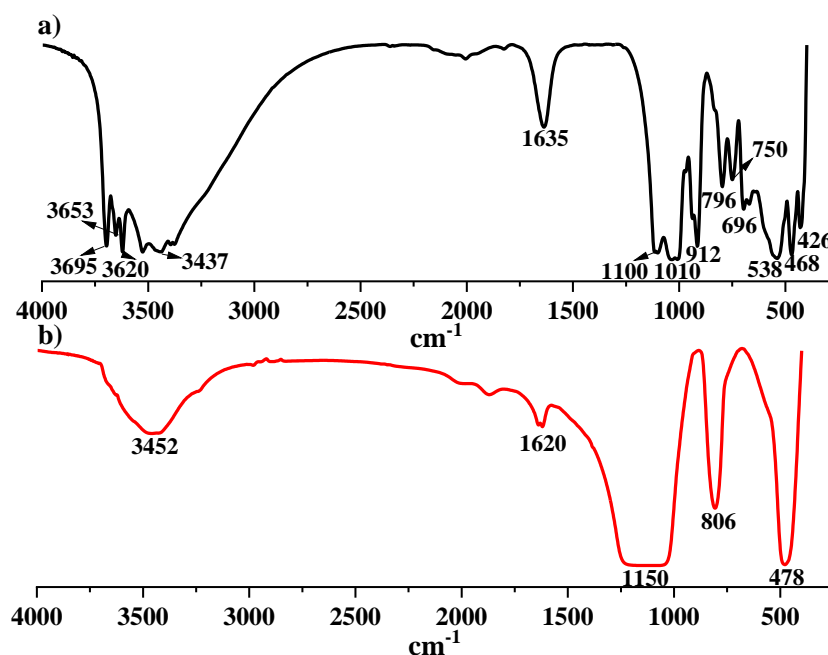
Figure 2- FT-IR spectra of the samples: a) ALB-1, b) MCR-1.

3.1.4 TG/DSC curves

The thermal behavior of ALB-1 is shown in Figure 3. The sample shows three endothermic events and one exothermic event. The first endothermic event occurs at a temperature of 293 °C, which can be attributed to the dehydroxylation of gibbsite. The second endothermic event occurs at a temperature of 358 °C and is related to the structural water loss of goethite. The third endothermic event is observed at 510 °C and is related to the structural water loss of kaolinite. The only exothermic event occurs at a temperature of 980 °C, characteristic of the formation of a new crystalline phase (mullite/spinel).

The dehydroxylation of the kaolinite begins at a temperature of 437.6 °C (onset). This temperature guided the selection of the maximum geopolymer curing temperature of 450 °C, considering that at this temperature, only some kaolinite has undergone complete dehydroxylation, allowing the influence of this behavior on the synthesis of geopolymers to be evaluated.
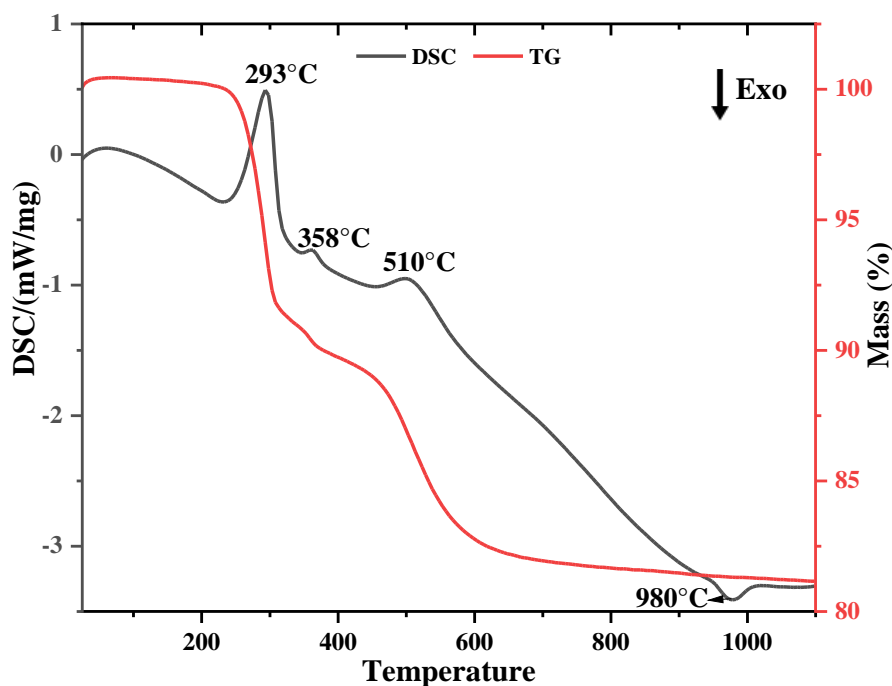
Figure 3- TG/DSC curves of ALB-1.

3.2 CHARACTERIZATION OF GEOPOLYMERS

3.2.1 Mineralogy obtained by XRD

The phase assembly of the synthesized geopolymers includes all the minerals originally present in ALB-1, plus zeolite and hydrosodalite, formed by the reaction of the sample with NaOH (Figure 4).

The semiquantitative results show that the kaolinite and gibbsite contents decreased in all geopolymers when compared to the percentages in the in natura sample (Table 3 and Figure 5), indicating that some kaolinite has been transformed (zeolite and/or hydrosodalite) during the geopolymerization reaction.

A simple comparison between the XRD diffractograms of ALB-1 and the geopolymers shows a greater background in the diffractograms of the geopolymers (Figure 4-B), which is characteristic of a high percentage of amorphous compounds. According to the semiquantitative results, the amorphous percentage ranged from 30 to 39% in the geopolymers. This percentage of amorphous material can be attributed to both the formation of geopolymers and the formation of other components from the dehydroxylation of kaolinite and gibbsite.

In the diffractograms of geopolymers G1 and G2, cured at the highest temperature (450 °C), the characteristic peaks of gibbsite and goethite are no longer noticeable. On the other hand, the amorphous percentage is higher than that of the G4 and G5 geopolymers, which were produced at the same Na/Al ratio but cured at 100 °C. This difference in the amorphous percentage is due to the decomposition of gibbsite and goethite (loss of structural water), which occurs at temperatures of 270 °C and 340 °C, respectively. The dehydroxylation of goethite results in the formation of hematite[33], while gibbsite decomposes and forms amorphous ρ-Al_2O_3[34], as shown by the high percentage of amorphous phases in the G1 and G2 geopolymers cured at 450 °C (Table 3).

Comparing the mineralogical composition of geopolymers G1, G2, G4 and G5 (Table 2) to each other's, it is observed that the formation of hydrosodalites was favored at a Na/Al ratio of 0.8 (highest Na/Al ratio), regardless of the curing temperature used. In contrast, the formation of zeolite (zeolite Na-ZK-4) was only observed at a Na/Al ratio of 0.6 (geopolymers G2 and G4).

Table 3-XRD-Rietveld semiquantitative results for the mineral phases in ALB-1 and in the produced geopolymers.

| Phases / samples	ALB-1	G1	G2	G4	G5	G9
kaolinite ($Al_2Si_2O_5(OH)_4$)	45	28	35	32	26	29
gibbsite ($Al(OH)_3$)	34	- -	- -	6	4	5
Al-goethite ($Fe_{0.83}Al_{0.17})O(OH)$	11	- -	- -	11	9	10
hematite (Fe_2O_3)	7	11	13	7	8	7
anatase (TiO_2)	2	2	2	2	2	2
hydrosodalite ($Na_8(Al_6Si_6O_{24})(OH)_2(H_2O)_2$)	- -	15	8	3	16	11
hydrosodalite ($Na_8(Al_6Si_6O_{24})(OH)_2$)	- -	- -	1	- -	- -	- -
hydrosodalite ($Na_{3.68}(Al_{3.6}Si_{8.4}O_{24})(H_2O)_{1.2}$)	- -	5	2	6	5	4
zeolite Na-ZK-4 (($Na_{7.36}H_{1.64})Al_9Si_{15}O_{48}(H_2O)_{4.68}$)	- -	- -	1	2	- -	- -
amorphous	1	39	39	30	31	33
quartz (SiO_2)	- -	- -	- -	- -	1	- -
total	100	100	100	100	100	100
curing temperature	- -	450	450	100	100	275
Na/Al ratio	- -	0.8	0.6	0.6	0.8	0.7
GOF	1.72	1.5	1.42	1.58	1.46	1.46
Rwp	12.68	11.08	10.51	11.35	10.46	10.86
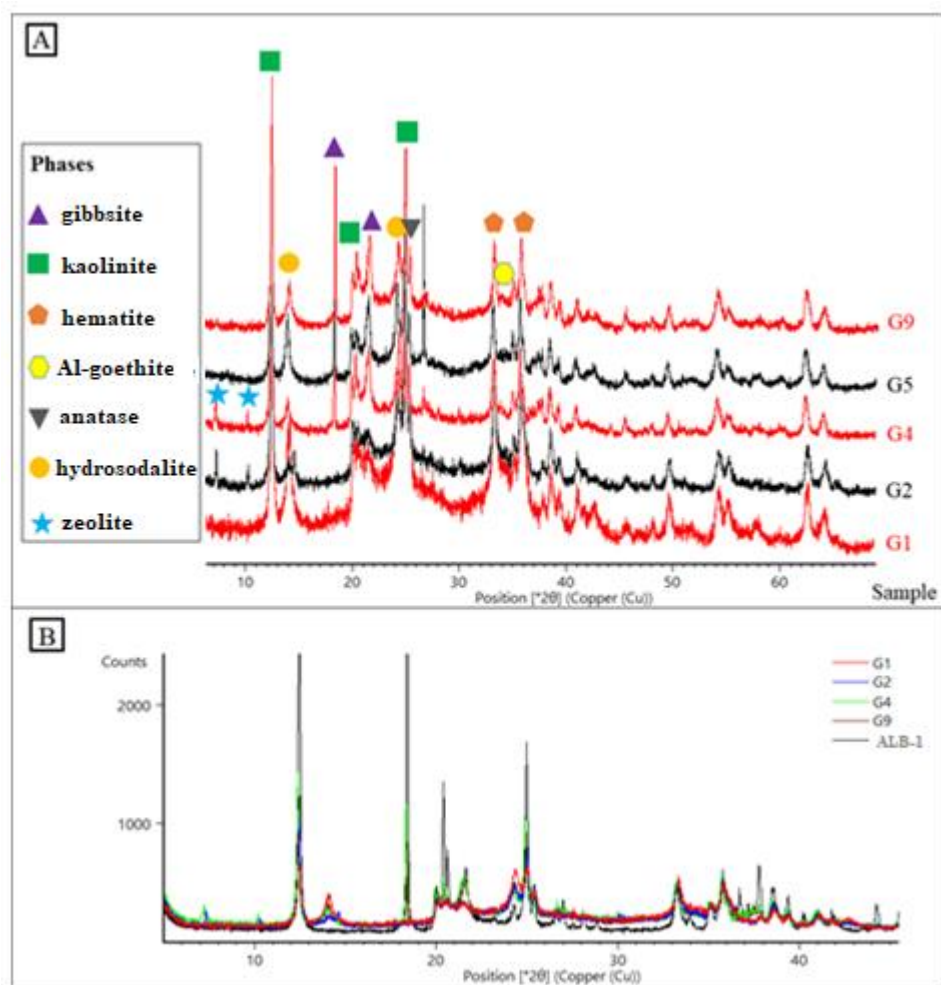
Figure 4- A- XRD patterns of the geopolymers. B: Same patterns overlapped with the pattern of ALB-1, demonstrating the higher background of the former.
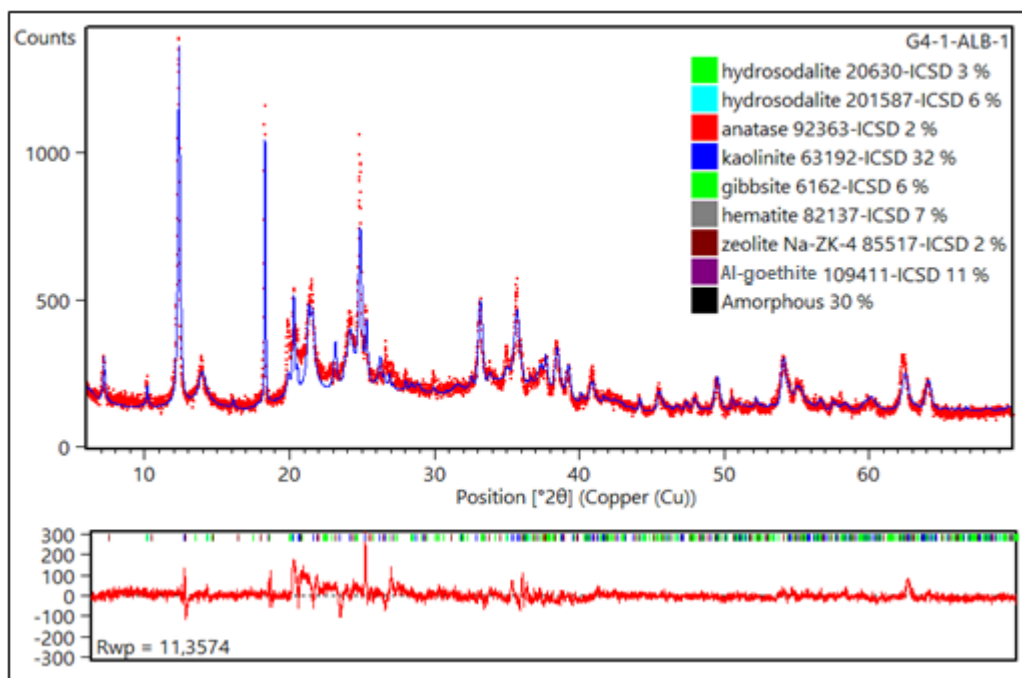

Figure 5- XRD-Rietveld semiquantitative results for the mineral phases in G4-1 produced geopolymers.

3.2.2 FT-IR spectra

Figure 6 shows the FT-IR results for the geopolymers. The permanence of the bands exhibited by the in natura samples was observed (3622-3620 cm^{-1}, 370-3695 cm^{-1}, 3525 cm^{-1}, 3464-3452 cm^{-1}, 1660-1652 cm^{-1}, 1116-1100 cm^{-1}, 1006-1004 cm^{-1}, 914-910 cm^{-1}, 702-696 cm^{-1}, 543-540 cm^{-1}, 470-468 cm^{-1}). These bands are associated with the presence of O–H (3622-3620 cm^{-1}, 370-3695 cm^{-1}, 3525 cm^{-1}, 3464-3452 cm^{-1}), H–OH (1660-1637 cm^{-1}), Si–O–Si (1006-1004 cm^{-1}), Al–OH (914-910 cm^{-1}), Si–O–Al (702-696 cm^{-1} and 470-468 cm^{-1}) and Fe–O (543-540 cm^{-1}) groups.

The absorbance of the OH band in the region of 3622-3420 cm^{-1} is in accordance with the increase in temperature, showing the structural loss of gibbsite, goethite and kaolinite. The same behavior is observed in the region of 1660-1637 cm^{-1}, which corresponds the presence of surface water.

The difference in band intensity at 1004 cm^{-1} is a result of the increased dissolution of aluminosilicates, confirming the activation of the geopolymers[4]. The absorbance intensity differs among the geopolymers. The band at 794 cm^{-1} is slightly shifted compared to that of ALB-1 in natura, in addition to exhibiting a change in intensity, which is indicative of the formation of the geopolymer[10]. In addition, in ALB-1, there is a broad band at 538 cm^{-1} and a band at 468 cm^{-1}. These bands are also present in the geopolymer spectra; the 538 cm^{-1} band becomes thinner and is shifted to 543-540 cm^{-1}, and the 468 cm^{-1} band is shifted to 468-470 cm^{-1}; this change may be indicative of the presence of hydrosodalites/zeolites[35], agreeing with the XRD results. The absorption band in the region of 1035-1031 cm^{-1} corresponds to the vibration of Si–O–T bonds[32].
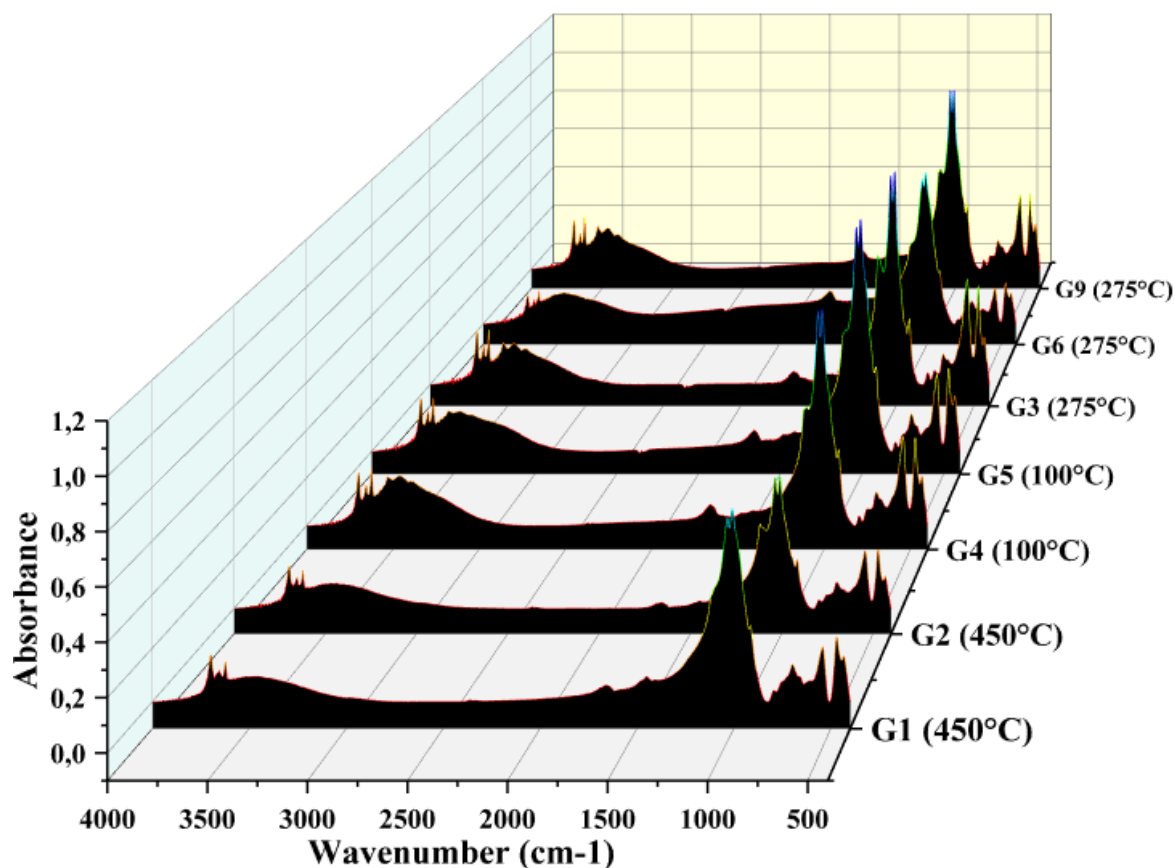
Figure 6- FT-IR spectra of the geopolymer samples.

3.2.3 FT-IR spectra of the "white spot" formed in the geopolymers

Figure 7 shows the FT-IR spectrum of the "white spot" that appears in the geopolymers. The absorption band at 1413 cm⁻¹ can be attributed to the asymmetric stretching of C–O–C bonds due to the formation of Na_2CO_3 or $NaHCO_3$ resulting from the reaction of the CO_2 in the environment with excess NaOH that did not react in the geopolymerization process[36–38]. The presence of the band at 1637 cm⁻¹ may be related to the O–H bonds of physically adsorbed water on the sample surface, which may react with the C–O–C bond of sodium bicarbonate[39–41]. Absorption in the 3465 cm⁻¹ region is characteristic of the stretching of O–H bonds, which may be related to the presence of sodium bicarbonate ($NaHCO_3$).42]. The other bands in the spectrum have already been described in Figure 6.
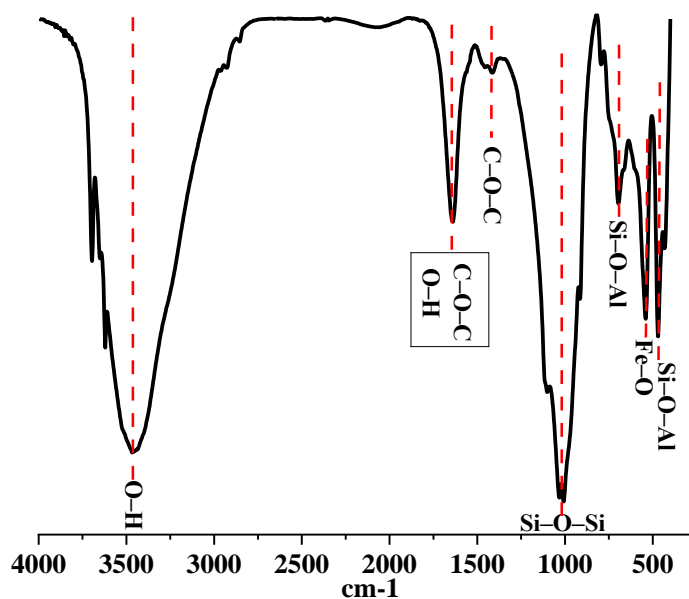
Figure 7- FT-IR spectrum of the white spot.

3.2.4 Compressive strength

Figure 8 shows the compressive strength results for the geopolymers. The compressive strength values range from 8.99 to 41.89 MPa. The lowest strength (8.99 MPa) is obtained at a Na/Al ratio of 0.9 and curing temperature of 275 °C, while the highest value is achieved at a Na/Al ratio of 0.6 and curing temperature of 100 °C.

The compressive strength results follow a trend inversely proportional to the Na/Al molar ratio and the percentage of hydrosodalite formed in the geopolymers.

For example, the lowest strength values are obtained at ratios of 0.8 and 0.9 (8.99, 19.51 and 23.08 MPa), corresponding to the highest percentages of hydrosodalite (Table 2). Based on these results, it can be inferred that the presence of a considerable percentage of hydrosodalite negatively affects the strength gain of the geopolymers. Another factor that may have contributed to lower resistance is the carbonation process (Figure 7), which occurred mainly at the highest ratios studied (0.8 and 0.9) due to excess NaOH that did not react in the geopolymerization process.

The highest compressive strength values are obtained at the lowest ratios (0.5, 0.6 and 0.7). At these ratios, the percentage of the all hydrosodalite types is much lower than that at ratios of 0.8 and 0.9, which favored strength gain.
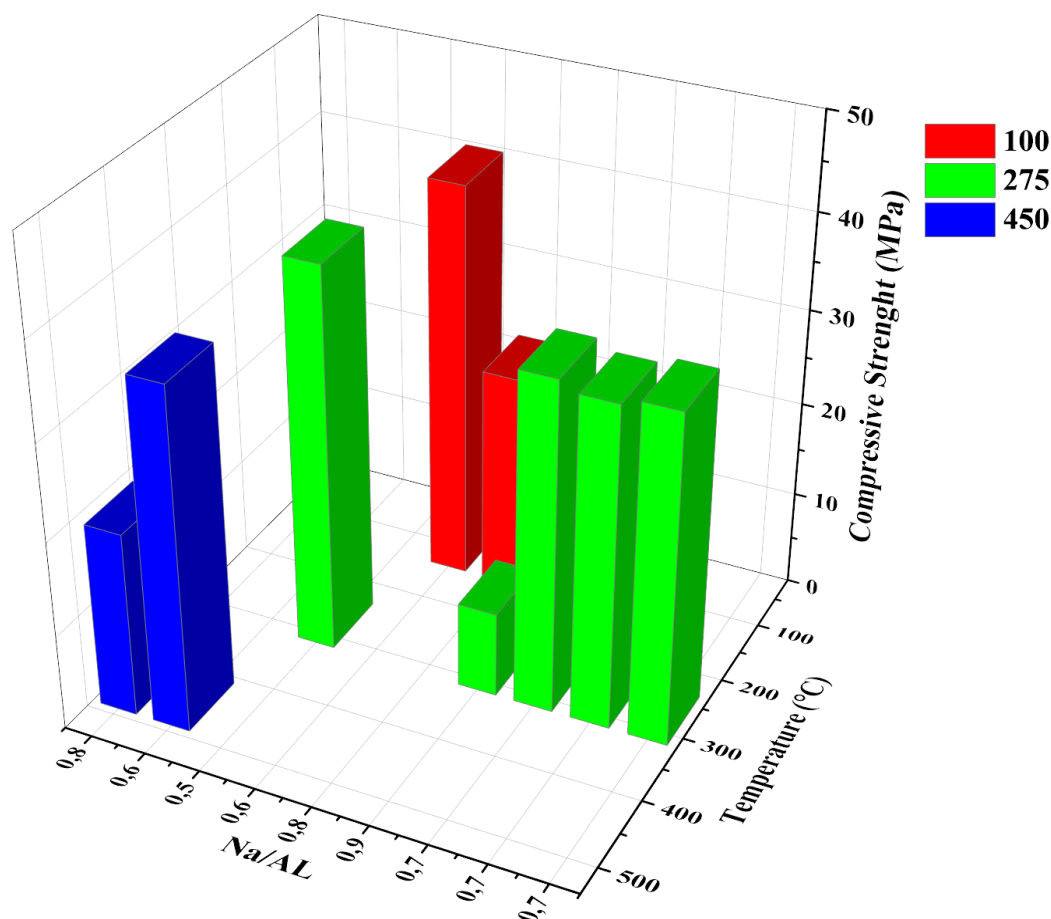
Figure 8- Compressive strength of the geopolymer samples.

3.2.6 Statistical parameters

Regression analysis was performed to evaluate the effect of the dependent variables (Na/Al ratio and temperature) on the compressive strength of the geopolymers (Table 4).

From the analysis of variance (ANOVA) results (Table 5), it can be seen that the regression model fails the lack of fit test because the ratio of the calculated pure error F value (9.34)/tabulated F value (18.48) is lower than 1. The model also shows a good regression according to the ratio of the model F value (192.15)/tabulated F (9.03). The correlation coefficient (explained variation, 0.99) and adjusted R^2 (maximum explained variation, 0.99) values are close to 1, reinforcing that the studied model is statistically adequate.

Considering the points highlighted above, the coefficients of the model were calculated based on the squared sum of the residuals (0.98) and a t value of 4.3027, with 95% confidence.

Table 4- Conditions of geopolymer synthesis according to the Doehlert statistical design.

Exp. No.	Temperature (X1)		Na/Al (X2)		Response variable: Compressive
	Coded	Real	Coded	Real	strength (MPa) (Y)
1	0.866	450	0.5	0.8	19.51
2	0.866	450	-0.5	0.6	36.09
3	0	275	-1	0.5	40.56
4	-0.866	100	-0.5	0.6	41.89
5	-0.866	100	0.5	0.8	23.08
6	0	275	1	0.9	8.99
7	0	275	0	0.7	34.86
8	0	275	0	0.7	33.88
9	0	275	0	0.7	34.61

Table 5- Analysis of variance (ANOVA) results for the full model.

Source	SS	Degrees of freedom	MS	Model F	Tabulated F	R^2	Adjusted R^2
Model	944.95	5	188.99	192.15	9.03	0,99	0,99
Error	2.95	3	0.98				
Total	947.91	8	118.49				
Pure error	0.52	2	0.26	9.34	18.48		
Lack of fit	2.43	1	2.43				

3.2.7 Coefficients of the RM (Regression Model)

Figure 9 shows the coefficients of the model. Six coefficients were calculated: X0, X1, X2, $X1^2$, $X2^2$, and (X1 × X2). Among the calculated coefficients and their confidence intervals, the coefficients $X1^2$ (T^2) and (X1 × X2) ((Na/Al) × T) were not significant for the proposed model according confidences intervals.
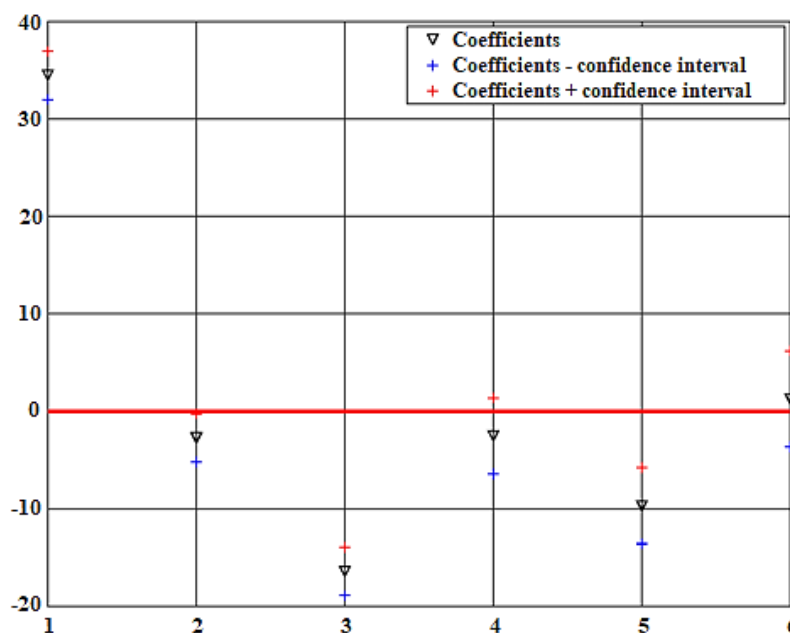
Figure 9- Regression coefficients.

3.2.8 New regression model with only significant coefficients

The ANOVA results (Table 6) for the recalculated model including only significant coefficients demonstrate that the model fails the lack of fit test (calculated F (0.26)/tabulated F (19.19) is less than 1) and has a good regression. The R^2 value (0.98) shows that the regression equation is satisfactory for predicting the mechanical compressive strength within the experimental parameters studied. The R^2 value implies that 98% of the variation in mechanical strength was described by the independent variables.

The coefficients of the model were calculated based on the squared sum of the residuals (2.36) and a t value of 2.7764 with 95% confidence.

Table 6- Analysis of variance (ANOVA) results for the recalculated model.

Source	SS	Degrees of freedom	MS	Model F	Tabulated F	R^2	Adjusted R^2
Model	936.10	3	312.03	132.17	5.41	0,98	0,99
Error	11.80	5	2.36				
Total	947.91	8	118.49				
Pure error	0.52	2	0.26	14.46	19.19		
Lack of fit	11.28	3	3.76				

3.2.9 Coefficients of the new regression model (RM)

The coefficients of the new model are shown in Figure 10. Four coefficients were calculated: X0, X1, X2, and $X2^2$. All coefficients of the model are significant. The model equation can be described as follows:

Mechanical strength RM = 33.44 - 2.70X1 - 16.42X2 – 9.17X1^2
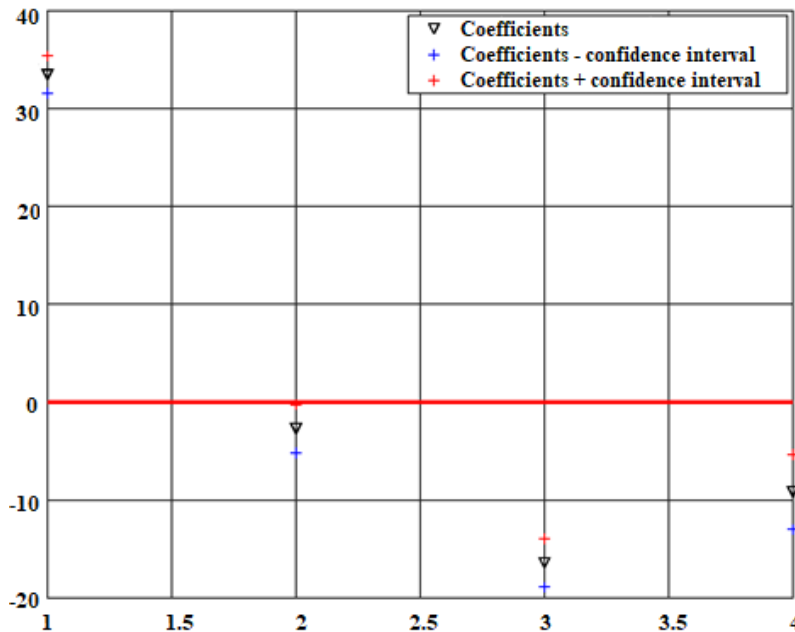
Figure 10- Recalculated regression coefficients.

3.2.10 Response surface and optimization of mechanical strength

The response surface for mechanical compressive strength in relation to the two experimental factors studied (Na/Al and temperature) is shown in Figure 11. Analyzing the three-dimensional graph, it can be seen that the experimental optimum region (40 to 45 MPa) is located in the range of Na/Al ratios between 0.5 and 0.6 and temperatures between 100 and 275 °C. The optimal region includes conditions that have already been tested in experiments 3 (Na/Al 0.5, 275 °C) and 4 (Na/Al 0.6, 100 °C); however, considering energy costs, the conditions of experiment 4 would be better because the resulting material exhibits high resistance at low temperature.
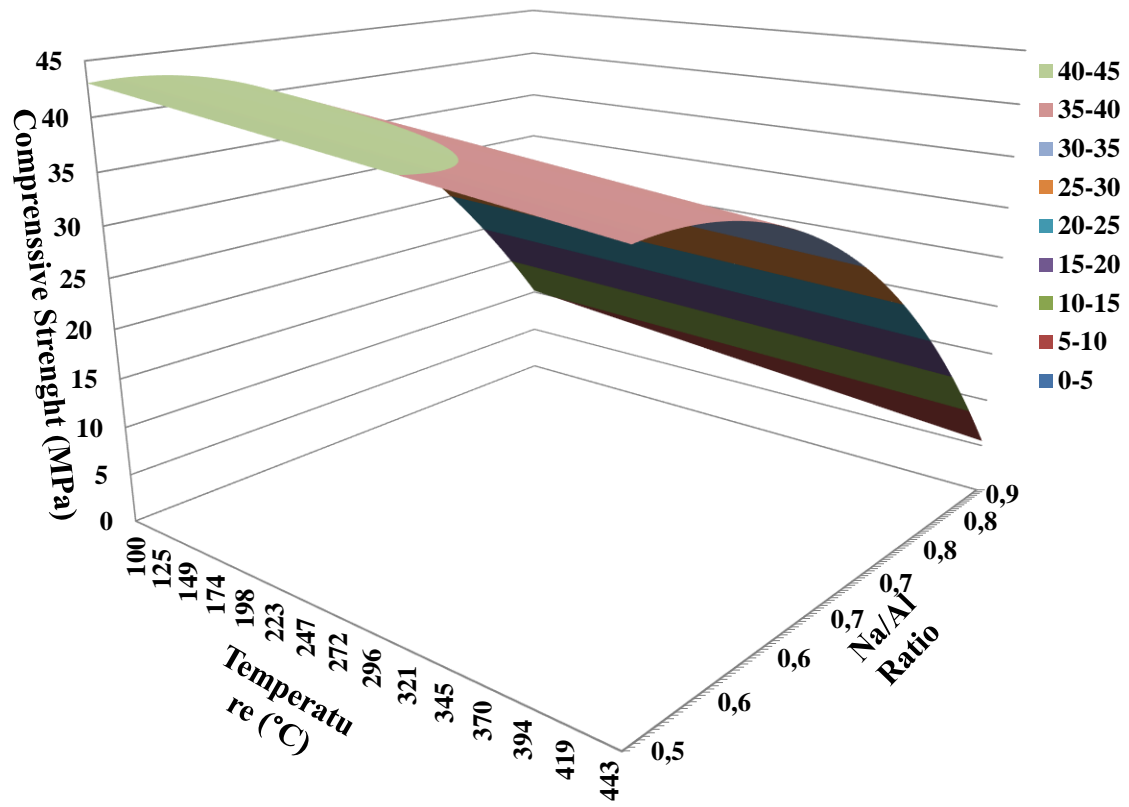
Figure 11- Response surface plot for compressive strength.

4 CONCLUSIONS

Bauxite washing clay contains 45% kaolinite, which allows it to be applied together with amorphous microsilica and NaOH as an alkaline activator in the synthesis of geopolymers. However, the XRD and FT-IR results for the geopolymers showed that not all kaolinite present in the samples reacted and that the reacted percentage formed not only amorphous aluminosilicates, which are sometimes common in geopolymers, but also the crystalline phases hydrosodalite and zeolite; thus, the product formed can be defined as a hybrid material (a mixture of crystalline phases and amorphous material).

The fact that not all kaolinite reacted with the NaOH solution provided NaOH to react with CO_2 and H_2O from the environment, favoring the carbonation process and the formation of sodium carbonate (Na_2CO_3) and sodium bicarbonate ($NaHCO_3$).

Due to the reaction mechanism under the studied synthesis conditions, which favored the formation of hydrosodalite and sodium carbonate/sodium bicarbonate, the mechanical resistance of the geopolymers was negatively affected, especially at a higher Na/Al ratio (0.9 and 0.8) and higher temperature (450 °C). However, the best compressive strength results were obtained at Na/Al ratios of 0.5-0.6 (40.56-41.89 MPa) and temperatures of 100-250 °C, which were defined as the optimal region by the response surface graph.

Considering the points highlighted above, it can be inferred that washing clay is a good starting material for the synthesis of geopolymers, with no need for thermal treatment (formation of metakaolinite) to obtain good mechanical strength. Another favorable factor is the low Na/Al ratio (0.5-0.6), which is necessary to achieve good mechanical properties.

This geopolymer synthesized from bauxite mining waste at low temperature and with a low Na/Al ratio represents a sustainable alternative for the replacement of construction products (cement, concrete, among others), drastically contributing to decreases in energy expenditure and CO_2 emissions in the atmosphere, which is derived of limestone used in Portland manufacture. In addition this product is cheaper than traditional geopolymers that require a Na/Al ratio of 1.1.

5 ACKNOWLEDGMENTS

REFERENCES

[1]   M.F. Zawrah, H.E.H. Sadek, R.E.A. Ngida, S.E.A. Sawan, A.A. El-Kheshen, Effect of low-rate firing on physico-mechanical properties of unfoamed and foamed geopolymers prepared from waste clays, Ceramics International. (2022). https://doi.org/10.1016/j.ceramint.2021.12.356.

[2]   L.N. Assi, K. Carter, E. Deaver, P. Ziehl, Review of availability of source materials for geopolymer/sustainable concrete, Journal of Cleaner Production. 263 (2020) 121477. https://doi.org/10.1016/j.jclepro.2020.121477.

[3]   S. Das, P. Saha, S. Prajna Jena, P. Panda, Geopolymer concrete: Sustainable green concrete for reduced greenhouse gas emission – A review, Materials Today: Proceedings. (2021). https://doi.org/10.1016/j.matpr.2021.11.588.

[4]   N.C. Gomes Silveira, M.L. Figueiredo Martins, A.C. da S. Bezerra, F. Gabriel da Silva Araújo, Ecological geopolymer produced with a ternary system of red mud, glass waste, and Portland cement, Cleaner Engineering and Technology. 6 (2022) 100379. https://doi.org/10.1016/j.clet.2021.100379.

[5]   O. Ayeni, A.P. Onwualu, E. Boakye, Characterization and mechanical performance of metakaolin-based geopolymer for sustainable building applications, Construction and Building Materials. 272 (2021) 121938. https://doi.org/10.1016/j.conbuildmat.2020.121938.

[6]   A.Z. Khalifa, Ö. Cizer, Y. Pontikes, A. Heath, P. Patureau, S.A. Bernal, A.T.M. Marsh, Advances in alkali-activation of clay minerals, Cement and Concrete Research. 132 (2020). https://doi.org/10.1016/j.cemconres.2020.106050.

[7]   D. dos S. da Silva Godinho, F. Pelisser, A.M. Bernardin, High temperature performance of geopolymers as a function of the Si/Al ratio and alkaline media, Materials Letters. 311 (2022) 131625. https://doi.org/10.1016/j.matlet.2021.131625.

[8]   P. Rożek, M. Król, W. Mozgawa, Geopolymer-zeolite composites: A review, Journal of Cleaner Production. 230 (2019) 557–579. https://doi.org/10.1016/j.jclepro.2019.05.152.

[9]   K.M. Klima, K. Schollbach, H.J.H. Brouwers, Q. Yu, Enhancing the thermal performance of Class F fly ash-based geopolymer by sodalite, Construction and Building Materials. 314 (2022). https://doi.org/10.1016/j.conbuildmat.2021.125574.

[10]   D.M. González-García, L. Téllez-Jurado, F.J. Jiménez-Álvarez, L. Zarazua-Villalobos, H. Balmori-Ramírez, Evolution of a natural pozzolan-based geopolymer alkalized in the presence of sodium or potassium silicate/hydroxide solution, Construction and Building Materials. 321 (2022) 126305. https://doi.org/10.1016/j.conbuildmat.2021.126305.

[11]   J.C. Kuri, P.K. Sarker, F.U.A. Shaikh, Sulphuric acid resistance of ground ferronickel slag blended fly ash geopolymer mortar, Construction and Building Materials. 313 (2021) 125505. https://doi.org/10.1016/j.conbuildmat.2021.125505.

[12]   A.L. Freire, C.D. Moura-Nickel, G. Scaratti, A. de Rossi, M.H. Araújo, A. de Noni Júnior, A.E. Rodrigues, E.R. Castellón, R. de Fátima Peralta Muniz Moreira, Geopolymers produced with fly ash and rice husk ash applied to CO2 capture, Journal of Cleaner Production. 273 (2020). https://doi.org/10.1016/j.jclepro.2020.122917.

[13]   R. Snellings, A. Bazzoni, K. Scrivener, The existence of amorphous phase in Portland cements: Physical factors affecting Rietveld quantitative phase analysis, Cement and Concrete Research. (2014). https://doi.org/10.1016/j.cemconres.2014.03.002.

[14]   T.E. Weirich, M. Winterer, S. Seifried, H. Hahn, H. Fuess, Rietveld analysis of electron powder diffraction data from nanocrystalline anatase, TiO 2, Ultramicroscopy. (2000). https://doi.org/10.1016/S0304-3991(99)00189-8.

[15]   H. Saalfeld, M. Wedde, Refinement of the crystal structure of gibbsite, A1(OH)3, Zeitschrift Fur Kristallographie - New Crystal Structures. 139 (1974) 129–135. https://doi.org/10.1524/zkri.1974.139.1-2.129.

[16]   D. Li, B.H. O'Connor, I.-M. Low, A. van Riessen, B.H. Toby, Mineralogy of Al-substituted goethites, Powder Diffraction. (2006). https://doi.org/10.1154/1.2358358.

[17]   V.A. Sadykov, L.A. Isupova, S. V. Tsybulya, S. V. Cherepanova, G.S. Litvak, E.B. Burgina, G.N. Kustova, V.N. Kolomiichuk, V.P. Ivanov, E.A. Paukshtis, A. V. Golovin, E.G. Avvakumov, Effect of mechanical activation on the real structure and reactivity of iron (III) oxide with corundum-type structure, Journal of Solid State Chemistry. (1996). https://doi.org/10.1006/jssc.1996.0168.

[18]   O. Bondareva, Y.A. Malinovskii, Low-temperature investigation of the structure of hydrosodalite, Sov. Phys. Crystallogr. 28 (1983) 273–276.

[19]   S. Luger, J. Felsche, P. Fischer, Structure of hydroxysodalite Na8[AlSiO4]6(OH)2, a powder neutron diffraction study at 8 K, Acta Crystallographica Section C: Crystal Structure Communications. 43 (1987) 1–3.

[20]   S. Cartlidge, W.M. Meier, Solid state transformations of synthetic CHA-and EAB-type zeolites in the sodium form, Zeolites. 4 (1984) 218–225.

[21]   D.L. Bish, R.B. Von Dreele, Rietveld refinement of non-hydrogen atomic positions in kaolinite, Clays & Clay Minerals. (1989). https://doi.org/10.1346/CCMN.1989.0370401.

[22]   H. d'Amour, W. Denner, H. Schulz, Structure determination of α-quartz up to 68 x 10 8 Pa , Acta Crystallographica Section B Structural Crystallography and Crystal Chemistry. (1979). https://doi.org/10.1107/s056774087900412x.

[23]   M.M. Eddy, A.K. Cheetham, W.I.F. David, Powder neutron diffraction study of zeolite Na-ZK-4; an application of new functions for peak shape and asymmetry, Zeolites. 6 (1986) 449–454.

[24]   I. A.R. Barreto, M. L. Costa, Use of the clayey cover of bauxite deposits of the Amazon region for geopolymer synthesis and its application in red ceramics, Construction and Building Materials. 300 (2021) 124318. https://doi.org/10.1016/j.conbuildmat.2021.124318.

[25]   L.B.A. Negrão, M.L. da Costa, H. Pöllmann, The Belterra Clay on the bauxite deposits of Rondon do Pará, Eastern Amazon, Brazilian Journal of Geology. 48 (2018) 473–484. https://doi.org/10.1590/2317-4889201820180128.

[26]   L.B.A. Negrão, T.K.C. Alves, H. Pöllmann, Mineralogical Appraisal of Bauxite Overburdens from Brazil, Minerals. (2021). https://doi.org/https://doi.org/10.3390/min11070677.

[27]   S.P.A. Paz, R.S. Angélica, H. Kahn, Optimization of the reactive silica quantification method applied to Paragominas-type gibbsitic bauxites, International Journal of Mineral Processing. 162 (2017) 48–57. https://doi.org/10.1016/j.minpro.2017.03.003.

[28]   H.T. Roudouane, J.A. Mbey, E.C. Bayiga, P.D. Ndjigui, Characterization and application tests of kaolinite clays from Aboudeia (southeastern Chad) in fired bricks making, Scientific African. 7 (2020) e00294. https://doi.org/10.1016/j.sciaf.2020.e00294.

[29]   B.L. Zhu, C.L. Qi, Y.H. Zhang, T. Bisson, Z. Xu, Y.J. Fan, Z.X. Sun, Synthesis, characterization and acid-base properties of kaolinite and metal (Fe, Mn, Co) doped kaolinite, Applied Clay Science. 179 (2019) 105138. https://doi.org/10.1016/j.clay.2019.105138.

[30]   N. Sazali, Z. Harun, F.H. Azhar, S.S. Bahri, R.P.N.A.R. Ahmad, R. Hussinisa, N. Misdan, The effect of various molarity sodium hydroxide (NaOH) on the hydrosodalite formation from synthesis of Johor Kaolin, Malaysia by hydrothermal method, in: Materials Today: Proceedings, Elsevier Ltd, 2020: pp. 2045–2051. https://doi.org/10.1016/j.matpr.2021.03.135.

[31]   C.R. Kaze, G.L. Lecomte-Nana, A. Adesina, J.G.D. Nemaleu, E. Kamseu, U. Chinje Melo, Influence of mineralogy and activator type on the rheology behaviour and setting time of laterite based geopolymer paste, Cement and Concrete Composites. (2021) 104345. https://doi.org/10.1016/j.cemconcomp.2021.104345.

[32]   M. Li, R. Luo, L. Qin, H. Liu, P. Duan, W. Jing, Z. Zhang, X. Liu, High temperature properties of graphene oxide modified metakaolin based geopolymer paste, Cement and Concrete Composites. 125 (2022) 104318. https://doi.org/10.1016/j.cemconcomp.2021.104318.

[33]   D.G. Schulze, U. Schwertmann, The influence of aluminium on iron oxides: X. properties of Al-substituted goethites, Clay Minerals. (1984). https://doi.org/10.1180/claymin.1984.019.4.02.

[34]   C. Colombo, A. Violante, Effect of time and temperature on the chemical composition and crystallization of mixed iron and aluminum species, Clays and Clay Minerals. (1996). https://doi.org/10.1346/CCMN.1996.0440110.

[35]   M.A. Salam, M. Mokhtar, S.M. Albukhari, D.F. Baamer, L. Palmisano, A.A. AlHammadi, M.R. Abukhadra, Synthesis of zeolite/geopolymer composite for enhanced sequestration of phosphate (PO_4^{3-}) and ammonium (NH_4^+) ions; equilibrium properties and realistic study, Journal of Environmental Management. 300 (2021). https://doi.org/10.1016/j.jenvman.2021.113723.

[36]   V.H.J.M. dos Santos, D. Pontin, G.G.D. Ponzi, A.S. de G. e Stepanha, R.B. Martel, M.K. Schütz, S.M.O. Einloft, F. Dalla Vecchia, Application of Fourier Transform infrared spectroscopy (FTIR) coupled with multivariate regression for calcium carbonate ($CaCO_3$) quantification in cement, Construction and Building Materials. 313 (2021) 125413. https://doi.org/10.1016/j.conbuildmat.2021.125413.

[37]   M. Vafaei, A. Allahverdi, P. Dong, N. Bassim, M. Mahinroosta, Resistance of red clay brick waste/phosphorus slag-based geopolymer mortar to acid solutions of mild concentration, Journal of Building Engineering. 34 (2021). https://doi.org/10.1016/j.jobe.2020.102066.

[38]   P. Baran, M. Nazarko, E. Włosińska, A. Kanciruk, K. Zarębska, Synthesis of geopolymers derived from fly ash with an addition of perlite, Journal of Cleaner Production. 293 (2021). https://doi.org/10.1016/j.jclepro.2021.126112.

[39]   G. Huang, Y. Ji, J. Li, Z. Hou, C. Jin, Use of slaked lime and Portland cement to improve the resistance of MSWI bottom ash-GBFS geopolymer concrete against carbonation, Construction and Building Materials. 166 (2018) 290–300. https://doi.org/10.1016/j.conbuildmat.2018.01.089.

[40]   H. Bekhti, Y. Boucheffa, A.H.A. Blal, A. Travert, In situ FTIR investigation of CO2 adsorption over MgO–Impregnated NaY zeolites, Vibrational Spectroscopy. 117 (2021). https://doi.org/10.1016/j.vibspec.2021.103313.

[41]   T. Belin, C. Mve Mfoumou, S. Mignard, Y. Pouilloux, Study of physisorbed carbon dioxide on zeolites modified by addition of oxides or acetate impregnation, Microporous and Mesoporous Materials. 182 (2013) 109–116. https://doi.org/10.1016/j.micromeso.2013.08.020.

[42]   V. Fiore, T. Scalici, F. Nicoletti, G. Vitale, M. Prestipino, A. Valenza, A new eco-friendly chemical treatment of natural fibres: Effect of sodium bicarbonate on properties of sisal fibre and its epoxy composites, Composites Part B: Engineering. 85 (2016) 150–160. https://doi.org/10.1016/j.compositesb.2015.09.028.

5 CONCLUSÕES GERAIS

A composição mineralógica das duas amostras evidenciada pelas análises de DRX, FTIR e TG/DSC, confirmaram a predominância de caulinita em ambas as amostras. Elas apresentaram gibbsita, goethita, hematita, quartzo e antásio como minerais acessórios. A hematita só está presente na amostra de Argila de Lavagem, enquanto que o quartzo, apenas, na amostra de Argila de Belterra.

Apesar da predominância de caulinita nas amostras ser bastante favorável para síntese de geopolímeros, a presença dos outros minerais afeta negativamente o ganho de resistência dos geopolímeros sintetizados com KOH.

Se compararmos as amostras de Argila de Belterra e a amostra de Argila de Lavagem da Bauxita, ambas apresentam vantagens para aplicação na síntese de geopolímeros. A Argila de Lavagem apresenta vantagens por ter passado por um processo de tratamento (britagem, moagem e classificação) que contribui para que essa amostra seja bastante homogênea e não exija mais etapas de preparação quando aplicada na síntese de geopolímeros. Por outro lado, apesar da amostra de Argila de Belterra não ser uma amostra pré-tratada durante o processo de extração, ela apresenta vantagens por ter maior percentual de caulinita em sua composição.

A resistência a compressão dos geopolímeros sintetizados com as duas amostras, acima de 40 MPa, favorecem a sua aplicação em diversas áreas da construção civil (diferentes tipos de cerâmica, cimento, concreto, entre outros). Por outro lado, as condições de síntese utilizadas com a Argila de Lavagem da Bauxita, colaboram para o que seu uso seja ainda mais atrativo, considerando que a maior resistência foi exibida em razões bem mais baixas de Na/Al (0,5 e 0,6) que as dita como ideal (1,1), reduzindo o consumo de NaOH pela metade, barateando o processo. Outro fato positivo pra o uso da Argila de Lavagem da Bauxita, foi a comprovação da não necessidade de calcinação da amostra, reduzindo o consumo energético.

Analisando os relatos acima, podemos concluir que a aplicação das duas matérias-primas em geopolímero contribui para que esses materiais tenham uma finalidade nobre, que tem ganhado bastante destaque, não só pela comunidade cientifica, mas, também pela indústria da construção civil, por ser considerado um produto Eco-friendly, de baixo consumo energético e um possível substituto do cimento, um produto com alta emissão de CO_2 na atmosfera.

REFERÊNCIAS

Associação Brasileira de Normas Técnicas-ABNT. 2017. *Alvenaria estrutural* - Blocos cerâmicos Parte 3: Métodos de ensaio. 09/08, 34.

Associação Brasileira de Normas Técnicas-ABNT. 2005. *NBR 15270-1*: Componentes cerâmicos. Parte 1: Blocos cerâmicos para alvenaria de vedação - Terminologia e requisitos. Associação Brasileira de Normas Técnicas, 15.

Associação Brasileira de Normas Técnicas-ABNT. 2017. *NBR 15270-2*: componentes cerâmicos Parte 2: Blocos cerâmicos para alvenaria estrutural – Terminologia e requisitos. Associação Brasileira de Normas Técnicas, 15.

Adjei S., Elkatatny S., Aggrey W. N., Abdelraouf Y. 2022. Geopolymer as the future oil-well cement: a review. *Journal of Petroleum Science and Engineering*, **208:**109485, Elsevier B.V.

Albach B., Santos P. H.Vianna dos, Rampon D.da Silveira, Barbosa R. V. 2019. An evaluation of modified Kaolinite surface on the crystalline and mechanical behavior of polypropylene. *Polymer Testing*, **75**:237–245, Nov.

Al-Majidi M. H., Lampropoulos A., Cundy A., Meikle S. 2016. Development of geopolymer mortar under ambient temperature for in situ applications. *Construction and Building Materials*, **120**: 198–211.

Alonso S. & Palomo A. 2001. Calorimetric study of alkaline activation of calcium hydroxide-metakaolin solid mixtures. *Cem Concr Res*., **31**(1):25–30.

Alnahhal A. M., Alengaram U. J., Yusoff S., Darvish P., Srinivas K., Sumesh M. 2022. Engineering performance of sustainable geopolymer foamed and non-foamed concretes. *Construction and Building Materials*, **316**: 125601.

Assi L. N., Carter K., Deave, E., Ziehl, P. 2020. Review of availability of source materials for geopolymer/sustainable concrete. *Journal of Cleaner Production*, **263**: 121477.

ASTM C20-00. 2015. Standard test methods for apparent porosity, water absorption , apparent specific gravity , and bulk density of burned refractory brick and shapes by boiling water. *American Society for Testing and Materials*, 00(Reapproved 2015), 1–3.

Autef A., Joussein E., Poulesquen A., Gasgnier G., Pronier S., Sobrados I., Sanz J., Rossignol S. 2013. Influence of metakaolin purities on potassium geopolymer formulation: The existence of several networks. *Journal of Colloid and Interface Science*, **408**(1): 43–53.

Ayeni O., Onwualu A. P., Boakye E. 2021. Characterization and mechanical performance of metakaolin-based geopolymer for sustainable building applications. *Construction and Building Materials*, **272**: 121938.

Barba A 1997. *Materias primas para lafabricación de soportes de baldosas cerámicas*. 1ª ed. Castellón-Espanha, Instituto de Tecnologia Cerámica-AICE p. 239-255.

Baran P., Nazarko M., Włosińska E., Kanciruk A., Zarębska K. 2021. Synthesis of geopolymers derived from fly ash with an addition of perlite. *Journal of Cleaner Production*, **293**:126-112.

Barbosa T. R., Foletto E. L., Dotto G. L., Jahn S. L. 2018. Preparation of mesoporous geopolymer using metakaolin and rice husk ash as synthesis precursors and its use as potential adsorbent to remove organic dye from aqueous solutions. *Ceramics International*, **44**(1): 416–423.

Barreto I.A.R. & Costa M.L. 2021. Use of the clayey cover of bauxite deposits of the Amazon region for geopolymer synthesis and its application in red ceramics. *Construction and Building Materials*, **300**: 124318, Feb.

Bekhti H., Boucheffa, Y., Blal, A. H. A., Travert, A. 2021. In situ FTIR investigation of CO_2 adsorption over MgO–Impregnated NaY zeolites. *Vibrational Spectroscopy*, **117:**103313.

Belin T., Mve Mfoumou C., Mignard S., Pouilloux Y. 2013. Study of physisorbed carbon dioxide on zeolites modified by addition of oxides or acetate impregnation. *Microporous and Mesoporous Materials*, **182**: 109–116.

Belmokhtar N., Ammari M., Brigui J., Ben Allal L. 2017. Comparison of the microstructure and the compressive strength of two geopolymers derived from Metakaolin and an industrial sludge. *Construction and Building Materials*, **146**: 621-629.

Bergaya F. & Lagaly G. 2006. General introduction: clays, clay minerals, and clay Science. *In:* Bergaya F., Theng B.K.G., Lagaly G. (eds.). *Handbook of clay science*: developments in clay science, Amsterdam, Elsevier, p. 1-18.

Bish D. L. & Von Dreele R. B. 1989. Rietveld refinement of non-hydrogen atomic positions in kaolinite. *Clays & Clay Minerals*. **117**: 103313,

Bhattacharyya S.K. & Singh B. 2012. *High performance materials and construction technologies for sustainable built space*. Supra Institutional Project Report (SIP 29), CSIR-Central Building Research Institute, Roorkee, India.

Bondareva O. & Malinovskii Y. A. 1983. Low-temperature investigation of the structure of hydrosodalite. *Sov. Phys. Crystallogr*, **28**: 273–276.

Buchwald A., Hohmann M., Posern K., Brendler E. 2009. The suitability of thermally activated illite/smectite clay as raw material for geopolymer binders. *Appl. Clay Sci.* **46**: 300–304.

Caglar B., Afsin B., Tabak A. 2007. Benzamide species retained by DMSO composites at a kaolinite surface. *Journal of Thermal Analysis and Calorimetry*, **87**(2): 429–432.

Cartlidge S., Meier W. M. 1984. Solid state transformations of synthetic CHA-and EAB-type zeolites in the sodium form. *Zeolites*, **4**(3): 218–225.

Cheng T., Lee M., Ko M., Ueng T., Yang S. 2012. The heavy metal adsorption characteristics on metakaolin-based geopolymer. *Applied Clay Science*. **56**: 90-96.

Chindaprasirt P., Chareerat, T., Sirivivatnanon V. 2007. Workability and strength of coarse high calcium fly ash geopolymer. *Cement and Concrete Composites*, *29*(3): 224–229.

Colangelo F., Roviello G., Ricciotti L., Ferrándiz-Mas V., Messina F., Ferone C., Tarallo O., Cioffi R., Cheeseman C. R. 2018. Mechanical and thermal properties of lightweight geopolymer composites. *Cement and Concrete Composites*, *86*: 266–272.

Colombo C., Violante A. 1996. Effect of time and temperature on the chemical composition and crystallization of mixed iron and aluminum species. *Clays and Clay Minerals*.

Costa L. M., Almeida N. G. S., Houmard M., Cetlin P. R., Silva G. J. B., Aguilar M. T. P. 2021. Influence of the addition of amorphous and crystalline silica on the structural properties of metakaolin-based geopolymers. *Applied Clay Science*, *215*: 106312.

Cui, X.M., Liu, L.P., He, Y., Chen, J.Y., Zhou, J., 2011. A novel aluminosilicate geopolymermaterial with low dielectric loss. *Mater. Chem. Phys.* **130**: 1–4.

d'Amour H., Denner W., Schulz H. 1979. Structure determination of α-quartz up to 68 x 10 8 Pa. *Acta Crystallographica Section B Structural Crystallography and Crystal Chemistry*.

da Silva Godinho D. dos S., Pelisser F., Bernardin A. M. 2022. High temperature performance of geopolymers as a function of the Si/Al ratio and alkaline media. *Materials Letters*, *311*: 1316-25.

Das S., Saha P., Prajna Jena S., Panda P. 2021. Geopolymer concrete: Sustainable green concrete for reduced greenhouse gas emission – A review. *Materials Today: Proceedings*.

Davidovits J. 1991a. Geopolymers. *Journal of Thermal Analysis*, **37**(8): 1633–1656.

Davidovits, J. 1991b. GEOPOLYMERS Inorganic polymerie new materials. In *Journal of ThamalAnalysis* (Vol. 37).

Davidovits J., Morris, M. 1988. "***The Pyramids, an Enigma Solved***", Dorset Press, New York.

Dimas D, Giannopoulou L, Panias D. 2009. Polymerization in sodium silicate solutions: a fundamental process in geopolymerization technology. *J Mater Sci*;**44**: 3719–30.

Drweesh S. A., Fathy N. A., Wahba M. A., Hanna A. A., Akarish A. I. M., Elzahany E. A. M., El-Sherif I. Y., Abou-El-Sherbini K. S. 2016. Equilibrium, kinetic and thermodynamic studies of Pb(II) adsorption from aqueous solutions on HCl-treated Egyptian kaolin. *Journal of Environmental Chemical Engineering*, **4**(2): 1674–1684.

Dupuy C., Havette J., Gharzouni A., Texier-Mandoki N., Bourbon X., Rossignol S. 2019. Metakaolin-based geopolymer: Formation of new phases influencing the setting time with the use of additives. *Construction and Building Materials*, **200**: 272–281.

Duxson P., Fernández-Jiménez A., Provis J. L., Lukey G. C., Palomo A., Van Deventer J. S. J. 2007. Geopolymer technology: The current state of the art. *Journal of Materials Science*, **42**(9): 2917–2933.

Eddy M. M., Cheetham A. K., David W. I. F. 1986. Powder neutron diffraction study of zeolite Na-ZK-4; an application of new functions for peak shape and asymmetry. *Zeolites*, **6**(6): 449–454.

Farmer V. C. 2000. *Transverse and longitudinal crystal modes associated with OH stretching vibrations in single crystals of kaolinite and dickite*. **56**: 927–930.

Fialips C., Petit, S., Decarreau A., Beaufort D., Umr-cnrs L. H. A. S. A., Poitiers U. de, Pineau R., & Cedex F.-P. 2000. Influence of synthesis pH on kaolinite " crystallinity " and surface properties. *Clays and Clay Minerals*, **48**(2): 173–184.

Filipponi A., Masi G., Bignozzi M. C. 2021. Pressing metakaolin-based one-part geopolymers: Influence of the mix design on microstructural and physical properties. *Ceramics International* **48**: 5814-5823.

Fiore V., Scalici T., Nicoletti F., Vitale G., Prestipino M., Valenza A. 2016. A new eco-friendly chemical treatment of natural fibres: Effect of sodium bicarbonate on properties of sisal fibre and its epoxy composites. *Composites Part B: Engineering*, **85**: 150–160.

Freire A. L., Moura-Nickel C. D., Scaratti G., de Rossi A., Araújo M. H., de Noni Júnior A., Rodrigues A. E., Castellón E. R., de Fátima Peralta Muniz Moreira R. 2020. Geopolymers produced with fly ash and rice husk ash applied to CO2 capture. *Journal of Cleaner Production*, **273**: 122917 .

Frost R. A. Y. L., Vassallo A. M. 1996. The Dehydroxylationof the kaolinite clay mineral susingin frared emission spectroscopy. *Clays and Clay minerals*, **44**(5): 635–651.

Granizo, N., Palomo, A., Fernandez-Jim_enez, A., 2014. Effect of temperature and alkaline concentration on metakaolin leaching kinetics. Ceraamic International **40**: 8975-8985.

Greig W. 1977. *Trombetas and Other Amazon Bauxites*. [S.l.], Society Mining Engineers AIME, Brazil, 34 p.

Glid M., Sobrados I., Rhaiem H. Ben Sanz J., Amara A. B. H. 2017. Alkaline activation of metakaolinite-silica mixtures: Role of dissolved silica concentration on the formation of geopolymers. *Ceramics International*, **43**(15): 12641–12650.

Glukhovsky, V.D. 1994. "*Ancient, Modern and Future Cements*", *First International Conference on Alkaline Cements and Concretes*, Kiev State Technical University, pp. 1-8. Johansen, I.L., 2011. Chapter 2 29–63.

Gomes Silveira N. C., Figueiredo Martins M. L., Bezerra A. C. da S., Gabriel da Silva Araújo F. 2022. Ecological geopolymer produced with a ternary system of red mud, glass waste, and Portland cement. *Cleaner Engineering and Technology*, **6**: 100379.

González-García D. M., Téllez-Jurado L., Jiménez-Álvarez F. J., Zarazua-Villalobos L., & Balmori-Ramírez H. 2022. Evolution of a natural pozzolan-based geopolymer alkalized in the presence of sodium or potassium silicate/hydroxide solution. *Construction and Building Materials*, **321**: 126305.

Hajimohammadi A., Ngo, T., & Kashani A. 2018. Glass waste versus sand as aggregates: The characteristics of the evolving geopolymer binders. *Journal of Cleaner Production*, **193**: 593–603.

Hassan A., Arif M., Shariq M. 2019. Use of geopolymer concrete for a cleaner and sustainable environment – A review of mechanical properties and microstructure. *Journal of Cleaner Production*, **223**: 704–728.

Horbe A. M. C., da Costa M. L. 2005. Lateritic crusts and related soils in eastern Brazilian Amazonia. *Geoderma*, **126**(3–4): 225–239.

Hu S., Wang H., Zhang G., Ding Q. 2008. Bonding and abrasion resistance of geopolymeric repair material made with steel slag. *Cement and Concrete Compososition*: **30**: 239-244.

Huang G., Ji Y., Li J., Hou Z., Jin C. 2018. Use of slaked lime and Portland cement to improve the resistance of MSWI bottom ash-GBFS geopolymer concrete against carbonation. *Construction and Building Materials*, **166**: 290–300.

Hui-Teng N., Cheng-Yong H., Yun-Ming L., al Bakri Abdullah M. M., Hun K. E., Razi H. M., Yong-Sing N. 2021. Formulation, Mechanical Properties and Phase Analysis of Fly Ash Geopolymer with Ladle Furnace Slag Replacement. *Journal of Materials Research and Technology*, **12**: 1212–1226.

Ishwarya G., Singh, B., Deshwal S., Bhattacharyya S. K. 2019. Effect of sodium carbonate/sodium silicate activator on the rheology, geopolymerization and strength of fly ash/slag geopolymer pastes. *Cement and Concrete Composites*, **97**: 226–238.

Issaoui M., Limousy L., Lebeau B., Bouaziz J., Fourati, M. 2016. Design and characterization of flat membrane supports elaborated from kaolin and aluminum powders. *Comptes Rendus Chimie*, **19**(4): 496–504.

John S. K., Nadir Y., Girija K. 2021. Effect of source materials, additives on the mechanical properties and durability of fly ash and fly ash-slag geopolymer mortar: A review. *Construction and Building Materials*, **280**: 122443.

Junaid M. T., Khennane A., Kayali O., Sadaoui A., Picard D., Fafard M. 2014. Aspects of the APÊNDICES deformational behaviour of alkali activated fly ash concrete at elevated temperatures. *Cement and Concrete Research*, **60**: 24–29.

Kamseu E., Beleuk à Moungam L. M., Cannio M., Billong N., Chaysuwan D., Melo U. C., Leonelli C. 2017. Substitution of sodium silicate with rice husk ash-NaOH solution in metakaolin based geopolymer cement concerning reduction in global warming. *Journal of Cleaner Production*, **142**: 3050–3060.

Kaur M., Singh J., Kaur M. 2018. Synthesis of fly ash based geopolymer mortar considering different concentrations and combinations of alkaline activator solution. *Ceramics International*, **44**(2): 1534–1537.

Kaze C. R., Lecomte-Nana G. L., Adesina A., Nemaleu J. G. D., Kamseu E., & Chinje Melo U. 2021. Influence of mineralogy and activator type on the rheology behaviour and setting time of laterite based geopolymer paste. *Cement and Concrete Composites*, **126**: 104345.

Khale D., Chaudhary R. 2007. Mechanism of geopolymerization and factors influencing its development: A review. *Journal of Materials Science*, **42**(3): 729–746.

Khalifa A. Z., Cizer Ö., Pontikes Y., Heath A., Patureau P., Bernal S. A., Marsh A. T. M. 2020. Advances in alkali-activation of clay minerals. In *Cement and Concrete Research* (Vol. 132). Elsevier Ltd.

Klima K. M., Schollbach K., Brouwers H. J. H., Yu Q. 2022. Enhancing the thermal performance of Class F fly ash-based geopolymer by sodalite. *Construction and Building Materials*, **314**: 125574.

Komnitsas K. A. 2011. Potential of geopolymer technology towards green buildings and sustainable cities. In: International conference on green buildings and sustainable cities, procedia engineering, vol. **21**: p.1023–32.

Kotschoubey, B., Truckenbrodt, W., Hieronymus, B., 1997. Bauxite deposits of Paragominas. In: Carvalho, A., Boulangé, B., Melfi, A.J., Lucas, Y. (Eds.), Brazilian Bauxites. USP/FAPESP/ORSTOM, São Paulo, pp. 75–106.

Kotschoubey B., Calaf J.M.C., Lobato A.C.C., Leite A.S. Azevedo C.H.D. 2005. Caracterização e Gênese dos Depósitos de Bauxita da Província Bauxitífera de Paragominas, Noroeste da bacia do Grajaú, Nordeste do Pará/Oeste do Maranhão. In: HardyJost (ADIMB) e Emanuel Teixeira de Queiroz (DNPM), 65 (eds.) Caracterização de Depósitos Minerais em Distritos Mineiros da Amazônia. 23.

Koshy N., Dondrob K., Hu L., Wen Q., Meegoda J. N. 2019. Synthesis and characterization of geopolymers derived from coal gangue, fly ash and red mud. *Construction and Building Materials*, **206**: 287–296.

Król M., & Mozgawa W. 2019. Zeolite layer on metakaolin-based support. *Microporous and Mesoporous Materials*, **282**: 109–113, November 2018.

Kuri J. C., Sarker P. K., Shaikh F. U. A. 2021. Sulphuric acid resistance of ground ferronickel slag blended fly ash geopolymer mortar. *Construction and Building Materials*, **313**: 125505.

Lemougna P. N., Chinje Melo U. F., Delplancke M. P., Rahier H. 2014. Influence of the chemical and mineralogical composition on the reactivity of volcanic ashes during alkali activation. *Ceramics International*, **40**(1 PART A): 811–820.

Lemougna P. N., Wang K. tuo, Tang Q., Cui X. min. 2017. Synthesis and characterization of low temperature (<800 °C) ceramics from red mud geopolymer precursor. *Construction and Building Materials*, **131**: 564–573.

Liew Y. M., Heah C. Y., Mohd Mustafa A. B., Kamarudin H. 2016. Structure and properties of clay-based geopolymer cements: A review. *Progress in Materials Science*, **83**: 595–629.

Li D., O'Connor B. H., Low I.-M., Riessen A. van, Toby B. H. 2006. Mineralogy of Al-substituted goethites. *Powder Diffraction*.

Li M., Luo R., Qin L., Liu H., Duan P., Jing W., Zhang Z., Liu X. 2022. High temperature properties of graphene oxide modified metakaolin based geopolymer paste. *Cement and Concrete Composites*, **125**: 104318.

Liu X., Jiang J., Zhang H., Li M., Wu Y., Guo L., Wang W., Duan P., Zhang W., Zhang Z. 2020. Thermal stability and microstructure of metakaolin-based geopolymer blended with rice husk ash. *Applied Clay Science*, **196**: 105769.

Luger S., Felsche J., Fischer P. 1987. Structure of hydroxysodalite Na8[AlSiO4]6(OH)2, a powder neutron diffraction study at 8 K. *Acta Crystallographica Section C: Crystal Structure Communications*, **43**(1): 1–3.

Luukkonen, T., Abdollahnejad, Z., Yliniemi, J., Kinnunen, P., Illikainen, M., 2018. Onepart alkali-activated materials: a review. *Cement Concr. Res*. **103**: 21-34.

Luna F.J., Schuchardt U. 1999. Argilas pilarizadas - uma introdução. *Química nova*, **22** (1):104-109.

Ma C. K., Awang A. Z., Omar W. 2018. Structural and material performance of geopolymer concrete: A review. *Construction and Building Materials*, **186**: 90–102.

Mbey J. A., Thomas F., Ngally Sabouang C. J., Liboum, Njopwouo D. 2013. An insight on the weakening of the interlayer bonds in a Cameroonian kaolinite through DMSO intercalation. *Applied Clay Science*, **83–84**: 327–335.

McLellan B. C., Williams R. P., Lay J., van Riessen A., Corder G. D. 2011. Costs and carbon emissions for geopolymer pastes in comparison to ordinary portland cement. *Journal of Cleaner Production*, **19**(9–10): 1080–1090.

Mohajerani A., Suter D., Jeffrey-Bailey T., Song T., Arulrajah A., Horpibulsuk S., Law D. 2019. Recycling waste materials in geopolymer concrete. *Clean Technologies and Environmental Policy*, **21**(3): 493–515.

Moore D. M. & Reynolds R. C. 1997. X-ray diffraction and the identification and analysis of clay minerals. Second ed. Oxford University Press, Oxford.

Moutinho S., Costa C., Cerqueira Â., Rocha F., Velosa A. 2019. Geopolymers and polymers in the conservation of tile facades. *Construction and Building Materials*, **197**: 175–184.

Naghsh M. & Shams K. 2017. Synthesis of a kaolin-based geopolymer using a novel fusion method and its application in effective water softening. *Applied Clay Science*, **146**: 238–245.

Nazari A. 2013. Compressive strength of geopolymers produced by ordinary Portland cement: Application of genetic programming for design. *Materials and Design*, **43**: 356–366.

Negrão L. B. A., Alves T. K. C., Pöllmann H. 2021. Mineralogical Appraisal of Bauxite Overburdens from Brazil. *Minerals*.

Negrão L. B. A., Costa M. L. da, Pöllmann H. 2018. The Belterra Clay on the bauxite deposits of Rondon do Pará, Eastern Amazon. *Brazilian Journal of Geology*, **48**(3): 473–484.

Negrão L. B. A., Costa M. L., Pöllmann H., Horn A. 2018. An application of the Rietveld refinement method to the mineralogy of a bauxite-bearing regolith in the Lower Amazon. *Mineralogical Magazine*, **82**(2): 413–431.

Negrão L. B. A., da CostaM. L., Pöllmann H. 2018. The Belterra Clay on the bauxite deposits of Rondon do Pará, Eastern Amazon. *Brazilian Journal of Geology*, **48**(3): 473–484.

Negrão L. B. A., Pöllmann H., Cortinhas Alves T. K. 2021. Mineralogical appraisal of bauxite overburdens from Brazil. *Minerals*, **11**(7): 677.

Nikolov A., Nugteren H., Rostovsky I. 2020. Optimization of geopolymers based on natural zeolite clinoptilolite by calcination and use of aluminate activators. *Construction and Building Materials*, **243**: 118257.

Oliveira S.B., Costa M.L., Prazeres Filho H. 2016. The lateritic bauxite deposit of Rondon do Pará: a new giant deposit in the Amazon Region, northern Brazil. Economic Geology, **111**: 1–14.

Olivia M., Nikraz H. 2012. Properties of fly ash geopolymer concrete designed by Taguchi method. *Materials and Design*, **36**: 191–198.

Panda B., Singh G. B., Unluer C., Tan M. J. 2019. Synthesis and characterization of one-part geopolymers for extrusion based 3D concrete printing. *Journal of Cleaner Production*, **220**: 610–619.

Paz S. P. A., Angélica R. S., Kahn H. 2017. Optimization of the reactive silica quantification method applied to Paragominas-type gibbsitic bauxites. *International Journal of Mineral Processing*, **162**: 48–57.

Perná I., Šupová M., Hanzlíček T., Špaldoňová A. 2019. The synthesis and characterization of geopolymers based on metakaolin and high LOI straw ash. *Construction and Building Materials*, **228**: 116765.

Petrus H. T. B. M., Fairuz F. I., Sa'dan N., Olvianas M., Astuti W., Jenie S. N. A., Setiawan F. A., Anggara F., Ekaputri J. J., Bendiyasa I. M. 2021. Green geopolymer cement with dry activator from geothermal sludge and sodium hydroxide. *Journal of Cleaner Production*, **293**(2): 126143.

Phoo-Ngernkham T., Maegawa A., Mishima N., Hatanaka S., Chindaprasirt P. 2015. Effects of sodium hydroxide and sodium silicate solutions on compressive and shear bond strengths of FA-GBFS geopolymer. *Construction and Building Materials*, **91**: 1–8.

Provis J. L., van Deventer J. S. J. 2007. Geopolymerisation kinetics. 1. In situ energy-dispersive X-ray diffractometry. *Chemical Engineering Science*, **62**(9): 2309–2317.

Prud'Homme E., Michaud P., Joussein E., Clacens J. M., Arii-Clacens S., Sobrados I., Peyratout C., Smith A., Sanz, J., Rossignol S. 2011. Structural characterization of geomaterial foams - Thermal behavior. *Journal of Non-Crystalline Solids*, **357**(21): 3637–3647.

Prud'homme E., Michaud P., Joussein E., Peyratout C., Smith A., Rossignol S. 2011. In situ inorganic foams prepared from various clays at low temperature. *Applied Clay Science*, **51**(1–2): 15–22.

Qureshi T. S., Panesar D. K. 2019. Impact of graphene oxide and highly reduced graphene oxide on cement based composites. *Construction and Building Materials*, **206**: 71–83.

Qtaitat M. A., Al-Trawneh I. N. 2005. Characterization of kaolinite of the Baten El-Ghoul region/south Jordan by infrared spectroscopy. *Spectrochimica Acta - Part A: Molecular and Biomolecular Spectroscopy*, **61**(7): 1519–1523.

Rasaki S. A., Bingxue Z., Guarecuco R., Thomas T., Minghui Y. 2019. Geopolymer for use in heavy metals adsorption, and advanced oxidative processes: A critical review. *Journal of Cleaner Production*, **213**: 42–58.

Rahier H., Simons W., Van Mele B., Biesemans M. 1997. Low-temperature synthesized aluminosilicate glasses. Influence of the composition of the silicate solution on production, structure and properties. Journal of Materials Science. **32**: 2237–2247.

Ríos C. A., Williams C. D., Fullen, M. A. 2009. Applied Clay Science Nucleation and growth history of zeolite LTA synthesized from kaolinite by two different methods. *Applied Clay Science*, **42**(3–4): 446–454.

Rodrigues S. F. S., Costa, M. L. Pöllmann H., Kern, D. C., Silveira M. I. Kipnis R. 2015. Pre-historic production of ceramics in the Amazon: Provenience, raw materials, and firing temperatures. *Applied Clay Science*, **107:** 145–155.

Roudouane H. T., Mbey J. A., Bayiga E. C., Ndjigui P. D. 2020. Characterization and application tests of kaolinite clays from Aboudeia (southeastern Chad) in fired bricks making. *Scientific African*, *7*, e00294.

Rożek P., Król M., Mozgawa W. 2019. Geopolymer-zeolite composites: A review. *Journal of Cleaner Production*, **230**: 557–579.

Saalfeld H., Wedde M. 1974. Refinement of the crystal structure of gibbsite, A1(OH)3. *Zeitschrift Fur Kristallographie - New Crystal Structures*, **139**(1–2): 129–135.

Sadykov V. A., Isupova L. A., Tsybulya S. V., Cherepanova S. V., Litvak G. S., Burgina E. B., Kustova G. N., Kolomiichuk V. N., Ivanov V. P., Paukshtis E. A., Golovin A. V., Avvakumov E. G. 1996. Effect of mechanical activation on the real structure and reactivity of iron (III) oxide with corundum-type structure. *Journal of Solid State Chemistry*.

Sagawa Y., Ota, S., Harada K., Nishizaki T., Goda H. 2015. Utilization of Fly Ash with Higher Loss on Ignition for Geopolymer Mortar. *Advanced Materials Research*, **1129**: 614–620.

Sagoe-Crentsil K., Weng L. 2007. Dissolution processes, hydrolysis and condensation reactions during geopolymer synthesis: Part II. High Si/Al ratio systems. *Journal of Materials Science*, **42**(9): 3007–3014.

Salam M. A., Mokhtar M., Albukhari S. M., Baamer D. F., Palmisano L., AlHammadi A. A., Abukhadra M. R. 2021. Synthesis of zeolite/geopolymer composite for enhanced sequestration of phosphate (PO_4^{3-}) and ammonium (NH_4^+) ions; equilibrium properties and realistic study. *Journal of Environmental Management*, **300**.

Samarakoon M. H., Ranjith P. G., Rathnaweera T. D., Perera M. S. A. 2019. Recent advances in alkaline cement binders: A review. *Journal of Cleaner Production*, **227**: 70–87.

Santos V. H. J. M. dos Pontin D., PonziG. G. D., Stepanha A. S. de G. e, Martel R. B., Schütz M. K., EinloftS. M. O., Dalla VecchiaF. 2021. Application of Fourier Transform infrared spectroscopy (FTIR) coupled with multivariate regression for calcium carbonate (CaCO3) quantification in cement. *Construction and Building Materials*, **313**: 125413.

Sazali N., Harun Z., Azhar F. H., Bahri S. S., Ahmad R. P. N. A. R., Hussinisa R., Misdan N. 2020. The effect of various molarity sodium hydroxide (NaOH) on the hydrosodalite formation from synthesis of Johor Kaolin, Malaysia by hydrothermal method. *Materials Today: Proceedings*, **46**: 2045–2051.

Schulze D. G., Schwertmann U. 1984. The influence of aluminium on iron oxides: X. properties of Al-substituted goethites. *Clay Minerals*.

Sedmale G., Randers M., Rundans M., Seglins V. 2017. Application of differently treated illite and illite clay samples for the development of ceramics. *Applied Clay Science*, **146**: 397–403.

Seiffarth, T., Hohmann, M., Posern, K., Kaps, C., 2013. Effect of thermal pre-treatmentconditions of common clays on the performance of clay-based geopolymeric binders. *Appl. Clay Sci.* **73**: 35–41.

Selmani S., Sdiri A., Bouaziz S., Joussein E., Rossignol S. 2017. Effects of metakaolin addition on geopolymer prepared from natural kaolinitic clay. *Applied Clay Science*, **146**: 457–467, July.

Selmani S., Sdiri A., Bouaziz S., Rossignol S. 2017. Geopolymers based on calcined tunisian clays: Effects of alkaline solution on vibrational spectra and mechanical properties. *International Journal of Mineral Processing*, **165**: 50–57.

Silva P. de, Sagoe-Crenstil K., Sirivivatnanon V. 2007. Kinetics of geopolymerization: Role of Al2O3 and SiO2. *Cement and Concrete Research*, **37**(4): 512–518.

Singh B., Ishwarya G., Gupta, M., Bhattacharyya S. K. 2015. Geopolymer concrete: A review of some recent developments. *Construction and Building Materials*, **85**: 78–90.

Siyal A. A., Azizli K. A., Man Z., Ismail L., Khan M. I. 2016. Geopolymerization kinetics of fly ash based geopolymers using JMAK model. *Ceramics International*, **42**(14): 15575–15584.

Snellings R., Bazzoni A., Scrivener K. 2014. The existence of amorphous phase in Portland cements: Physical factors affecting Rietveld quantitative phase analysis. *Cement and Concrete Research*.

Sousa S.J.G. 2003. *Formulação e caracterização de massas cerâmicas para revestimento Poroso Base Vermelha utilizando argilas da região de Campos dos Goytacazes*. MS Dissertation, Campos dos Goytacazes – RJ, Universidade Estadual do Norte Fluminense, UENF-RJ, 96p.

Sun Z., Lin X., Vollpracht A. 2018. Pervious concrete made of alkali activated slag and geopolymers. *Construction and Building Materials*, **189:** 797–803.

Tang J., Ji X., Liu X., Zhou W., Chang X., Zhang S. 2021. Mechanical and microstructural properties of phosphate-based geopolymers with varying Si/Al molar ratios based on the sol-gel method. *Materials Letters*, **308**(Part b): 131178.

Vafaei M., Allahverdi A., Dong P., Bassim N., Mahinroosta M. 2021. Resistance of red clay brick waste/phosphorus slag-based geopolymer mortar to acid solutions of mild concentration. *Journal of Building Engineering*, **34**: 102066.

Van Jaarsveld J. G. S., van Deventer J. . J., Lukey G. C. 2002. The effect of composition and temperature on the properties of fly-ash and kaolinite-based geopolymers. Chem Eng J;**89**: 63–73.

Van Jaarsveld J. G. S., Van Deventer J. S. J. 1999. Effect of metal contaminants on the formation and properties of waste-based geopolymers. *Cement and Concrete Research*, **29**(8): 1189–1200.

Velde, B., Meunier, A., 2008. The Origin of Clay Minerals in Soils and Weathered Rocks. Springer, Berlin Heidelberg.

Weirich T. E., Winterer M., Seifried S., Hahn H., Fuess H. 2000. Rietveld analysis of electron powder diffraction data from nanocrystalline anatase, TiO 2. *Ultramicroscopy*.

Wenk H.-R., Bulakh A.G., Andreǐ G. 2004. *Minerals*: their constitution and origin. Cambridge, Cambridge University Press.

Xu H. & van Deventer J. S. J. 2000. The geopolymerisation of alumino-silicate minerals. *International Journal of Mineral Processing*, **59**(3): 247–266.

Yan S., He P., Jia D., Yang Z., DuanX., Wang S., Zhou Y. 2016. Effects of treatment temperature on the reduction of GO under alkaline solution during the preparation of graphene/geopolymer composites. *Ceramics International*, **42**(16):18181-18188.

Yunsheng Z., Wei S., Zongjin, L. 2010. Composition design and microstructural characterization of calcined kaolin-based geopolymer cement. *Applied Clay Science*, **47**(3–4): 271–275.

Zawrah M. F., Sadek H. E. H., Ngida R. E. A., Sawan S. E. A., El-Kheshen A. A. 2022. Effect of low-rate firing on physico-mechanical properties of unfoamed and foamed geopolymers prepared from waste clays. *Ceramics International,*

Zhang H. Y., Liu J. C., Wu B. 2021. Mechanical properties and reaction mechanism of one-part geopolymer mortars. *Construction and Building Materials*, **273**: 121973

Zhang P., Zheng Y., Wang K., Zhang J. 2018. A review on properties of fresh and hardened geopolymer mortar. *Composites Part B: Engineering*, **152**: 79–95, June.

Zhang Z., Wang H., Provis J. L., Bullen F., Reid, A., Zhu Y. 2012. Quantitative kinetic and structural analysis of geopolymers. Part 1. the activation of metakaolin with sodium hydroxide. *Thermochimica Acta*, **539**: 23–33.

Zhuang X.Y., Chen L., Komarneni S., Zhou C.H., Tong D.S., Yang H.M., Wang H. 2016. Fly ash-based Geopolymer: clean production, properties and applications. *J. Clean. Prod.*, **125**: 253-267.

Zhu B. L., Qi C. L., Zhang Y. H., Bisson T., Xu, Z., Fan Y. J., Sun Z. X. 2019. Synthesis, characterization and acid-base properties of kaolinite and metal (Fe, Mn, Co) doped kaolinite. *Applied Clay Science*, **179**: 105138, May.

APÊNDICE A – COMPROVANTE DE SUBMISSÃO DO ARTIGO "SYNTHESIS OF GEOPOLYMER WITH KOH BY TWO KAOLINITIC CLAYS FROM THE AMAZON: INFLUENCE OF DIFFERENT SYNTHESIS PARAMETERS ON THE COMPRESSIVE STRENGTH"

28/02/2022 12:30   Gmail - A manuscript number has been assigned: MATCHEMPHYS-D-22-00716

M Gmail   Igor Barreto <igorrochaq@gmail.com>

A manuscript number has been assigned: MATCHEMPHYS-D-22-00716
1 mensagem

Materials Chemistry and Physics <em@editorialmanager.com>   25 de fevereiro de 2022 16:05
Responder a: Materials Chemistry and Physics <support@elsevier.com>
Para: Igor Alexandre Rocha Barreto <igorrochaq@gmail.com>

Ms. Ref. No.: MATCHEMPHYS-D-22-00716
Title: Synthesis of geopolymer with KOH by two kaolinitic clays from the Amazon: influence of different synthesis parameters on the compressive strength
Materials Chemistry and Physics

Dear Mr. Igor Alexandre Rocha Barreto,

Your submission entitled "Synthesis of geopolymer with KOH by two kaolinitic clays from the Amazon: influence of different synthesis parameters on the compressive strength" has been been assigned the following manuscript number: MATCHEMPHYS-D-22-00716.

You may check on the progress of your paper by logging on to the Editorial Manager as an author. The URL is https://www.editorialmanager.com/matchemphys/.

Your username is: IBarreto-489

If you need to retrieve password details, please go to: https://www.editorialmanager.com/matchemphys/l.asp?i=1441579&l=J7TGESSC

For guidelines on how to track your manuscript in EM please go the following address: For guidelines on how to track your manuscript in EM please go the following address: http://help.elsevier.com/app/answers/detail/p/7923/a_id/89

Thank you for submitting your work to this journal.

Kind regards,

Materials Chemistry and Physics

****
For further assistance, please visit our customer support site at http://help.elsevier.com/app/answers/list/p/7923. Here you can search for solutions on a range of topics, find answers to frequently asked questions and learn more about EM via interactive tutorials. You will also find our 24/7 support contact details should you need any further assistance from one of our customer support representatives.

#AU_MATCHEMPHYS#

To ensure this email reaches the intended recipient, please do not delete the above code

_____
In compliance with data protection regulations, you may request that we remove your personal registration details at any time. (Use the following URL: https://www.editorialmanager.com/matchemphys/login.asp?a=r). Please contact the publication office if you have any questions.

APÊNCIDE B – COMPROVANTE DE SUBMISSÃO DO ARTIGO "SYNTHESIS OF "ECOFRIENDLY" GEOPOLYMERS FROM BAUXITE WASHING WASTE: AN ALTERNATIVE TO MINIMIZE CO$_2$ EMISSIONS"

18/02/2022 22:18   Gmail - Submission to Cement and Concrete Composites - manuscript number

M Gmail   **Igor Barreto <igorrochaq@gmail.com>**

Submission to Cement and Concrete Composites - manuscript number
1 mensagem

Cement and Concrete Composites <em@editorialmanager.com>   18 de fevereiro de 2022 06:16
Responder a: Cement and Concrete Composites <support@elsevier.com>
Para: Igor Alexandre Rocha Barreto <igorrochaq@gmail.com>

This is an automated message.

Manuscript Number: CCC-D-22-00272
Synthesis of "ecofriendly" geopolymers from bauxite washing waste: An alternative to minimize CO2 emissions

Dear Mr Barreto,

Your above referenced submission has been assigned a manuscript number: CCC-D-22-00272.

To track the status of your manuscript, please log in as an author at https://www.editorialmanager.com/ccc/, and navigate to the "Submissions Being Processed" folder.

Thank you for submitting your work to this journal.

Kind regards,
Cement and Concrete Composites

More information and support

You will find information relevant for you as an author on Elsevier's Author Hub: https://www.elsevier.com/authors

FAQ: How can I reset a forgotten password?
https://service.elsevier.com/app/answers/detail/a_id/28452/supporthub/publishing/
For further assistance, please visit our customer service site: https://service.elsevier.com/app/home/supporthub/publishing/
Here you can search for solutions on a range of topics, find answers to frequently asked questions, and learn more about Editorial Manager via interactive tutorials. You can also talk 24/7 to our customer support team by phone and 24/7 by live chat and email

#AU_CCC#

To ensure this email reaches the intended recipient, please do not delete the above code

_____
In compliance with data protection regulations, you may request that we remove your personal registration details at any time. (Use the following URL: https://www.editorialmanager.com/ccc/login.asp?a=r). Please contact the publication office if you have any questions.

ANEXO A – CORPOS DE PROVA DOS GEOPOLIMEROS SINTETIZADOS A PARTIR DA AMOSTRA BTC-1 CALCINADA A 750°C
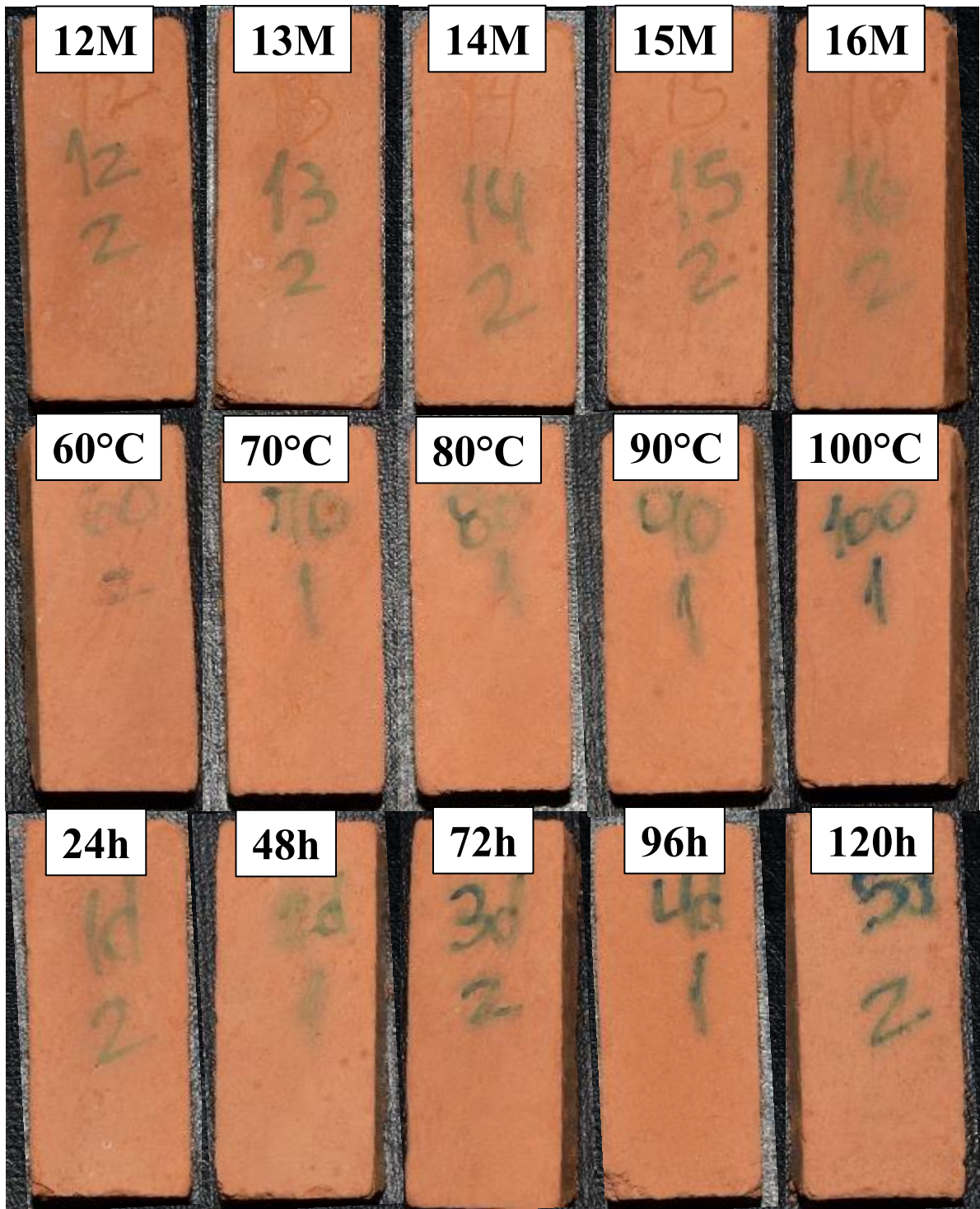
10mm

ANEXO B – CORPOS DE PROVA DOS GEOPOLIMEROS SINTETIZADOS A PARTIR DA AMOSTRA CIM-1 CALCINADA A 750°C
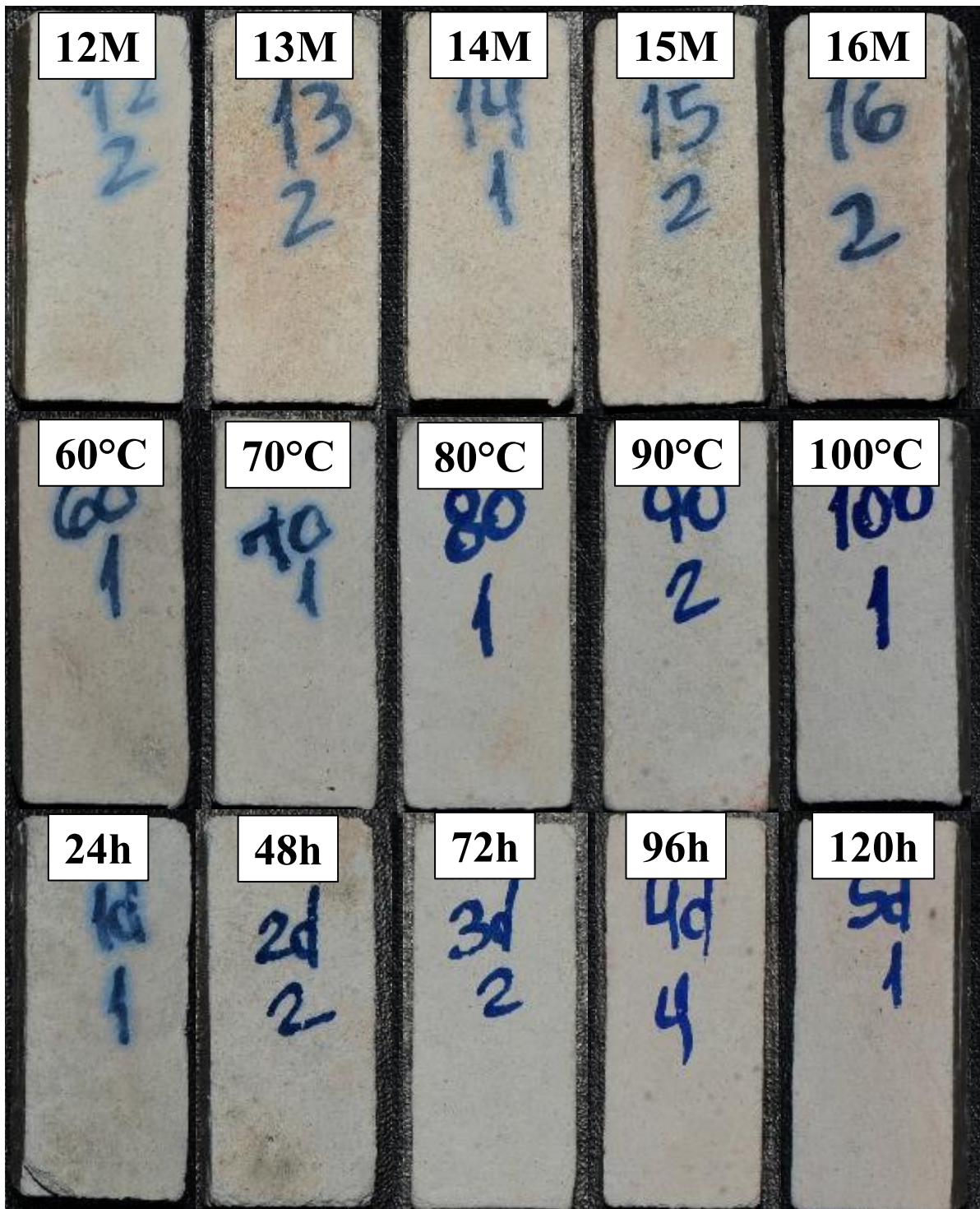
10mm

PARECER

Sobre a Defesa Pública da Tese de Doutorado de
IGOR ALEXANDRE ROCHA BARRETO

A banca examinadora da Tese de Doutorado de **IGOR ALEXANDRE ROCHA BARRETO** orientando do Prof. Dr. Marcondes Lima da Costa (UFPA) e composta pelos professores doutores Herbert Pöllmann (Martin-Luther Universität Halle-Wittenberg, Alemanha), Guilherme Frederico Bernardo Lenz e Silva (USP), José Roberto Zamian (UFPA), e Rômulo Simões Angélica (UFPA), após apresentação da sua tese intitulada **"APLICAÇÃO DE RESÍDUOS DA MINERAÇÃO DE BAUXITA NA SÍNTESE DE GEOPOLIMEROS"** emite o seguinte parecer:

O candidato realizou sua apresentação de forma clara, organizada e segura no tempo estipulado. Na arguição mostrou domínio da temática abordada e respondeu às perguntas formuladas pela banca, porém foi evidenciando que o texto apresentado necessita de alguns ajustes. São eles: ajustar o foco ou reescrever os objetivos, adequar a metodologia de forma a melhorar o entendimento e o encadeamento dos artigos publicados e/ou enviados para publicação. E no caso das conclusões, também é necessário fazer um ajuste de modo a melhor integrar os resultados obtidos nos três artigos, respondendo aos objetivos iniciais.

Finalmente, a banca examinadora decidiu por unanimidade aprovar a tese de doutorado.

Belém, 08 de abril de 2022

Prof. Dr. Marcondes Lima da Costa (Orientador – UFPA)

Prof. Dr. Herbert Pöllmann (Martin-Luther Universität Halle-Wittenberg)

Prof. Dr. Guilherme Frederico Bernardo Lenz e Silva (USP)

Prof. Dr. José Roberto Zamian (UFPA)

Prof. Dr. Rômulo Simões Angélica (UFPA)